The Study of Fatigue Life Discrepancy on High-Strength Steel Springs Used in Automotive Engine Application

by

Keivan HEIDARI

THESIS PRESENTED TO ÉCOLE DE TECHNOLOGIE SUPÉRIEURE IN PARTIAL FULFILLMENT FOR A MASTER'S DEGREE WITH THESIS IN MECHANICAL ENGINEERING
M.A.Sc.

MONTREAL, DECEMBER 21, 2016

ÉCOLE DE TECHNOLOGIE SUPÉRIEURE UNIVERSITÉ DU QUÉBEC

BOARD OF EXAMINERS

THIS THESIS HAS BEEN EVALUATED

BY THE FOLLOWING BOARD OF EXAMINERS

Mr. Philippe Bocher, Thesis Supervisor
Mechanical Engineering Department, École de technologie supérieure

Ms. Nicole R. Demarquette, Chair, Board of Examiners
Mechanical Engineering Department, École de technologie supérieure

Mr. Ricardo Zednik, Member of the jury
Mechanical Engineering Department, École de technologie supérieure

THIS THESIS WAS PRESENTED AND DEFENDED

IN THE PRESENCE OF A BOARD OF EXAMINERS AND THE PUBLIC

ON DECEMBER 8, 2016

AT ÉCOLE DE TECHNOLOGIE SUPÉRIEURE

ACKNOWLEDGMENTS

Foremost, I would like to express my sincere gratitude to my advisor, Professor Philippe Bocher, for the opportunity he has given me to work at the Laboratoire d'Optimisation des Procédés de Fabrication Avancés (LOPFA). Without his guidance, patience, and continuous support my master study would not have been successful. Definitely, he was the most influential person during my research. His guidance helped me in all the time of research and writing of this thesis. I could not have imagined having a better advisor and mentor for my master study.

My immense appreciation extends to Ms. Nicole R. Demarquette and Mr. Ricardo Zednik, professors at ETS, for accepting to be part of my board of examiners and for providing valuable comments.

I would like to thank Professor Hamid Jahed, for the experiments have done at the University of Waterloo. I would like to appreciate the help provided by Ms. Bahareh Marzbanrad, for running the rotating bending fatigue tests.

This work was made possible by the financial support provided by Liberty Spring Inc. Special thanks to Mr. Jean-François Fournier and Mr. René Fournier from Liberty Spring Inc. for their enthusiastic help and supports.

Sincere thanks are extended to my colleagues at LOPFA for their discussions and assistance in different parts of this research project. Special thanks go to Dr. Hossein Monajati, Dr. Sébastien Le Corre, Dr. Jianqiang Chen, Dr. Abdelhalim Loucif, Dr. Samir Mourad , Dr. Mohsen Mokhtabad, and Dr. Ali Niknam. I would like to acknowledge the help of entire materials laboratory at ETS, particularly Radu Romanica, Serge Plamondon, and Olivier Bouthot.

I wish to give my wholehearted thanks to my parents and my sisters for their unwavering supports, wise counsel, well wishing, encouragements, and endless love.

ETUDE DES DIFFRENCES DE COMPORTEMENT EN FATIGUE DE RESSORTS A HAUTE LIMITE D'ELASTICITE UTILISES DANS LE SECTEUR AUTOMOBILE

Keivan HEIDARI

RÉSUMÉ

Les aciers à haute limite élastique sont des aciers bainitique-martensitique utilisés dans la production de ressort. Ils sont utilisés en industrie automobile au niveau de la partie moteur. Leur fonction principale est d'amortir les vibrations générées par le moteur, ce qui implique que ces derniers soient soumis à un haut niveau de sollicitation. Les derniers progrès dans l'industrie automobile demandent le développement de ressort de haute résistance mécanique et ayant une meilleure résistance à la fatigue.

L'un des objectifs de cette étude est de caractériser les raisons principales contrôlant le comportement en fatigue des ressorts cassant pour différents nombres de cycle, allant de de 10^4 à 10^5 cycles. Pour ce faire, différentes microstructures et moyens de caractérisation ont été utilisés. Ces observations, réalisées sur des ressorts testés en contrainte imposée, montrent que la relaxation des contraintes et les microstructres initailes ne sont pas les mêmes dans le cas des ressorts à faibles durées de vie comparée à ceux de plus longues durées de vie. La relaxation des contraintes est plus prononcée pour les ressorts cassant à une faible nombre de cycle. Cette étude montre que les microstrustures de ces derniers contiennent plus de martenisite conférant au matériau une plus grande résistance à la déformation. Ainsi, les matéraiux les plus durs diminuent les peformences des ressorts en service.

En continuité de ces observations, cette étude a étudié le comportement en fatigue en fonction de l'état de surface de plusieurs matériaux et conditions de chargement. Les essais de fatigue ont été réalisés par flexion rotative (R =-1) à une contrainte de 1000 MPa. Les résultats obtenus montrent que la rupture des échantillons ne présentant pas de défauts de surface ni de contraintes résiduelles est due à la présence d'inclusions. Ces inclusions sont composées d'aluminium et de calcium. Elles ne contrôlent pas le comportement en fatigue des échantillons grenaillés. C'est plutôt la rugosité générée par le traitement de grenaillage qui est la cause de l'amorçage de fissure. La plupart des défauts de surface ont été supprimés par electro-polissage et la plus haute durée de vie a été atteinte par les échantillons grenaillés puis electro-polis.

Mot-clés: Aciers à très haute limite d’élasticité, Contraintes résiduelles, La vie en fatigue, Structure bainitique et martensitique, Grenaillage

THE STUDY OF FATIGUE LIFE DISCREPANCY ON HIGH-STRENGTH STEEL SPRINGS USE IN AUTOMATIVE ENGINE APPLICATION

Keivan HEIDARI

ABSTRACT

High-strength steels are the bainitic-martensitic steels that are used for coil spring products. Coil springs are particular components of the engine system that are widely used in automotive industries. Their main function is to absorb vibrations of the engine system, which imposes a high level of energy to these coil springs. Recent developments in automotive industries require the coil springs with high fatigue life and strength.

One of the objectives of this study is to assess the main reasons for fatigue life discrepancy of coil springs that broken in different numbers of cycles, varying in the range of 10^4 to 10^5 cycles. To that end, different material and microstructural characterization methods were used. These characterizations on coil springs, tested with controlled stress, revealed that the stress relaxation, and initial microstructure, was not the same in the coils with low life cycles (10^4) and high life cycles (10^5). Stress relaxation during fatigue test was more in springs failed at low numbers of cycles than the ones failed at high numbers of cycles. This work showed that microstructure of these low fatigue life springs have more martensite, which allows the harder material be formed. However, hard materials decreased the performance of the coil in service.

The other objective of this research work is to study the fatigue life of the parts as a function of the surface integrity conditions for different materials and process parameters. The fatigue testing was performed by rotating bending method (R=-1) with a stress of 1000 MPa. Fatigue life studies showed that failure for the steels without surface defects and residual stress came from inclusion particles. The chemical composition of these inclusions is rich in Aluminum-Calcium (Al-Ca). It was investigated that these inclusion particles do not control fatigue life after surface shot peening. It was shown that surface defects induced by shot peening cause failure. Surface defects after chemical polishing were removed and the best fatigue life obtained when specimens were shot peened and chemically polished.

Keywords: High-strength steels, Spring steels, Residual Stress, Fatigue life, Bainitic-martensitic structures, Shot peening.

TABLE OF CONTENTS

Page

LIST OF TABLES

Page

LIST OF FIGURES

Page

LIST OF ABBREVIATIONS

Al	Aluminium
ASM	American Society for Metals
ASTM	American Society for Testing and Materials
AT	After Tempering
BCT	Body-Centered Tetragonal
C	Carbon
Ca	Calcium
Co	Company
cos	Cosine
Cr	Chromium
EDX	Energy-Dispersive X-ray
e.g.	Example
Fe	Iron
Inc	Incorporated
ISO	International Organization for Standardization
Mn	Manganese
Mo	Molybdenum
Ni	Nickel
OT	Oil Tempered
SAE	Society of Automotive Engineers
SiCr	Silicon Chromium

SEM	Scanning Electron Microscope
Si	Silicon
TEM	Transmission Electron Microscopy
TTT	Time-Temperature-Transformation
V	Vanadium
VC	Vanadium Carbide
XRD	X-ray Diffraction

LIST OF SYMBOLS AND UNITS OF MEASUREMENTS

a_c	Critical flaw size (μm)
d_{max}	Depth of maximum residual stress (μm)
d_0	Depth where residual stress become zero (μm)
dV	Vickers diagonal
E	Young's modulus (MPa)
gf	Gram force
GPa	Giga Pascal
HV	Hardness Vickers
Kc	Fracture toughness
kV	Kilovolt
mA	Milliamps
mm	Millimeter
MPa	Mega Pascal
Ra	Arithmetic average height (μm)
Rp	Maximum height of peaks (μm)
Rt	Maximum height of profile (μm)
Rv	Maximum depth of valleys (μm)
Rz	Ten-point height (μm)
s	Second
V	Voltage
wt.	Weight
σ_a	Alternating stress (MPa)

σ_{max}	Maximum stress (MPa)
σ_{min}	Minimum stress (MPa)
σ_m	Mean stress (MPa)
σ_s	Stress at the surface (MPa)
σ_u	Ultimate tensile stress (MPa)
$P\sigma_0$	Residual stress depth
σ_{-1}	Experimental alternating stress in R=-1 (MPa)
λ_c	Cut-off length
μm	Micrometer
α_{Gb}	Granular bainite
α_M	Tempered martensite
m/sec	Meter per second
θ	Beam diffraction angle
λ	Wavelength
β	Bragg angle
φ	X-ray beam incident angle
ε_a	Strain parameter
ϑ	Poisson's ratio
°C	Degree Celsius
°	Degree
%	Percentage

INTRODUCTION

Coil springs absorb the vibrations of stop-start automotive engine systems. This vibration absorption imposes a high level of energy, causing a demand for coil springs with high strength and high fatigue life. Liberty Spring Inc. is one of the companies that produce coil springs in different sizes and geometries for these engine systems. Liberty Spring Inc. uses high-strength steels for its products. The high-strength steels commercially named 'OTEVA ® 75 SC' are oil tempered (OT) steels. They have good tensile strength and formability (Suda and Ibaraki, 2005). The companies that supply coil springs, which need high fatigue properties, are using these steels. Different processes such as shaping, grinding, stress relieving, and double shot peening are applied to these steels to produce coil springs.

The general objective of this study is to investigate a proper production procedure that would improve the fatigue life in coil spring specimens. For this regard, this study is divided into two phases. The first phase investigates the failure reasons for the coil springs that failed at different life cycles. The second phase documents the material durability for different surface integrity conditions. These phases are developed with more details as follows:

Phase I:

The fatigue life discrepancy is studied for six broken coil specimens that failed at significant numbers of cycles. These six coils were chosen randomly from a large set of low life (10^4 cycles) and high life (10^5 cycles) coils that were fatigue tested by Liberty Spring Inc. under stress-controlled condition. Different characterization methods such as fractography of the fracture surface and measurement of the surface roughness, residual stress, microhardness, and microstructural characterization have been used in this phase.

Phase II:

Fatigue performance is studied for the specimens that have different production procedures using rotating bending method of fatigue test (R= –1). Liberty Spring Inc. provides the specimens with eight surface integrity conditions. These conditions show the fatigue behavior of the steels with no residual stress and surface defects, chemically polished specimens after machining and after shot peening. Broken specimens after fatigue test have been characterized with different characterization methods, including fractography of the fracture surface, measuring the stress relaxation during fatigue test, and characterizing the material softening due to fatigue test for each condition.

This thesis has consequently three chapters. Chapter 1 will present an overview of the recent studies on mechanical properties and fatigue life improvement of high-strength steels. In this chapter production steps of coil springs and recent developments of these steps will be introduced. Chapter 2 will present the material characterization techniques as well as the equipment that have been used in this research. In chapter 3 the results of material characterization for both coil springs and rotating bending test specimens will be discussed. Summary of the obtained results as well as suggestions to further control and enhance the fatigue life of coil springs under study will be presented at the end of the thesis.

CHAPTER 1

LITERATURE REVIEW

Developments in automotive industries are toward lighter cars and smaller engine system resulting in fuel consumption and cost saving. Coil springs as one of the automotive engine components should have a smaller diameter, higher level of durability, and improved fatigue life properties. This chapter reviews recent developments in spring steels as well as the strengthening methods, which have positive effects on mechanical properties. Developments in coil springs production will also be explained in detail in this chapter.

1.1 Spring Steels Developments

High-strength steels are oil tempered and have been used in the spring industry in recent years. These steels have replaced 'Piano Wire,' oil tempered wire, and Chromium-Vanadium (Cr-V) steels. Piano wire was the early material used for the small size springs (Izumida, Matsumoto and Murai, 2016); (Jinbo, Fujiwara and Suda, 2007). Piano wires had high carbon content, high tensile strength, and toughness, as well as uniform mechanical properties. On the other hand, springs made of Piano wire could be used at room temperature up to 150°C, and they could be used under dynamic or static stress. Higher temperature leads Piano wires to have lower endurance limit (Dove, 1990); (Yamada and Kuwabara, 2007). Springs made by piano wires had limited sizes, in the range of 0.12 mm to 3 mm. Therefore, spring industries replaced the piano wire with oil tempered steels. Oil tempered steels were cheaper and could be used for bigger spring sizes (3 mm to 12 mm). These steels were good for the working temperature below 180°C. However, they were not usable in shocking or impact loading conditions (Sarna, 2013). Cr-V steels were then used because of their improved properties such as absorbing shock and impact loading, usable at high working temperature (up to 220°C), and high fatigue life. The size of the springs made by Cr-V steels could be in the range of 0.8 mm to 12 mm.

Finally, high-strength steels have Silicon-Chromium-Vanadium (Si-Cr-V) alloying elements with excellent fatigue behavior, mechanical properties, and strength than the steels were used earlier. Advances in the strengthening methods such as alloying elements and mixed microstructures together with fatigue life improvements have summarized in the following subsections.

1.1.1 Alloying Elements

Strengthening methods in high-strength steels are a solid solution and precipitation hardening (Izumida, Matsumoto and Murai, 2016). These two strengthening methods are the result of various alloying elements in the chemical composition. Alloying element of the high-strength steels in the present study are Si, Cr, and V. Each of these elements has different strengthening method, which will explain in following subsections.

1.1.1.1 Silicon

Si postpones material softening in tempering process as it delays the conversion of carbide to cementite during tempering process (Izumida, Matsumoto and Murai, 2016); (Nam, Lee and Deok, 2000). As a result of the delay in material softening, tempering can be applied at higher temperatures, leading to further reduction of dislocations density and toughness improvement. Also, stress relieving will be applied at a higher temperature resulting in more stress relaxation (Izumida, Matsumoto and Murai, 2016).

1.1.1.2 Chromium

Cr increases the hardenability, corrosion resistance, and oxidation resistance of high-strength steels (Totten, 2006). Cr carbides increase the required stress for dislocations movement, which resulted in higher yield strength (Terentyev, Bonny and Malerba, 2008).

1.1.1.3 Vanadium

V strengthens the steels by the precipitation hardening mechanism. V is a carbide former and forms fine particles of VC (Vanadium Carbide) precipitates. These precipitates improve the yield strength of steels (Nam, Lee and Deok, 2000).

1.1.2 Mixed Microstructure

A microstructure with an optimum combination of toughness and ductility has been desired for high-strength steels. The work of Htun, Kyaw and Lwin (2008) showed that after quenching, high-strength steels have martensitic structures plus a small amount of retained austenite. By tempering process retained austenite will transform to carbide precipitations or bainitic structures depending on tempering temperatures. Bainitic structures in high-strength steels obtained by tempering at the range of 400°C to 450°C. These authors observed that at higher tempering temperature range (500°C-550°C) retained austenite transformed to the cementite precipitation (tempered martensite).

Recent studies show that high-strength steels with mixed bainitic-martensitic structures have better mechanical properties than steels with tempered martensite structures. For instance, Htun, Kyaw and Lwin (2008) have shown that mixed bainitic-martensitic steels after tempering at 450 °C for 1 hour have maximum yield strength and endurance limit. Figure 1.1 (a) shows high-strength steels after tempering at 450 °C for 1 hour have maximum yield strength. These authors have proved that mixed bainitic-martensitic structures, after 1-hour tempering at 400 °C to 450 °C have the maximum endurance limit (Figure 1.1 (b)).

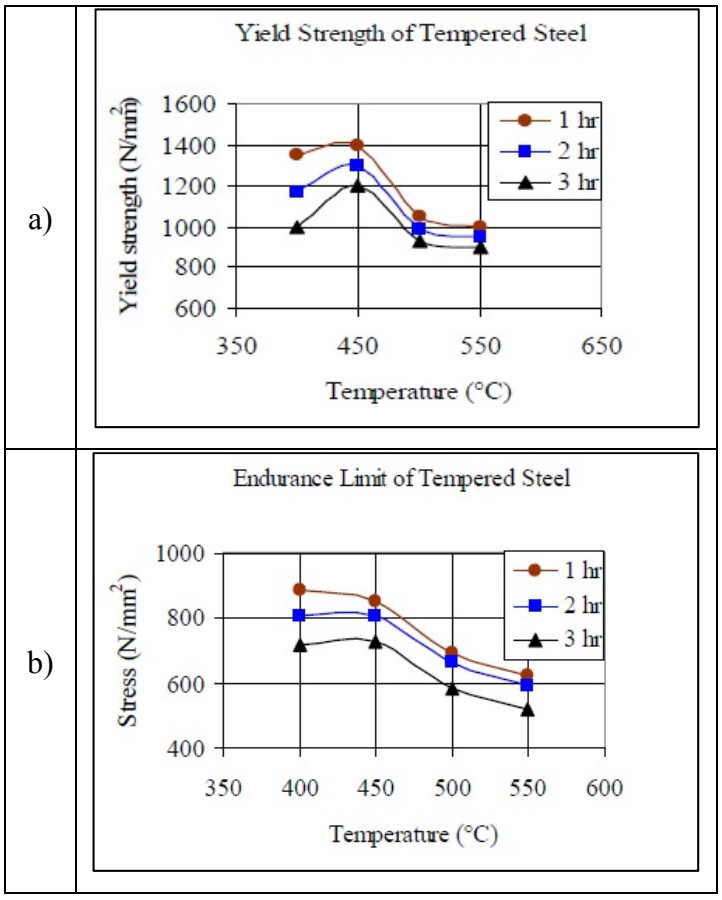

Figure 1.1 Show the yield strength (a) and endurance limit (b) of high-strength steels in different tempering temperatures and holding times, the figure reported from Htun, Kyaw and Lwin (2008).

Serbino and Tschiptschin (2014) have shown that bainitic-martensitic steels have higher fatigue life at stress amplitude of 500 MPa compare to tempered martensite (Figure 1.2). However, at lower stress amplitude (450 MPa and 475 MPa) fatigue lives of both steels were almost similar.

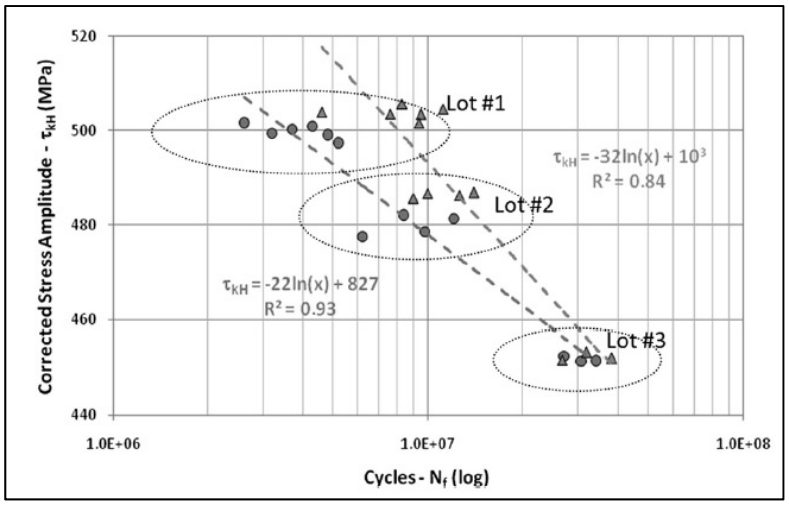

Figure 1.2 Comparison of the fatigue lives at different stress level for the bainitic-martensitic steels (▲) and martensitic steels (●), figure reported from Serbino and Tschiptschin (2014).

Tempered martensite and bainitic structures will be introduced respectively in following subsections.

1.1.2.1 Tempered Martensite

Martensitic structures are formed at low transformation temperature by rapid cooling from austenitization temperature. Martensite is a hard and brittle structure that causes high yield strength in the material. These structures have high dislocations density and low carbon diffusion (Bramfitt, 2002). Usually, tempering process is applied to these structures, and some of the mechanical properties, such as ductility and toughness are restored (Htun, Kyaw and Lwin, 2008). The work of Lee and al. (1998) showed that in martensitic steels elevation of tempering temperature up to 450 °C, increases the fatigue limit of the material (σ_f=910 MPa). While at higher tempering temperature (500°C), fatigue limit has decreased (σ_f=790 MPa (Figure 1.3).

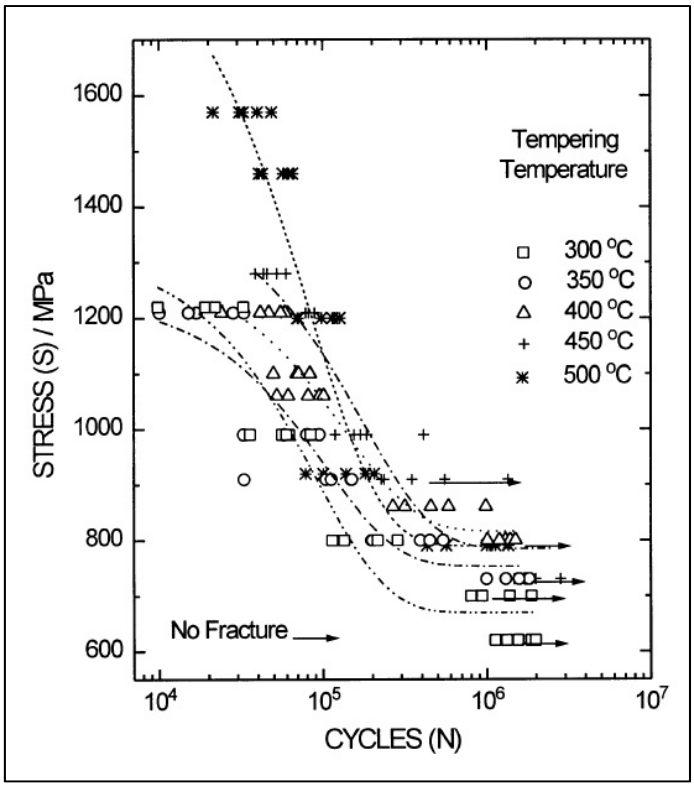

Figure 1.3 S-N curves for different tempering temperatures of high-strength steels, figure reported from Lee and al. (1998).

One of the issues with martensitic structures is the possibility of material softening during the cyclic test. This material softening would cause the stress level to decrease when operated in constant strain test. The material softening in martensitic steels is due to rearrangement of dislocations (Dubey and al., 2005); (Sauzay and al., 2005); (Sauzay and al., 2008).

1.1.2.2 Bainitic Structure

Bainitic structures are formed in two ways. In one approach, these structures are formed during quenching by controlled cooling rate after austenitization. The other approach is through the transformation of retained austenite in the martensitic structure during tempering at high temperature.

In the first approach, depending on formation temperature, bainitic structures would be in the form of upper bainite or lower bainite. Upper bainite is formed at high transformation temperature range (400 °C to 500 °C), and lower bainite is formed at lower transformation temperature range (250 °C to 400 °C) (Campbell, 2008). Dislocations in bainitic structures have low density, and carbon precipitations have formed.

1.2 Coil Springs

Coil spring production process has different steps. The first step is the design of coil according to *Handbook of Spring Design* (SMI, 2002). Different properties of coil spring such as wire size and compositions, coil diameter, number of active coils, and the amount of expected external force are specified in this step. Different wires are used in coil springs such as round wire, keystoned wire, and rectangular wire. The wire of the coil springs in the present study are rectangular wire. Springs with rectangular wires are stored more energy than equivalent round wires, even though stress distribution around the rectangular wire is not as uniform as the round wire (SMI, 2002).

The shear stress (τ) in coils with low pitch angle (less than 10°) has been calculated by using Equation 1-1 and is known as the uncorrected shear stress. In this equation, ‘P’ is applied load, ‘R’ is coil radius, and ‘d’ is wire diameter. Figure 1.4 (a) shows distributions at the inner and outer side of the coil are perfectly inverted.

$$\tau = \frac{16PR}{\pi d^3} \tag{1-1}$$

This formulation of the shear stress equation ignores many factors that have an effect on the stress distribution in helical springs. Bending and compressive stresses are some of these factors. Wahl (1944) suggested a new equation for calculating the corrected shear stress in coil springs. Accordingly, corrected shear stress distributions (Figure 1.4) is higher at the inner side and lower on the other side of the coil, which is calculated from Equations 1-2 and 1-3 respectively. In these equations, 'c' is spring index, which is calculated by dividing coil diameter (D) by wire diameter (d) (Equation 1-4).

$$\tau_{a1} = \frac{16PR}{\pi d^3}\left[\frac{4c-1}{4c-4}\right] \quad (1\text{-}2)$$

$$\tau_{a2} = \frac{16PR}{\pi d^3}\left[\frac{4c+1}{4c+4}\right] \quad (1\text{-}3)$$

$$c = \frac{D}{d} \quad (1\text{-}4)$$

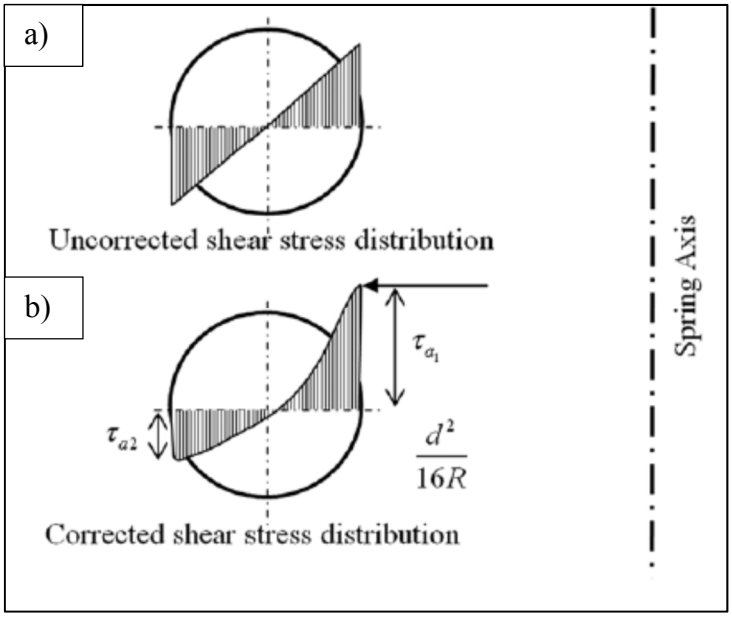

Figure 1.4 (a) Theoretical (uncorrected) and (b) real (corrected) shear stress distribution in coil springs, figure adapted from (Prawoto and al., 2008).

The next steps in the manufacturing of the coil springs following the design are shaping or coiling, stress relieving, shot peening, and surface finishing respectively. If these steps perform accurately, coil springs will have higher fatigue life and strengthening (Porteiro, 2010). These steps will be explained in detail in following subsections.

1.2.1 Shaping

Spring wires are shaped into the coils by using both mechanical and Computer-Numeric-Control (CNC) machines. This process is usually performed at room temperature when wire diameters are less than 20 mm and at an elevated temperature for wire diameters more than 20 mm.

1.2.2 Stress Relieving

Stress relieving is a heat treatment method that is applied at low temperature to release internal stresses induced during the previous production steps. If stress relieving is not applied, it could cause part distortion in the long term. In this process, the material is warmed up to a temperature in the range of 75 °C to 510 °C. Material is held at this temperature for a specific period and then is cooled down to the room temperature (Canonico, 1991); (Kovacs, 1991); (SMI, 2002). Holding time varies for different materials in the spring wire.

In the present work, two stress relieving methods known as batch and inline were used. Stress relieving in batch method is independent of the production line as steels are loaded into the furnace chamber to be heat treated together. Stress relieving with inline method is applied in the production line, and specimens are loaded on a conveyor belt, which passes through the furnace.

1.2.3 Double Shot Peening

Shot peening is a mechanical surface treatment that induces compressive residual stress at surface layers. In shot peening the specimen's surface is bombarded with hard, small, and high-speed spheres, called shots, causing plastic deformation of the surface (Vielma, Llaneza and Belzunce, 2014). Shot peening has a positive influence in reducing the effect of destructive stress concentrations on the surface such as notches, forging pits and other types of surface defects (Kostilnik, 1994). Layers of compressive residual stress, induced in shot peening process, prevent the microcrack propagation and increase fatigue life (Guagliano and Vergani, 2004); (Song and Wen, 1999). Compressive residual stress induced by shot peening extends up to hundreds of microns below the surface, which is balanced with internal tensile stress in deeper layers of the material (Figure 1.5) (Kostilnik, 1994).

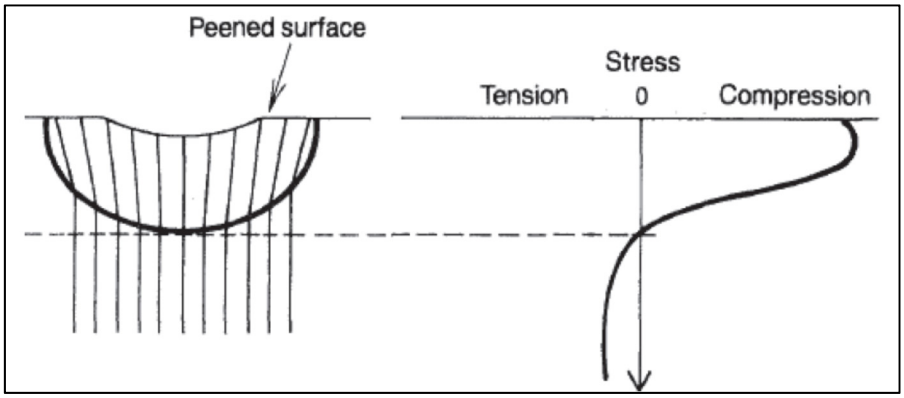

Figure 1.5 Compressive residual stress distribution in the material reported from (Gur and Savas, 2012).

Single shot peening and double shot peening are the two variant of same surface treatment. Single shot peening method applies using one shot size and constant peening intensity. On the other hand, double shot peening uses different shot size and peening intensity: the first peening is applied at high peening intensity with big shot size in order to produce a high level of compressive residual stress in depth. The second peening is applied at low peening

intensity with small shot size that improves the surface roughness and increases the residual stress value at the surface (Ishigami and al., 2000).

While single shot peening with very big shot size induces good depth of compressive residual stress and improves the fatigue life (Figure 1.6) (Tekeli, 2002) but shot peening in high peening intensity and big shot size create lots of surface damages causing early crack nucleation as damage can be induced by the process itself (Vielma, Llaneza and Belzunce, 2014). Figure 1.7 shows an example of surface damages after shot peening with big shot sizes.

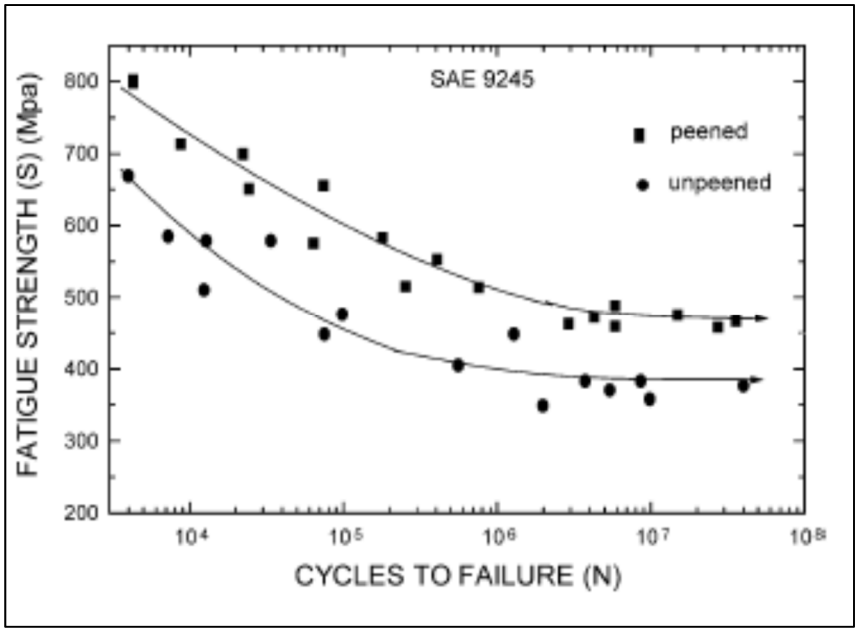

Figure 1.6 S-N curve for shot peened and unpeened specimens, figure reported from (Tekeli, 2002)

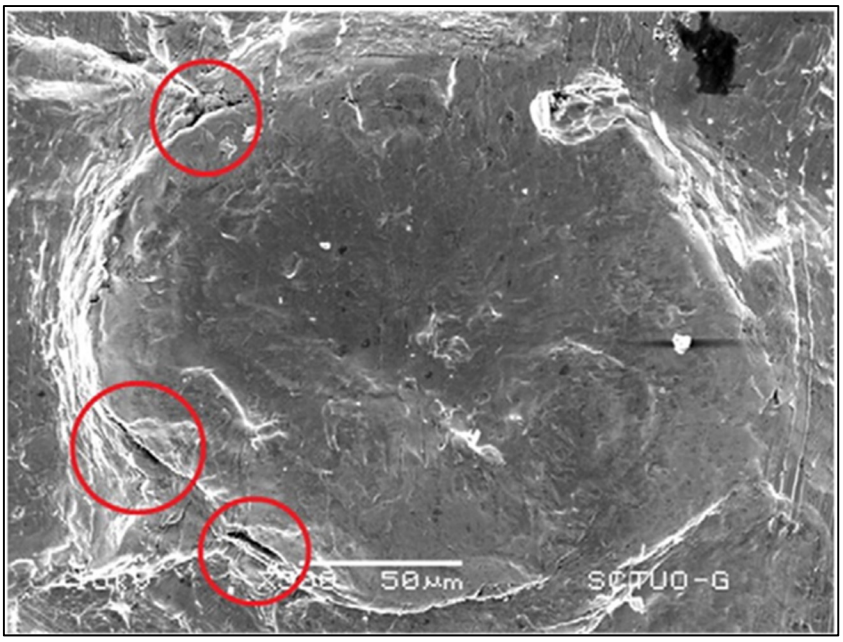

Figure 1.7 Surface damages due to the shot peening with big shot size. Red circles show the surface damages around the shot impact, reported from (Vielma, Llaneza and Belzunce, 2014).

Vielma, Llaneza and Belzunce (2014) have shown that double shot peening improves the surface roughness (Figure 1.8). They showed that an aggressive first peening intensity (0.7 mm shot size and high Almen intensity (21A)) followed by a gentle second peening (0.2 mm shot size and lower Almen intensity (5A)) improves the surface roughness considerably. It has been shown that better surface roughness obtained after electropolishing (EP) and mechanical grinding (MG). These authors found that fatigue life increased after second shot peening by smaller shot size (0.3 mm and 0.2 mm) (Figure 1.9). However, it has concluded that second peening with very low Almen intensity (5A) improved the fatigue life less than the moderate Almen intensity (8A). These authors have found than as high fatigue life as optimized double shot peening would be obtained by optimized single shot peening (10A).

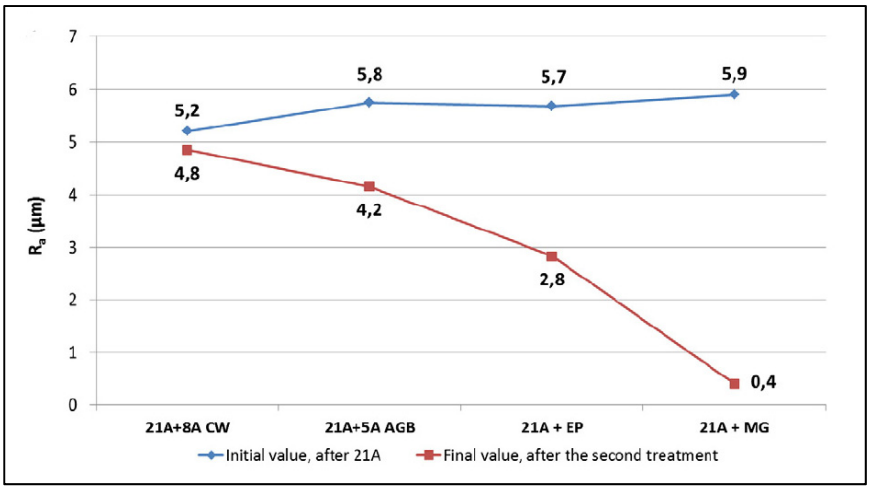

Figure 1.8 Roughness evolution after second surface treatments, figure reported from (Vielma, Llaneza and Belzunce, 2014).

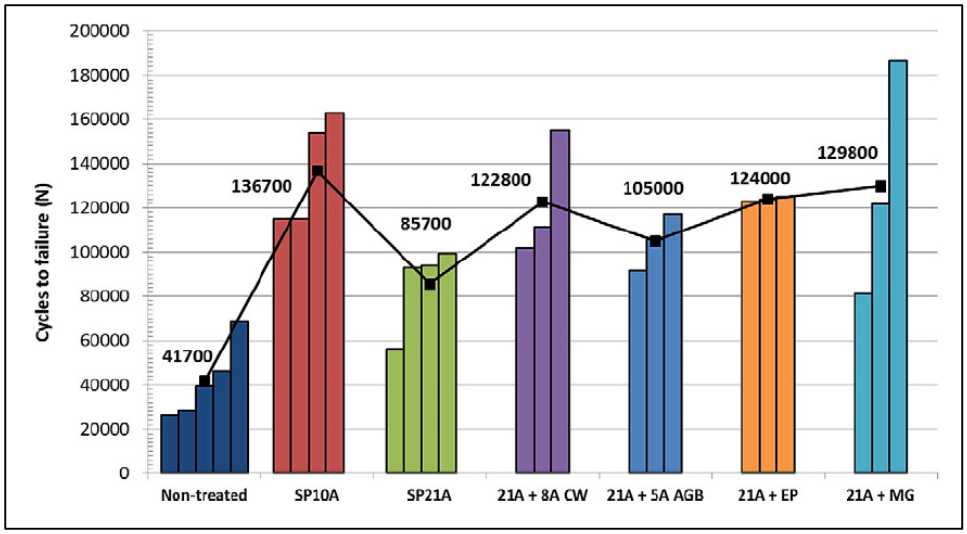

Figure 1.9 Fatigue lives of the steels with different surface treatments. Testing stress = 50% of the tensile strength of the steels, figure reported from (Vielma, Llaneza and Belzunce, 2014).

1.2.4 Finishing

Finishing is the last step in the manufacturing process of the coil springs. In this step, different polishing methods such as mechanical polishing, electropolishing, chemical polishing, and coating are used to further improvement of the surface roughness. It has shown by Vielma, Llaneza and Belzunce (2014) that fatigue lives after electropolishing have less dispersion (Figure 1.9). Chemical polishing method has been used in the present study for some of the specimens, hoping to increase the fatigue life of the specimens substantially. Sharp edges and notches are removed from the surface by chemical polishing resulting in the smoother surface (Balseal, 2016).

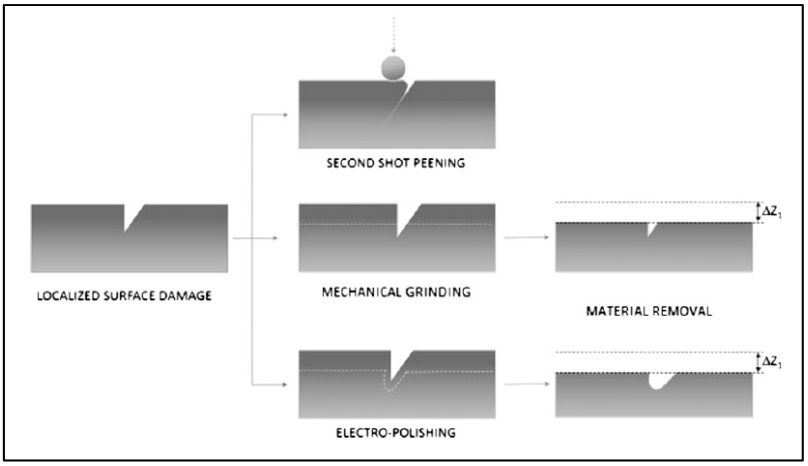

Figure 1.10 Comparison of removing surface damage with different surface finishing method, figure reported from (Vielma, Llaneza and Belzunce, 2014).

CHAPTER 2

EXPERIMENTAL DETAILS

This chapter will present the materials and specimens, equipment, and characterization methods that have been used in the present study. The first section of this chapter will introduce the chemical composition of the high-strength steels, specimen's geometries, and surface condition of the specimens. The second section will discuss the differences between strain-controlled and stress-controlled methods in fatigue. Coil springs in engine system are working under strain-controlled cyclic loading condition, whereas they were fatigue tested with the stress-controlled method by Liberty Spring Inc. Additionally, straight shank specimens with different surface integrity conditions were also fatigue tested in stress-controlled conditions. The third section will explain the methodology and equipment that were used for material characterizations before and after fatigue tests. These methods of material characterization were microhardness measurement, roughness measurement, residual stress measurement, microstructural characterization, and fractography of the fracture surfaces.

2.1 Material Specification

2.1.1 Chemical Composition

Different suppliers provide high-strength steels for Liberty Spring Inc. Their products should have the range of chemical composition presented in Table 2.1. These high-strength steels have a comparable range of chemical composition with two technical standards that are ASTM standard (A1000 Grade A) and SAE standard (Grade 9254); (ASTM, 2014); (SAE, 2015).

Table 2.1 Require range of chemical composition according to Liberty Spring Inc. proprietary standard.

Composition (wt. %)						
C	Si	Mn	P max	S max	Cr	V
0.5 to 0.7	1.2 to 1.65	0.5 to 0.9	0.025	0.025	0.5 to 1	0.05 to 0.25

2.1.2 Specimens Geometry and Specifications

In the present work, specimens were provided with two geometries coil spring and straight shank. One supplier provided the high-strength steels for the coil springs. These specimens had rectangular cross-section and coils had five rings (Figure 2.1). Coil springs were double shot peened at inner and outer sides by Liberty Spring Inc. The same shot size was used for the first peening and second peening. Peening intensity and balls hardness have been presented in Table 2.2.

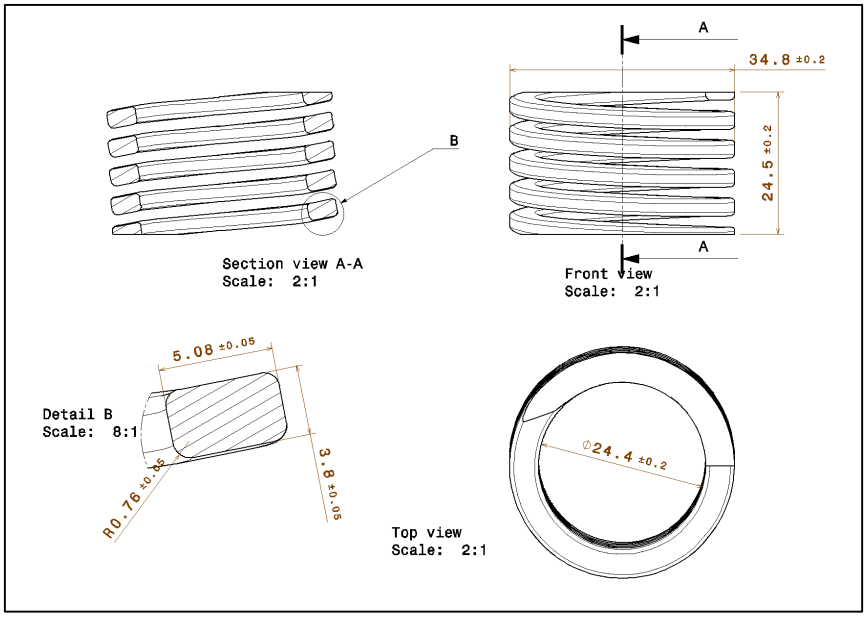

Figure 2.1 Shows the geometry of the coil specimen and the dimensions. All the dimensions are in millimeters.

Table 2.2 Double shot peening conditions according to Liberty Spring Inc. specification.

First peening intensity	Speed: 56 m/sec, for 20 minutes
Second peening intensity	Speed: 30 m/sec for 10 minutes
Balls hardness (HV)	610-670

Straight shank specimens were provided in eight different surface integrity conditions (Table 2.3). The high-strength steels for these specimens were provided by two suppliers, which named as a 'supplier A' and 'supplier B' in the present study. Figure 2.2 shows the geometry and dimensions of the straight shank specimens.

Table 2.3 Presents different conditions of the straight shank specimens.

Condition	Supplier	Stress relieving method	Surface condition
0	A	Inline	Mechanical polishing[1]
1	A	Batch	Mechanical polishing
2	B	Inline	Mechanical polishing
3	A	Batch	Superfinished [2]
4	A	Inline	Superfinished
5	B	Inline	Superfinished
6	A	Inline	Shotpeened
7	A	Inline	Shotpeened+Superfinished

[1] Mechanical polishing removes the surface defects and layers of residual stress.
[2] Superfinishing is a type of chemical polishing that is used by Liberty Spring Inc.

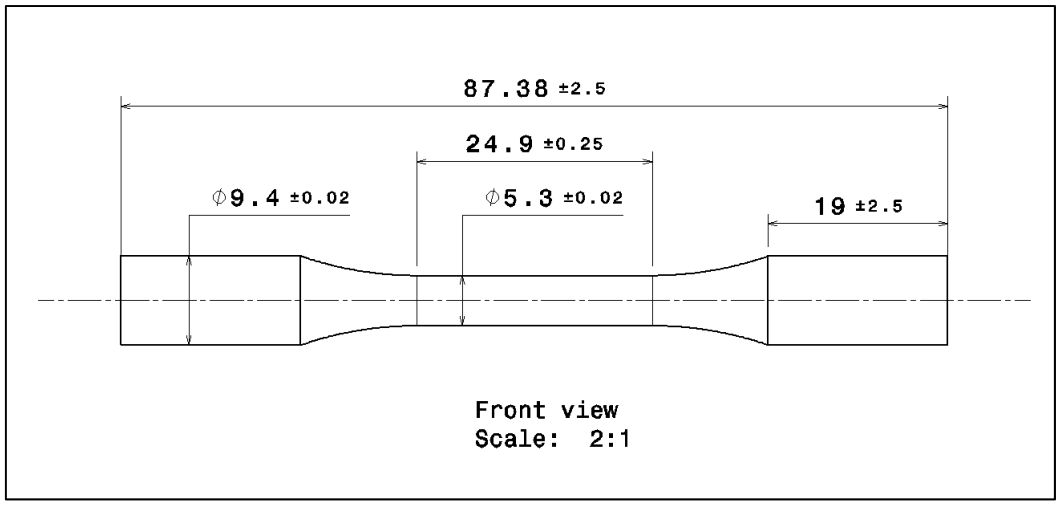

Figure 2.2 Specimen design for machining the straight shank specimens, all dimension are in millimeters.

Specimens in the early three conditions (conditions 0, 1, and 2) were mechanically polished after machining. In the mechanical polishing method, specimens do not have surface defects and residual stress. Therefore, fatigue life was studied for the base materials of two suppliers and two stress relieving methods (batch and inline).

Following three conditions (conditions 3, 4, and 5) were chemically polished after machining. Fatigue behaviors were studied in these conditions, and they were compared with the obtained results in mechanical polishing conditions.

Fatigue life developments after shot peening were studied in conditions 6 and 7. Specimens in these two conditions were provided by one supplier, and they were stress relieved with the inline method. In condition 6, specimens were only shot peened and in condition 7 they were shot peened and chemically polished. Fatigue results in these two conditions were compared with conditions 0 and 4. Specimens

2.2 Fatigue Conditions

2.2.1 Strain-Controlled Condition

Strain-controlled cyclic loading is the real working condition of coil springs in an automotive engine system in which coils undergo to the same amount of applied strain each time the engine turned on. If the global material properties of the steel changes when undergoing fatigue, the applied stress to the coils will not be constant and increase or decrease depending on the dynamic response of the material. Applied stress will increase if materials get harden resulted in lower fatigue life in the coils and will decrease in case of material softening leading to higher fatigue life. Figure 2.3 shows stress changes during strain-controlled cyclic loading condition in case of (a) material hardening and (b) material softening.

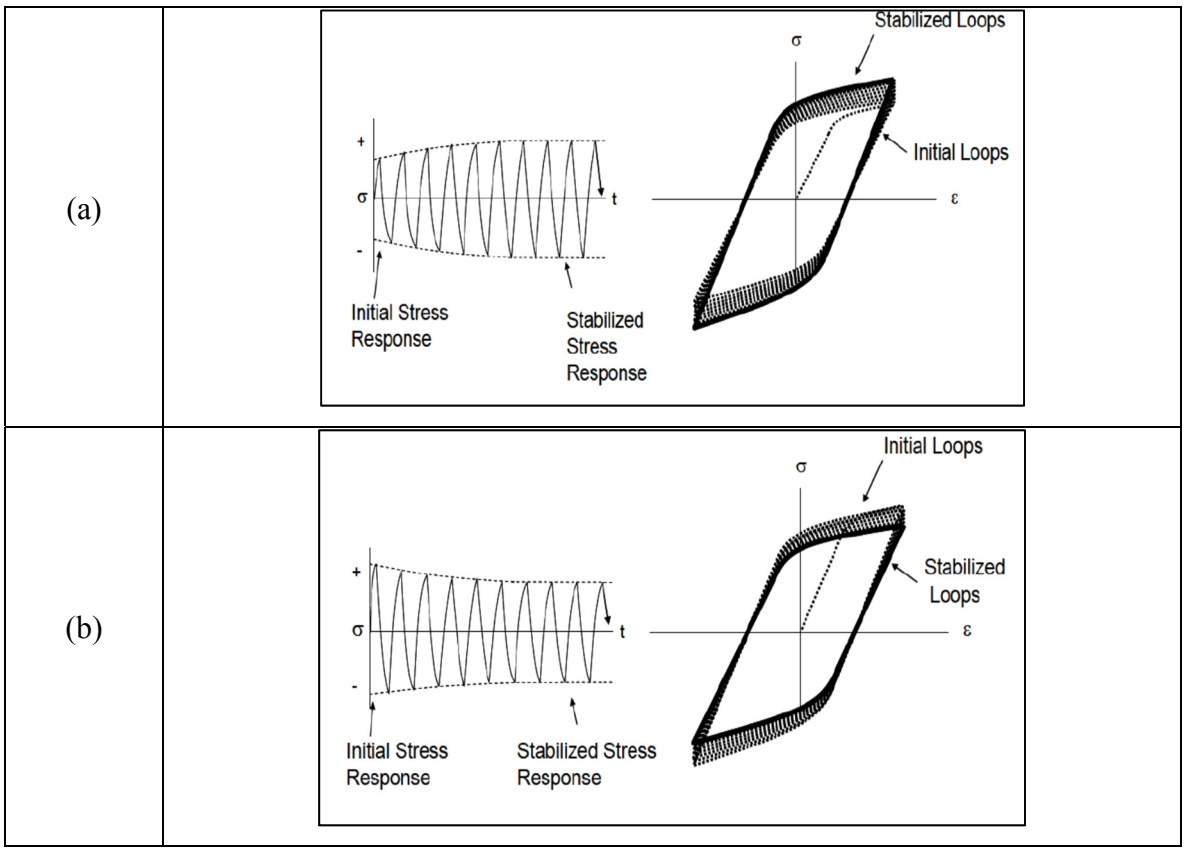

Figure 2.3 Showing the stress changes in strain-controlled cyclic loading in case of (a) material hardening and (b) material softening, figure reported from (Daubenspeck, 2010).

2.2.2 Stress-Controlled Condition

The available equipment at Libert Spring Inc. is a stress controlled equipment, as a consequence, a large number of coil springs tested in similar stress-controlled condition were available. Coils broken reaching different numbers of cycles were selected, some in the range of 10^4 (called here a low number of cycles) other reaching 10^5 (respectively high number of cycles). In the present study, six broken coils were chosen randomly, three coils in each category, and this in order to understand the reason of the fatigue life discrepancy. Fatigue life of the specimens broken at low numbers of cycles are 44552, 49758, and 60758 cycles, and those with high life cycles are 195391, 200319, and 320225 cycles.

Straight shank specimens were fatigue tested by rotating bending (R=-1) method. Rotating bending test has different loading methods such as single-point loading, two-point loading, and four-point loading (ISO, 2010). Four-point loading is the fatigue testing method that was used in the present study. In this method, specimens could have hourglass or straight shank geometries (ASTM, 2015); (ISO, 2010). Straight shank geometry is the preferred geometry as a larger volume of the material is subjected to applied stress (Figure 2.4) (ISO, 2010).

An ‘Instron R.R. Moore’ machine was used for performing the rotating bending fatigue tests in this study. Fatigue tests were performed at 30 Hz frequency and a constant stress level of 1000 MPa, which was the maximum possible stress for fatigue testing with this machine. This stress is close to the maximum applied stress to the coil springs by engine system.

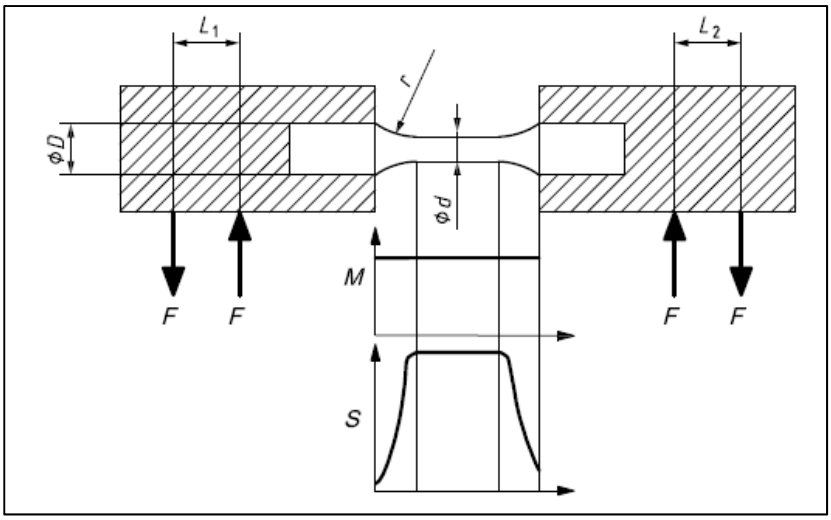

Figure 2.4 The schematic of a four-point loading method of rotating bending test fatigue test that shows the constant stress and moment distributions along the specimen's testing section reported from (ISO, 2010).

2.3 Methods of Material Characterizations

2.3.1 Microhardness Measurement

Automated microhardness tester (PSFilter) from Clemax Inc. was used for the microhardness measurement in Vickers method. Indent in Vickers method has square-based pyramid-shaped (Figure 2.5) (ASTM, 2012). The microhardness values in this method are presented in Vickers hardness (HV) representing the applied force divided by the surface area of the indent impact.

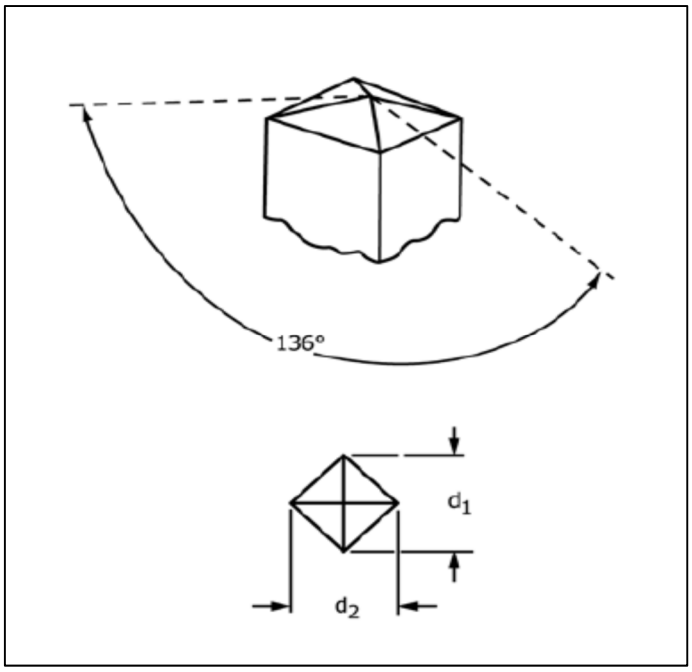

Figure 2.5 Indent shape in Vickers method of microhardness testing, reported from (ASTM, 2012).

Indentation for microhardness measurements of two supplier products was done on a determined pattern with 100 indents (10*10) at the center of the specimen's cross-section. These indentations were performed at low load range (25 gf), which had 8 to 10 microns impact on the surface. Adjacent indents in this pattern had 50 microns interval (Figure 2.6) as the minimum interval in Vickers method is 2.5 dV (Vickers Diagonal) (ASTM, 2012).

Changes in the material properties during fatigue test were studied by microhardness measurements from the surface into depth. These microhardness measurements were done at 10 gf, which had 6 to 7 microns impact on the surface. Indentation at 10 gf allowed to measure the microhardness at the nearest distance from the surface (15 microns) to the depth.

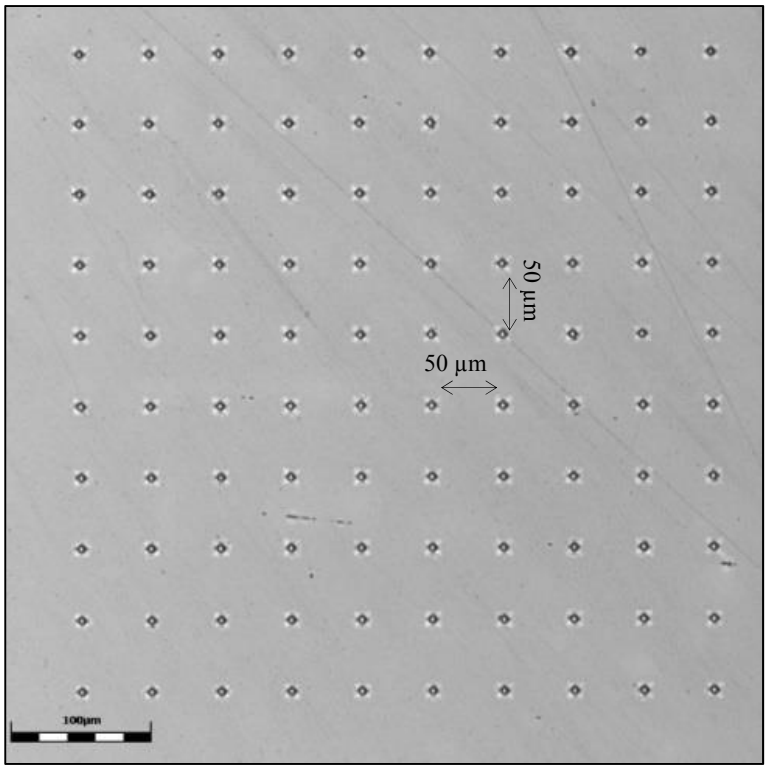

Figure 2.6 Shows a determined pattern for the indentation on specimen's cross-section as such the interval of the adjacent indents.

2.3.2 Surface Roughness Measurement

Two techniques of surface roughness measurement were used in this study, contact and non-contact methods. Surface roughness on the coil spring specimens was measured with contact method, and non-contact method was used for roughness measurements on straight shank specimens.

Surface roughness was measured on the third ring at the inner side of the coil spring specimens (Figure 2.7). As stress gradient during fatigue test is higher on the third ring and shear stress distribution is higher at the inner side. Therefore, surface roughness at the inner side of the third ring is more important than other rings.

Stylus profilometer model, S.J 400 from 'Mitutoyo,' was used for the measurements in contact method. Waviness features of the measured profile were filtered by using 0.8 mm cut-off length (λc=0.8mm), which was the largest cut-off length that could be used for coil springs. It has suggested using a large cut-off length to add more surface features into the measured profile (Chang, Hirvonen and Grönqvist, 2004). Each roughness measurement was repeated three times to ensure the repeatability of the results.

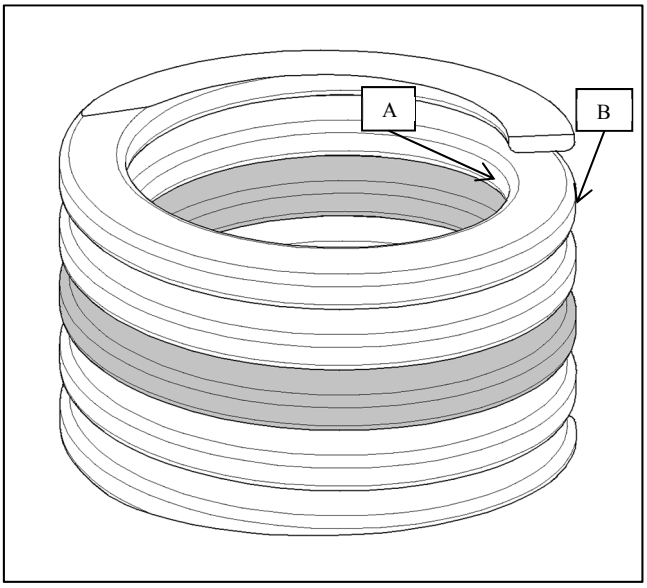

Figure 2.7 Shows the inner side (A) and outer side (B) in coil spring specimens and the third ring (the most stressed ring).

Surface roughness for the straight shank specimens was measured along the longitudinal axis with the non-contact method by using Laser confocal microscope from 'Olympus.' The same cut-off length with the contact method (λc=0.8mm) was used for the roughness measurements on straight shank specimens. Measurements in this method repeated three times to ensure the repeatability of the results.

2.3.3 Residual Stress Measurement

X-ray diffraction (XRD) is the non-destructive technique of residual stress measurement that was used in the present study. However, $Sin^2 \Psi$ is a well-known method for residual stress measurement in XRD technique, but in the present study, residual stress measurements were done with Cos α method. 'Cos α' is an alternative method uses by industries for calculating residual stress (Wang and al., 2015). In this method, the X-ray beam is radiated to a specimen's surface, and its diffraction forms a cone. The image of this cone on the image plate is in the form of a ring (Debye ring) as shown in Figure 2.8.

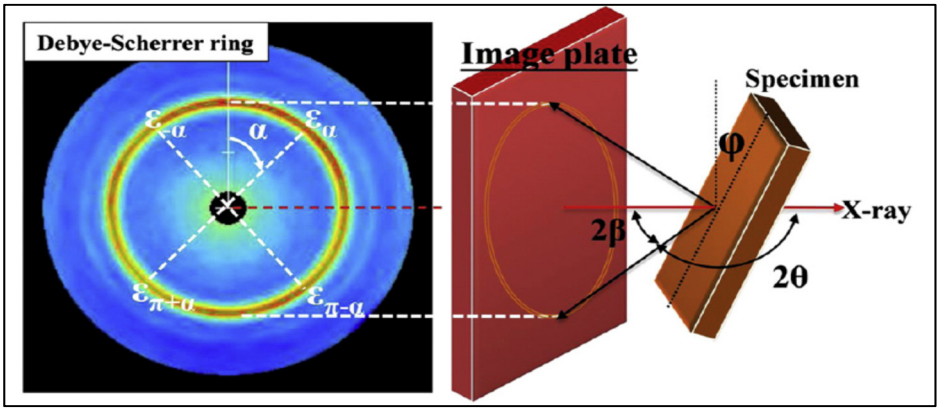

Figure 2.8 Schematic of the specimen, the position of the image plate, and Debye ring in Cos α method of residual stress measurement, the figure reported from (Wang and al., 2015).

In Figure 2.8, β is Bragg angle, φ is incidence angle of the X-ray beam, and α is surrounding angle of the Debye ring varies between 0 to 90º. In each α angle, the strain is considered in four points presenting as a ε_{α}, $\varepsilon_{-\alpha}$, $\varepsilon_{\alpha+\pi}$, $\varepsilon_{\alpha-\pi}$ (Figure 2.8). Equation (2-1) presents a new parameter (ε_a) from these four strains. Stress σ_x is the slope in the relation between ε_a versus cos α according to the Equation (2-2) (Wang and al., 2015).

$$\varepsilon_a = \frac{1}{2}\left((\varepsilon_{\alpha} - \varepsilon_{\pi+\alpha}) + (\varepsilon_{-\alpha} - \varepsilon_{\pi-\alpha})\right) \qquad (2\text{-}1)$$

$$\sigma_x = -\left(\frac{E}{1+\vartheta}\right)\frac{1}{sin2\beta}\frac{1}{sin2\varphi}\left(\frac{\partial \varepsilon a}{\partial cos\alpha}\right) \quad (2\text{-}2)$$

XRD technique gives peak profiles that are useful for obtaining different information about the material. For instance, measurements of the full-width at half-maximum (FWHM) indicates various information about the grain distortion, dislocation density, and residual stresses. FWHM in low alloy steels decreased in case of cyclic softening (Quesnel, Meshii and Cohen, 1978).

'μ-X360' X-ray residual stress analyzer from Pulstec Industrial Co. were used for the residual stress measurements in this study (Figure 2.9). The following parameters were used for measuring the lattice space in the family of planes {211}. CrKα radiation tube with 2.291 Angstroms wavelength, 30kV power, 1mA current, 1 mm aperture size, 30 s exposure time, 156.4º Bragg angle, and 38 mm focal distance.

Figure 2.9 Shows 'μ-X360' residual stress analyzer from Pulstec Industrial Co., as such presenting the X-ray apparatus and specimen, figure reported from (Puls-Tech, 2016).

Residual stress of the coil spring and straight shank specimens were measured at the surface and in depth. These measurements were in two directions, axial and hoop. Each measurement was repeated three times to ensure the repeatability of the results. Material removal for the

residual stress measurements in depth was carried out by using electropolishing technique. Used solution for high-strength steels was salt-water with 30% concentration and applied voltage was 50 V.

2.3.4 Microstructural Characterization

The microstructure of high-strength steels was characterized at high and low magnifications. These microstructural characterizations were done at the center of the specimen's cross-sections. Laser confocal microscope from Olympus was used for the characterizations at low magnification. Scanning Electron Microscope (SEM) models SU70 and SU8230 from 'Hitachi' performed the material characterizations at high magnifications.

Surface preparations were done according to the ASTM standard E3 (ASTM, 2007) for material characterizations at low and high magnifications. Since high-strength steels in this study are oxidized very fast, thus after each step of grinding and polishing surface was cleaned with Ethanol and dried and high-pressure air. Surface polishing was continued up to 1-micron solution, and they were etched in Nital 3% for 6 s.

2.3.5 Fractography of Fracture Surface

Fracture surfaces of the coil spring and straight shank specimens were characterized in two scales, macro and micro. Macro scale characterizations of the fracture surfaces were done by using Binocular stereomicroscope from AMscope. Microscale observations of the fracture surfaces were performed by using Scanning Electron Microscope (SEM) model S3600M from 'Hitachi.' Fracture surfaces before fractography were cleaned and contaminations were removed by immersing the fracture surface in Ethanol and holding for 10 minutes in ultrasonic cleaner model FS110D from 'Fisher Scientific.'

CHAPTER 3

RESULTS AND DISCUSSIONS

This chapter will present the results of the material characterizations and fatigue testing for the coil spring and straight shank specimens. The material characterizations for the coil specimens with the highest and the lowest numbers of cycles showed the reasons that may be behind the fatigue life discrepancy in coil springs. Moreover, the characterization results for the straight shank specimens before and after rotating bending fatigue test show the effect of different surface integrity conditions. The failure reason after shot peening is different from the one obtained on the base materials.

3.1 Investigation of Fatigue Life Discrepancy in Coil Springs

3.1.1 Fractography in Macroscale

Initial observation of the broken coil specimens shows that all the failures have initiated at the third ring of the coil, as stress gradient is higher at this ring. Optical observations of the fracture surfaces in macro scale show that all the rings have failed from the inner side (Figure 3.1) as shear stress distribution during fatigue test is higher at the inner side of the ring than the outer side (Prawoto and al., 2008).

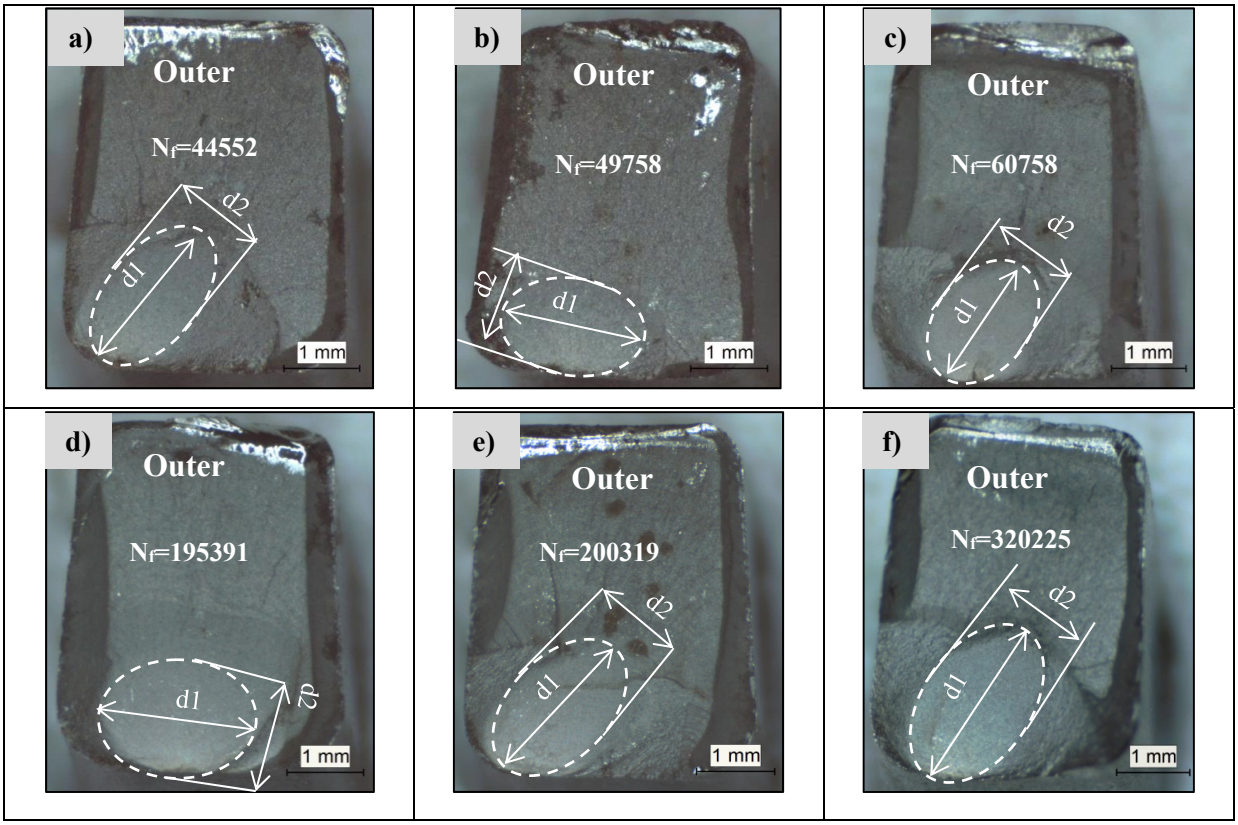

Figure 3.1 Images of the fracture surface in low magnifications for the specimens with low life cycles. (a), (b), (c) and high life cycles specimens (d), (e), (f). Failure happened on the inner side of the ring indicated. Dash ellipses show the propagations area at the fracture surface, big diameter (d1) and small diameter (d2).

3.1.2 Propagation Ellipse Measurement

The propagation ellipses are shown by white dash ellipses on the fracture surface in Figure 3.1, and the results of diameters measurements and ellipse area have been presented in Figure 3.2 (a) and (b) respectively. These measurements show that the size of the propagation ellipses does not have a constant trend. It means that the propagation ellipses have the lower size for the second specimen with low life cycle and the third specimen broken at the high life cycle.

These propagation ellipses will show the fracture toughness of the material (K_c) if fatigue test performs at a constant level (Dao and Sellami, 2012). Propagation ellipse measurements do not conclude much difference between low life cycle and high life cycle coils as the size of the propagation areas are not significantly different in low life and high life coils. The more information on the procedure of the propagation ellipse measurements is detailed in APPENDIX I.

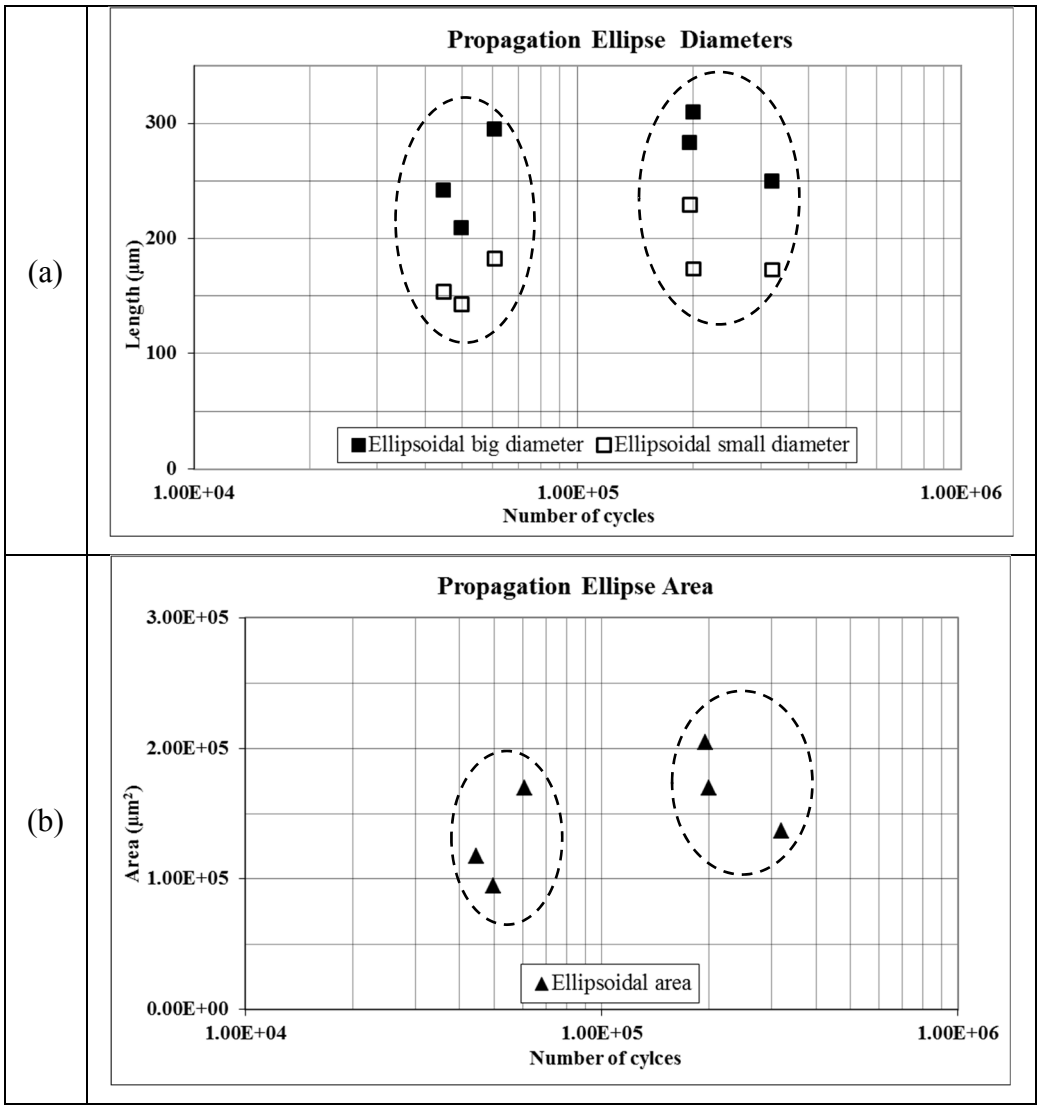

Figure 3.2 Showing the measurements of propagation ellipse for the coil specimens with different numbers of cycles, (a) ellipses diameters and (b) ellipses area.

3.1.3 Fractography in Microscale

Fractographies of coil springs at high magnification shows the crack initiation sites (white dash circles in Figure 3.3). This figure shows that coil specimens have crack initiations from the surface and subsurface. Crack initiation in the coil specimen with the lowest numbers of cycles (N_f=44552) is 100 microns below the surface (subsurface) (Figure 3.3 (a)). The other specimens with low life cycle (N_f=49758 and N_f=60758), have multiple crack initiations from the surface (Figure 3.3 (b) and (c)). Multiple crack initiation represents a high-stress level during the fatigue test (Torres and Voorwald, 2002).

Coil specimens with high life cycles have crack initiation from the surface. The broken coils at 195391 and 320225 numbers of cycles (Figure 3.3 (d) and (f)) have the crack initiation approximately 30 microns below the surface (almost surface). Crack initiation for the other high life cycle specimen that has Nf= 200319 is from the surface (Figure 3.3 (e)).

It was expected to have crack initiation from deeper layers, equal or more than 100 microns below the surface (subsurface) after double shot peening (where there is no compressive residual stress in the material (Uematsu and al., 2013)). Therefore, surface defects induced by shot peening process could be a reason of the crack initiation from the surface for those coils specimens at high and low life cycles.

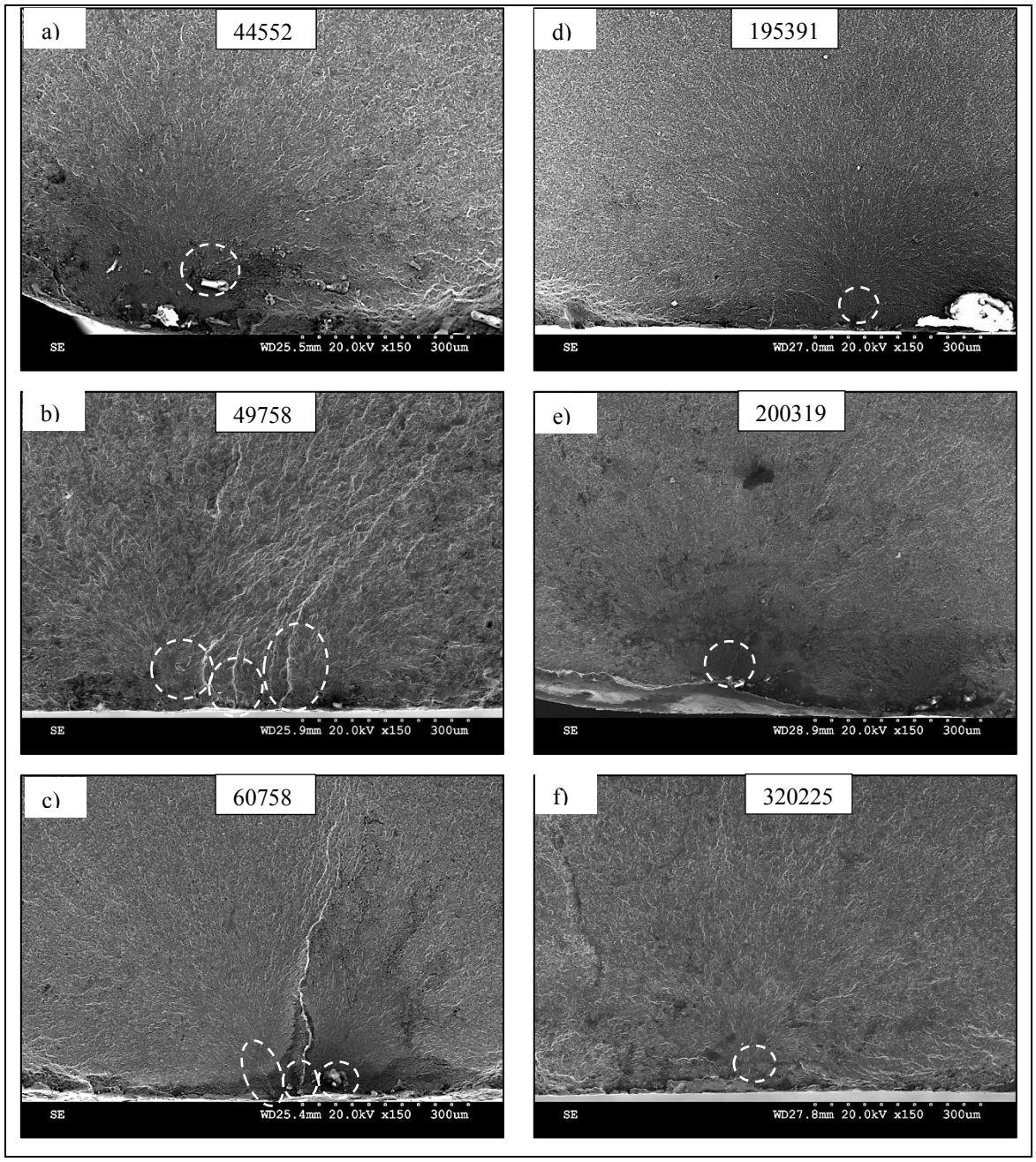

Figure 3.3 SEM images of fracture surfaces in micro scale for the broken coil specimens (a, b, c, d, e, and f), white dash circles are showing the crack initiations in coil specimens.

3.1.4 Surface Roughness Measurement

Five surface roughness parameters of the broken coil specimens in different numbers of cycles have been compared in Figure 3.4. These roughness parameters that have compared are:

- Rp: maximum height of peaks (μm);
- Rv: maximum depth of valleys (μm);
- Rz: ten-point height (μm);
- Rt: maximum height of profile (μm);
- Ra: arithmetic average height (μm).

Figure 3.4 presents five roughness parameters in logarithmic scale for coil specimens in high life cycles and low life cycles. These roughness measurements show that high fatigue life springs mostly have better surface roughness than low fatigue life springs. However, the surface roughness for the coil broken at the highest numbers of cycle (320225) is not as good as the coil broken after 200319 numbers of cycles. Moreover, the low life cycle specimens have an almost similar roughness values.

These measurements showed that although applied double shot peening was similar for these coil specimens, induced surface defects were not similar. Surface defects are bigger in low life cycle coils and less in high life cycle specimens. On the other hand, the difference of induced surface defects is not explaining the fatigue life discrepancy as the coil broken at 60758 numbers of cycles (low fatigue life) has an almost similar roughness value with the coil failed after 195391 numbers of cycles (high fatigue life) suggesting that other parameters play a significant role in fatigue performance.

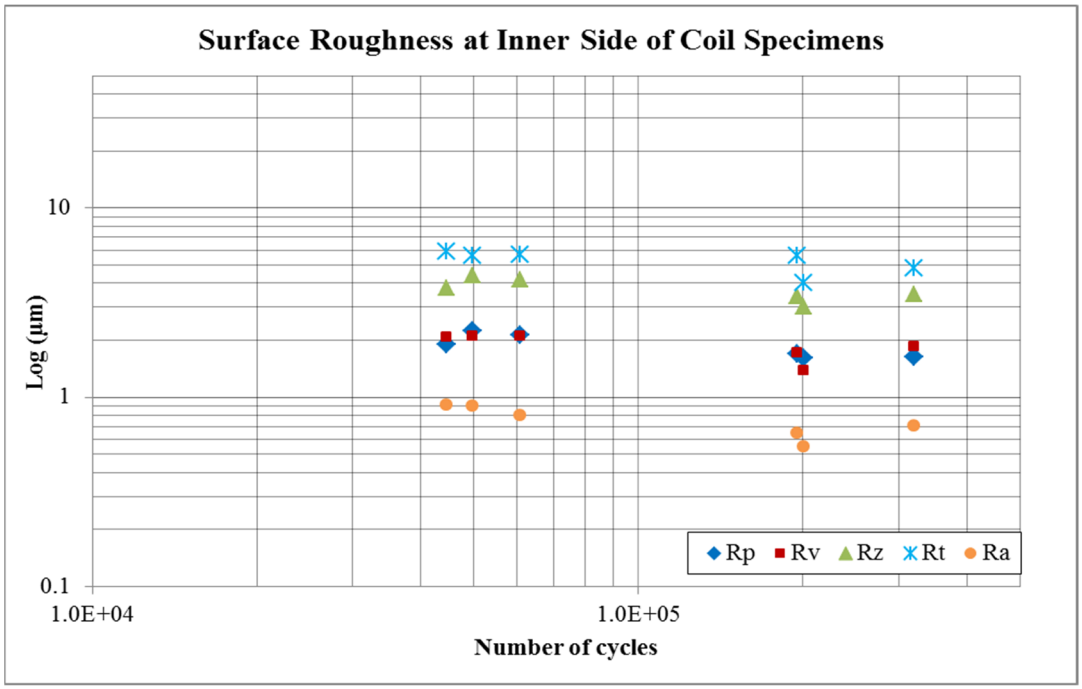

Figure 3.4 Surface roughness comparison for coil specimens in logarithmic scale.

3.1.5 Optical Characterization of Surface Defects

Optical characterizations of surface defects induced by double shot peening process are shown in Figure 3.5. Optical images in this figure were taken from the inner side of the ring where roughness was measured. These characterizations show that many surface defects induced by double shot peening process at the inner side and they have are big sizes. Optical characterizations of these peening defects are showing that they are similar to the specimens with high life cycles (Figure 3.5 (d) to (f)) and low life cycles (Figure 3.5 (a) to (c)). However, Figure 3.4 showed that peening defects are less in high fatigue life specimens. Corrosion marks (Figure 3.5 (d)) have been generated after fatigue test.

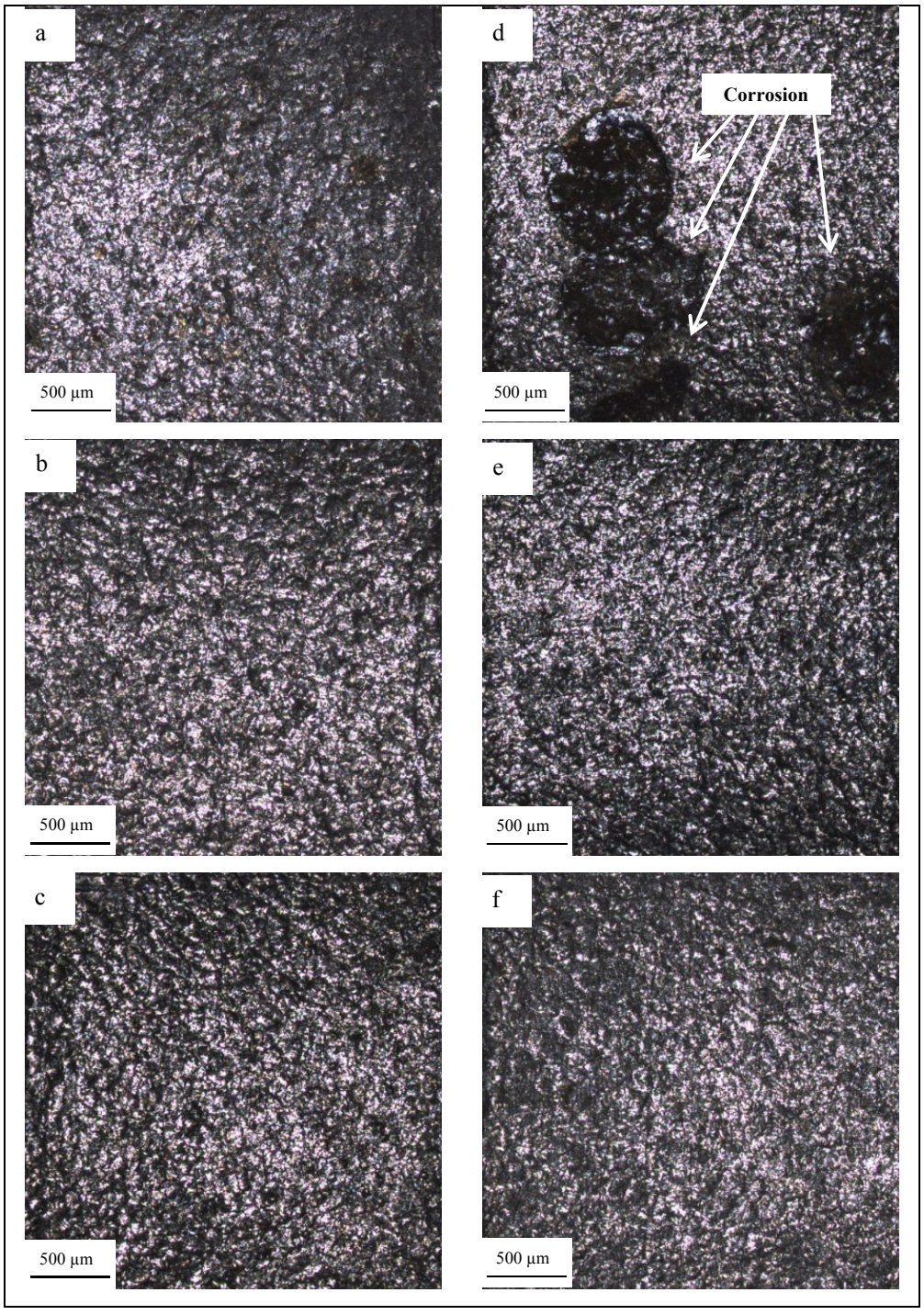

Figure 3.5 Peening defects induced by double shot peening for the broken coil specimens at Nf= 44552 (a), Nf=49758 (b), Nf=60758 (c), Nf=195391 (d), Nf=200319 (e), and Nf=320225 (f).

3.1.6 Residual Stress Measurement

Surface residual stresses were measured on the third ring for three set of coil specimens (one that was not fatigue tested, one broken at the lowest numbers of cycles (4.E+04), and one broken at the highest numbers of cycles (3.E+05)). Results of these measurements in axial and hoop directions have presented in Figure 3.6. These measurements show that the coil broken at the lowest numbers of cycles has the lowest residual stress values in axial and hoop directions. It means this specimen had more stress relaxation. The highest fatigue life specimen has undergone stress relaxation too but in the axial direction but to a similar extend. Surface residual stress measurements show that the lowest fatigue life specimen has more stress relaxation than the highest fatigue life specimen does, suggesting a different material behavior.

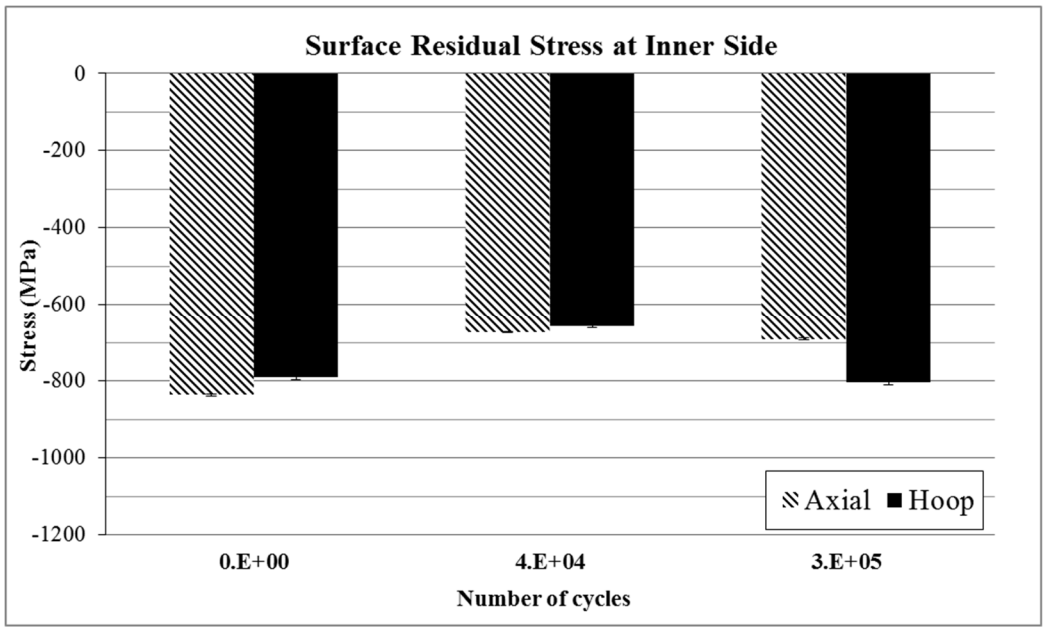

Figure 3.6 The residual stress measurements on the third ring at the surface of the coil specimens show the residual stress before fatigue test (0E+00), for the coil broken at the lowest numbers of cycles (4E+04), and the highest one (3E+05).

Figure 3.7 shows the uncorrected residual stress profiles at two directions in depth for the coil that was not fatigue tested, the coil broken at the lowest numbers of cycles, and the one failed at the highest numbers of cycles. Figure 3.7 (a) presents residual stress profile in axial direction and Figure 3.7 (b) is for the residual stress measurements in hoop direction. The maximum depth of compressive residual stress in both directions is almost 50 microns after manufacturing, but it becomes 80 microns for the lowest fatigue life specimen and 50 microns for the highest fatigue life one. In deeper layers, residual stress profiles become similar for the coil that was not fatigue tested and the one broken at the highest numbers of cycles. This is most likely due to some stress redistribution induced by stress relaxation during fatigue tests.

In axial direction both fatigued specimens display stress relaxations., Again, these are more significant for the coil with the lowest fatigue life and less for the highest fatigue life specimen. In hoop direction, only the low fatigue life specimen shows significant stress relaxation and the high fatigue life specimen has almost similar profile with no fatigue-tested specimen. The coil broken at the lowest numbers of cycles has different residual stress profile compared to the other two specimens. Compressive residual stress in this specimen was continued up to 200 microns in depth for both axial and hoop directions.

Residual stress profiles show important differences between high and low life cycle specimens meaning that for the same shot peening condition residual stress profiles are not the same. Furthermore, it is expected to have higher fatigue life for the specimen that has more depth of compressive residual stress as micro cracks stay for a longer time at compressed layers (Guagliano and Vergani, 2004); (Song and Wen, 1999) however, it was different in these coil specimens.

(a)

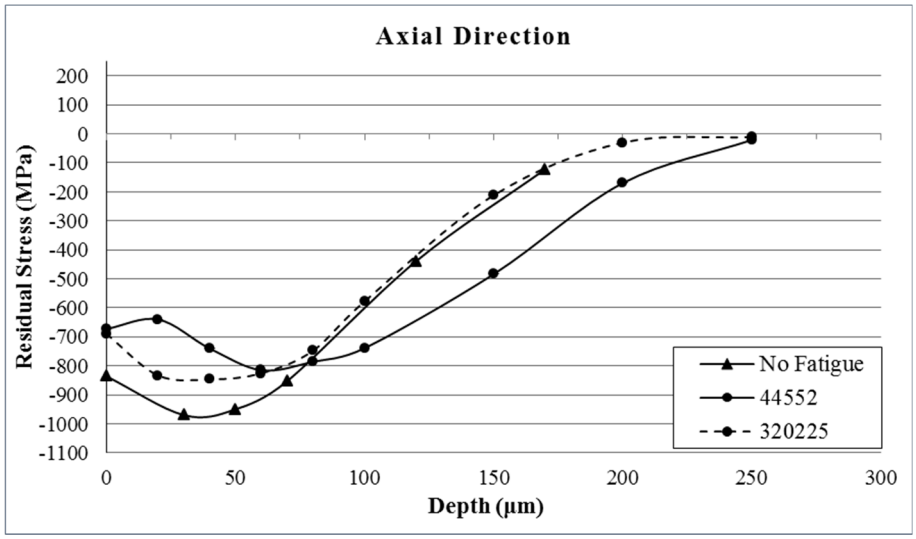

(b)

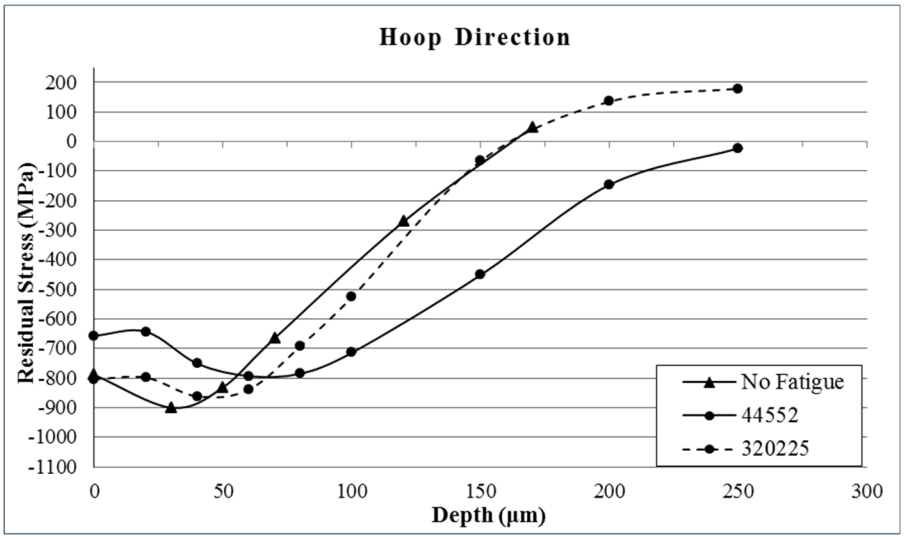

Figure 3.7 Residual stress distributions in depth for the specimens that was not fatigue tested, the coil broken at the lowest numbers of cycles, and the one broken at the highest numbers of cycles, in two directions (a) axial (b) hoop (error with cos α method are lower than ±10 MPa and they are not observable).

3.1.7 Microhardness Measurement

Microhardness measurements were done for the coil specimens that was not fatigue tested, the ones with the highest and the lowest numbers of cycles. These measurements were done on the inner side of the rings, close to the surface into the depth. These regions were more affected during fatigue test regarding the shear stress distribution in coil springs as discussed in chapter 1. Results of these microhardness measurements are presented in Figure 3.8 (a), (b), and (c). The lowest fatigue life specimen has higher microhardness value compare to no fatigue tested at the first 100 microns. The first 50 microns are showing dispersion in the results, which are most likely due to the residual stress redistribution at this region. In deeper layers, lower microhardness values can be seen in low life cycle specimen than the other one. However, compressive residual stress extends up to 200 microns in low life cycle specimen, and higher microhardness values were expected in these layers.

When microhardness profile of high life cycle specimen compared with no fatigue tested specimen (Figure 3.8 (b)), it can be seen that both specimens have relatively low microhardness values at the first 70 microns than deeper layers and no dispersions are found in the affected region by compressive stress (around 50 microns from the surface). Microhardness values in both specimens drop around 200 microns in depth suggesting the region where tension stress has found in residual stress profiles of the material.

In Figure 3.8 (c), the microhardness profiles for low life cycle and high life cycle coils have compared. Low life cycle specimen has relatively high microhardness values particularly at the first 100 microns below the surface suggesting the material hardening during fatigue test in this specimen however, 80 microns from the surface has affected by compressive residual stress in low life cycle specimen and 50 microns in high life cycle. After 150 microns, relatively lower microhardness values are observed in low life cycle specimen compare to high life cycle specimens suggesting different material properties in these two specimens.

(a)

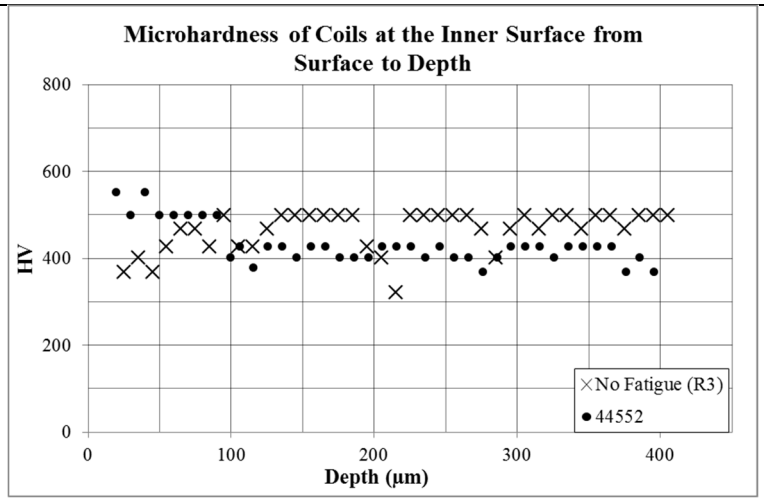

(b)

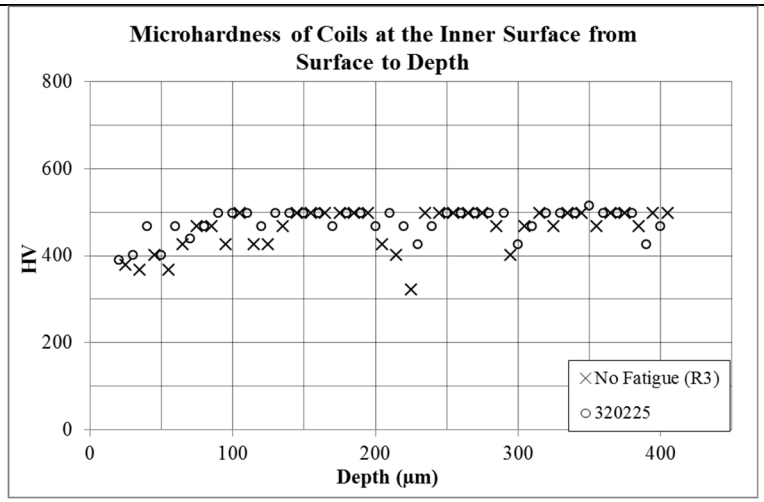

(c)

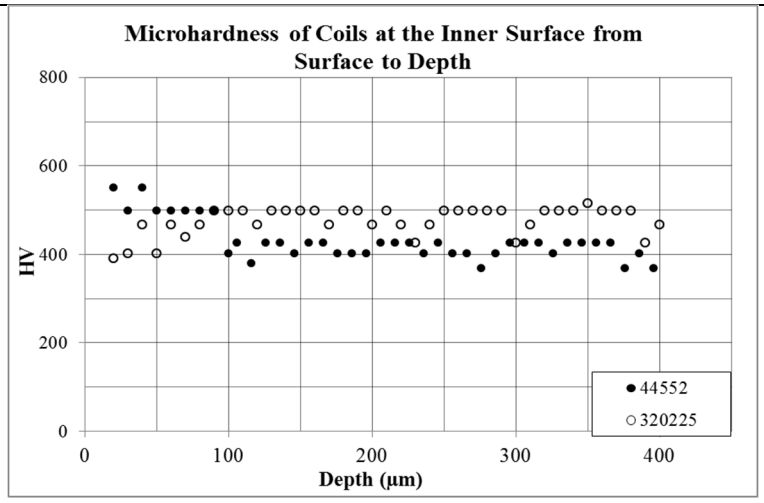

Figure 3.8 Microhardness profiles in depth at the third ring for (a) no fatigue tested coil and the one broken at the lowest life cycles, (b) no fatigue tested coil and the one broken at the highest numbers of cycles, and (c) the highest and the lowest fatigue life specimens.

3.1.8 Microstructural Characterization

The coil broken at the lowest numbers of cycles have different microhardness profile in depth showing lower values compared to the highest numbers of cycles. These coil specimens have bainitic-martensitic structures as seen in Figure 3.9. Bainitic structures are the dark regions that are shown by white arrows. The size of bainite in the coil with the highest numbers of cycles is bigger than the lowest numbers of cycles.

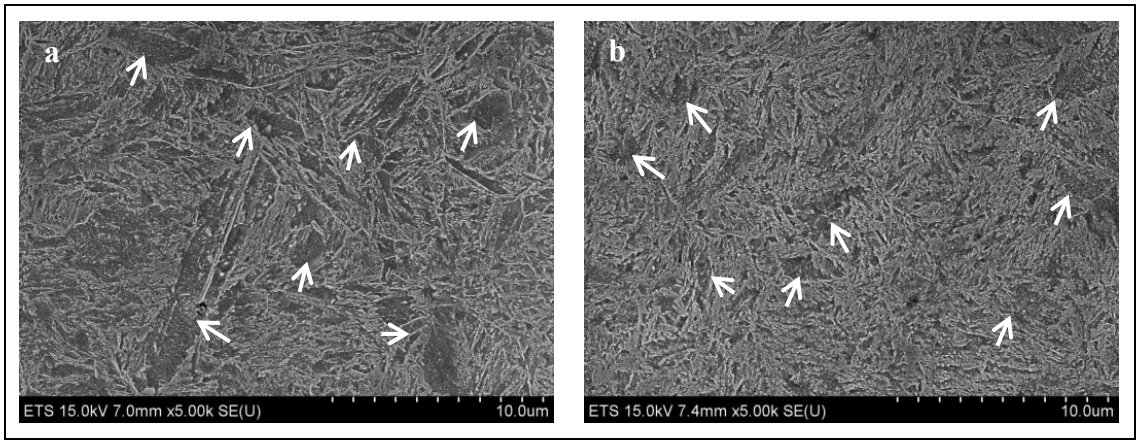

Figure 3.9 Microstructural characterizations of coil specimens broken at (a) the highest numbers of cycles and (b) the lowest numbers of cycles. Both microstructures have bainitic-martensitic structures. Bainite (white arrows) has bigger size in the coil broken at the highest numbers of cycles.

Figure 3.9 (a) shows that the coil broken at the highest numbers of cycles has big size of bainitic structures while they are smaller in the coil broken at the lowest numbers of cycles (Figure 3.9 (b)). Consequently, the coil with highest fatigue life has a big plate of bainite, and it has less martensite than the other one. Better fatigue behavior of the bainitic-martensitic steels has reported by Serbino and Tschiptschin (2014) as discussed earlier in chapter 1.

3.2 Fatigue Life Studies in Different Surface Integrity Conditions

The straight shank specimens were provided in eight different surface integrity conditions (Table 3.1). Fatigue life was compared to these conditions at the constant testing stress of 1000 MPa. These straight shank specimens were characterized before fatigue test in terms of microhardness, microstructure, surface roughness, and layers that affected by compressive residual stress. Results of these characterizations before fatigue test are presented in subsection 3.2.1. The fatigue testing results are presented in subsection 3.2.2. The following subsection (3.2.3) presents the results of the fractography of the fracture surfaces, stress relaxation during fatigue test, comparison of the dislocation density before and after fatigue test, and material softening.

Table 3.1 Different conditions of straight shank specimens and numbers of specimens for fatigue test in each condition

Condition Number	Supplier	Stress Relieving	Surface Condition	Number of Specimens for Fatigue Test
0	A	Inline	Machining + Mechanical Polishing (Base Material)	3
1	A	Batch		2
2	B	Inline		2
3	A	Batch	Machining + Chemical Polishing	2
4	A	Inline		3
5	B	Inline		2
6	A	Inline	Machining + Shot peening	3
7	A	Inline	Machining + Shot peening + Superfinishing	3

3.2.1 Characterizations before Fatigue Test

3.2.1.1 Microhardness Measurement

Microhardness distributions of the steels that were provided by 'supplier A' were compared after inline and batch methods of stress relieving (Figure 3.10). These measurements show that after both methods of stress relieving, steels have similar microhardness distributions.

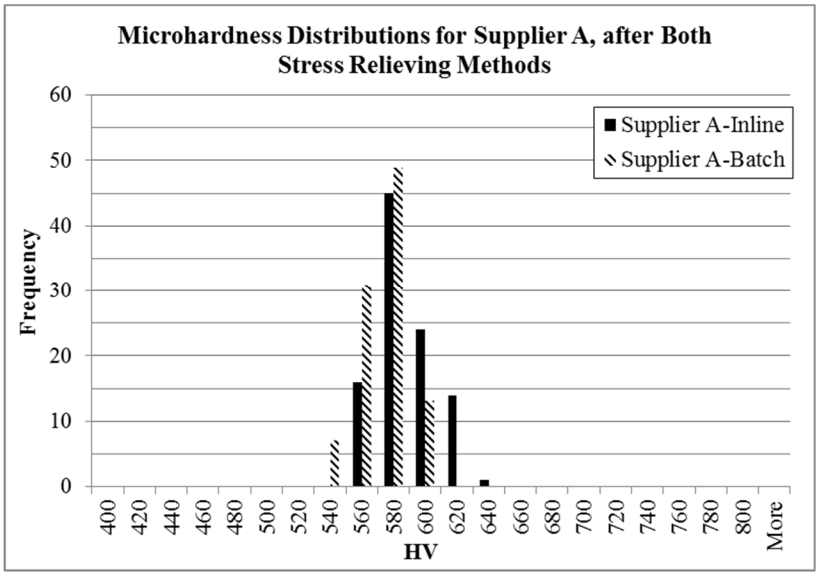

Figure 3.10 Showing the microhardness distributions of supplier A products after stress relieving with batch and inline methods.

The microhardness was measured for the suppliers 'A' and 'B' products after stress relieving with inline method. Figure 3.11 presents the microhardness distributions of these two suppliers. This figure shows that 'supplier B' products have higher microhardness distribution than 'supplier A' after the same method of stress relieving suggesting that more martensite is presented in the microstructure of the steels provided by supplier 'A.'

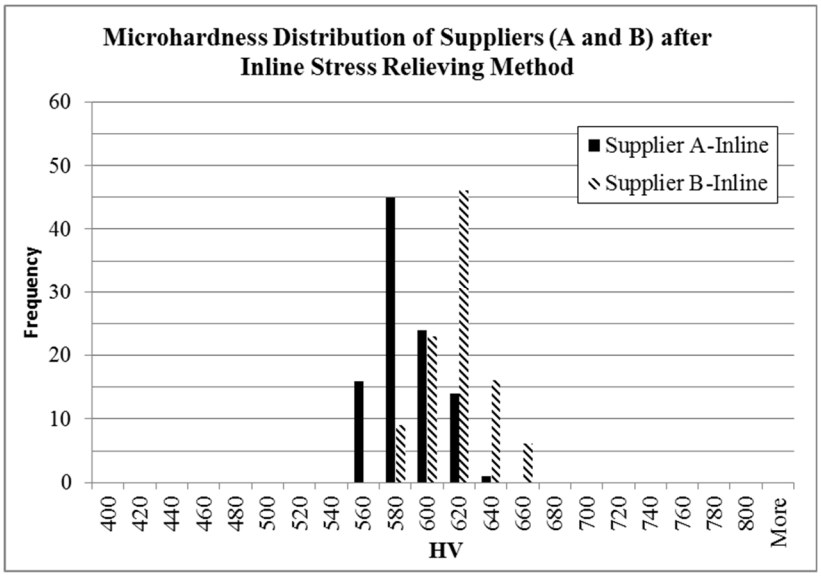

Figure 3.11 Showing the microhardness distributions of suppliers 'A' and 'B' after stress relieving with inline method.

3.2.1.2 Microstructural Characterization

Microstructural characterizations for 'supplier A' products after inline and batch methods of stress relieving show almost similar microstructures (Figure 3.12 (a) and (b)). Both microstructures are bainitic-martensitic, and white arrows in Figure 3.12 are showing some of the bainitic structures. Bainitic structures in both stress-relieving methods have same size and distributions.

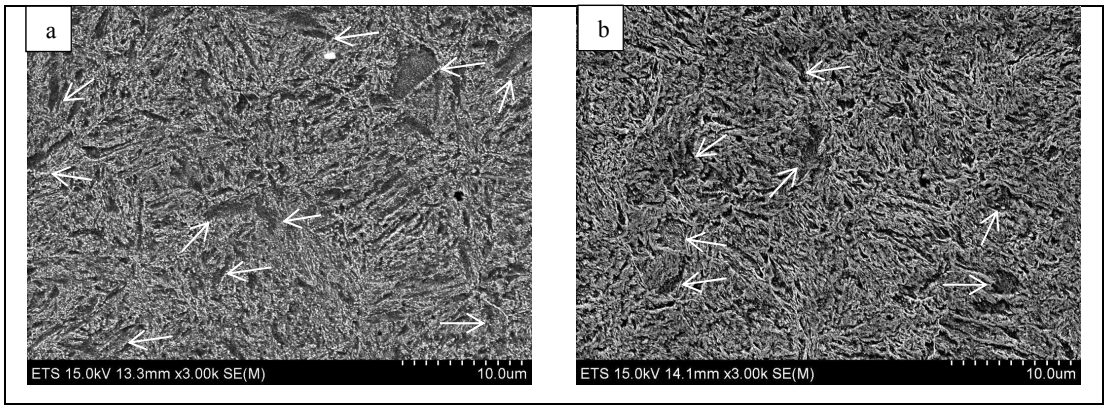

Figure 3.12 Microstructural characterizations of 'supplier A' products after stress relieving with (a) Inline and (b) Batch method. Microstructures look similar after both methods of stress relieving.

Microstructural characterizations of ‘suppliers A and B’ products after stress relieving with inline method show bainitic-martensitic structures, which are smaller in the microstructure of the supplier ‘B’ products (Figure 3.13 (a) and (b)). White arrows in Figure 3.13 are showing some of the bainitic structures.

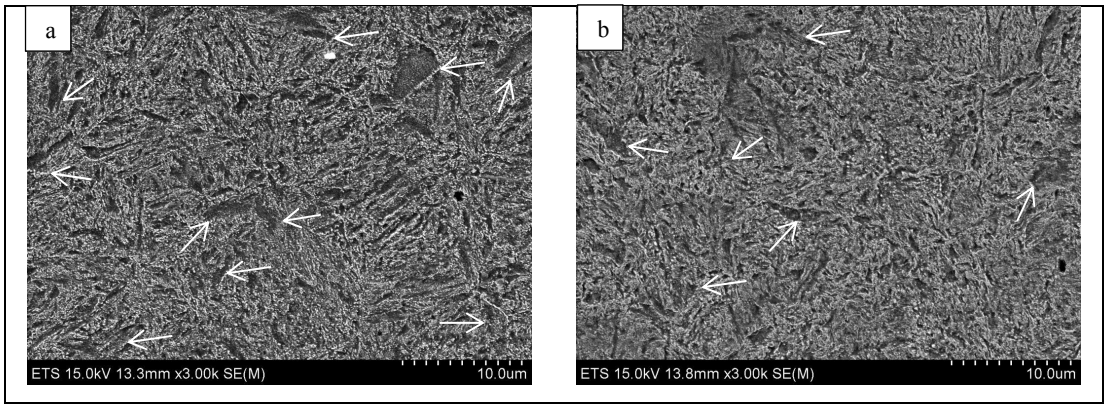

Figure 3.13 Microstructural characterizations of (a) ‘supplier A’ and (b) ‘Supplier B’ products after stress relieving with Inline method. Bainitic structures have shown by white arrows.

3.2.1.3 Surface Roughness

Surface roughness of the straight shank specimens was characterized regarding their roughness values and optical inspection of surface defects. Figure 3.14 shows the comparison in logarithmic scale of five roughness parameters (Rp, Rv, Rz, Rt, and Ra).

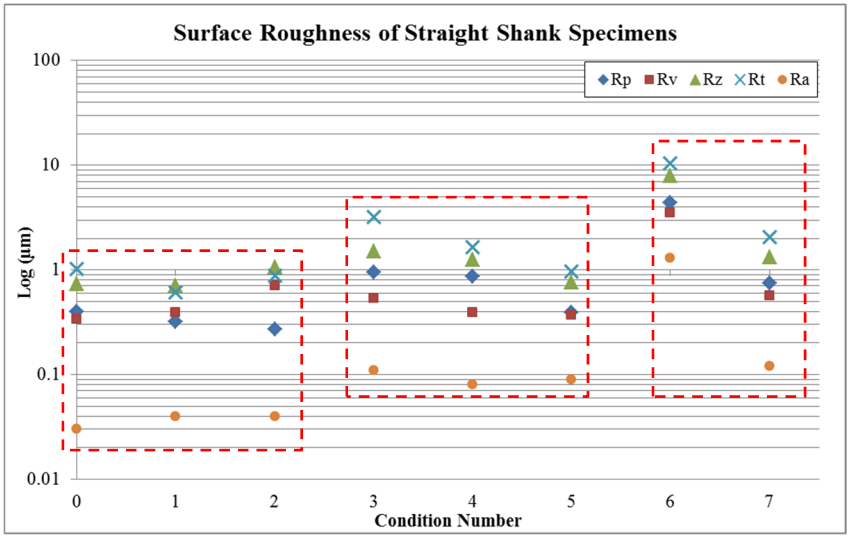

Figure 3.14 Surface roughness values in logarithmic scale for different conditions of straight shank specimens (Table 3.1).

Each surface condition in Figure 3.14 is shown by dash boxes. The first box on the left shows the specimens that were mechanically polished (conditions 0, 1, and 2). Specimens in these conditions have the lowest roughness values compare to other conditions. The box in the middle displays the specimens after chemical polishing (conditions 3, 4, and 5). Roughness values are higher for the specimens after chemical polishing than the mechanically polished specimens. The box at the right side presents the roughness after shot peening (condition 6) and shot peening plus chemical polishing (condition 7). High surface roughness values after shot peening decrease significantly by chemical polishing.

The optical comparison of the surface defects for the specimens in different conditions are shown in Figure 3.15, Figure 3.16, and Figure 3.17. Specimens after mechanical polishing have no surface defects (Figure 3.15 (a)) while after chemical polishing method still, some defects have left on specimen's surface (Figure 3.15 (b)). These defects would be the long range machining marks, which have not been removed by chemical polishing.

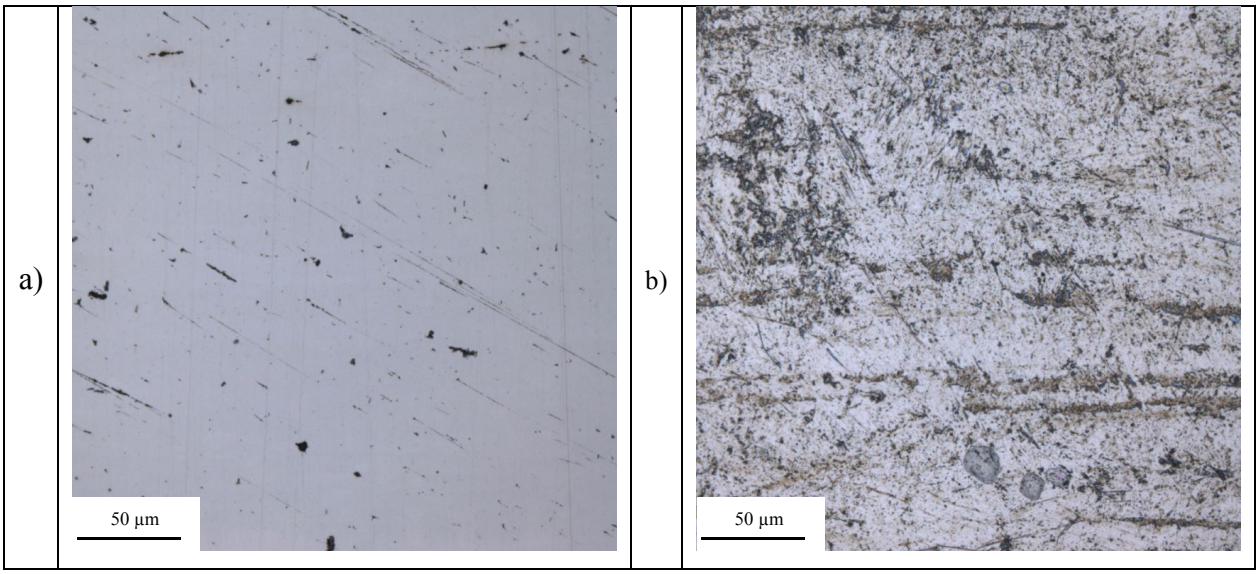

Figure 3.15 Optical characterizations of surface defects for straight shanks specimens that (a) mechanically polished (conditions 0, 1, and 2) and (b) chemically polished (conditions 3, 4, and 5).

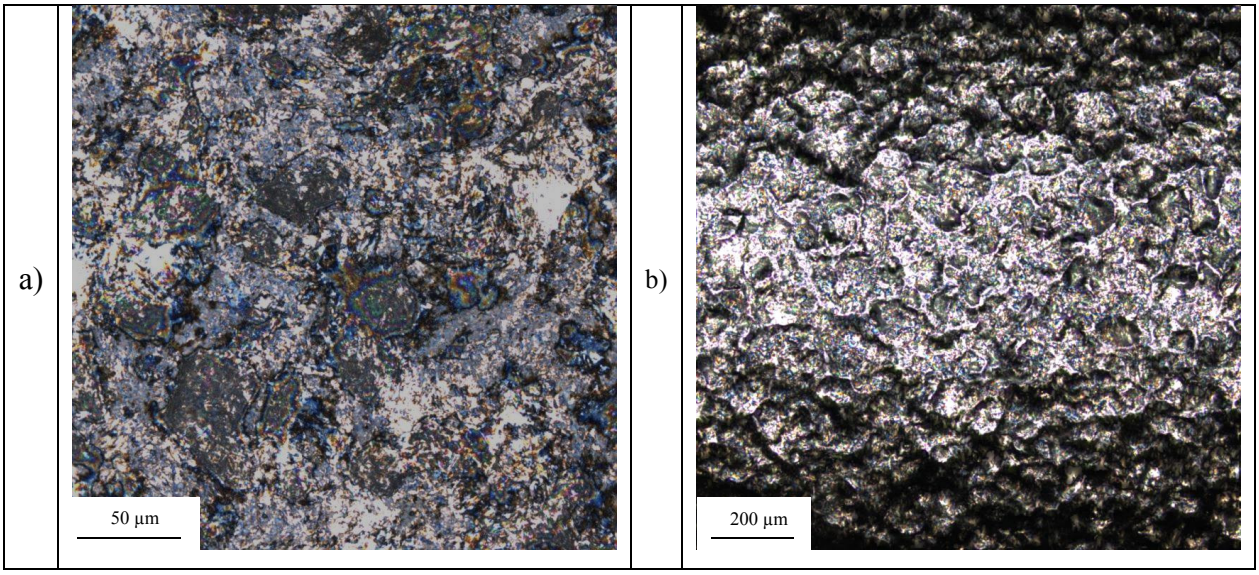

Figure 3.16 Optical characterizations of surface defects for straight shanks specimens after shot peening in two magnifications (a)500x and (b)100x.

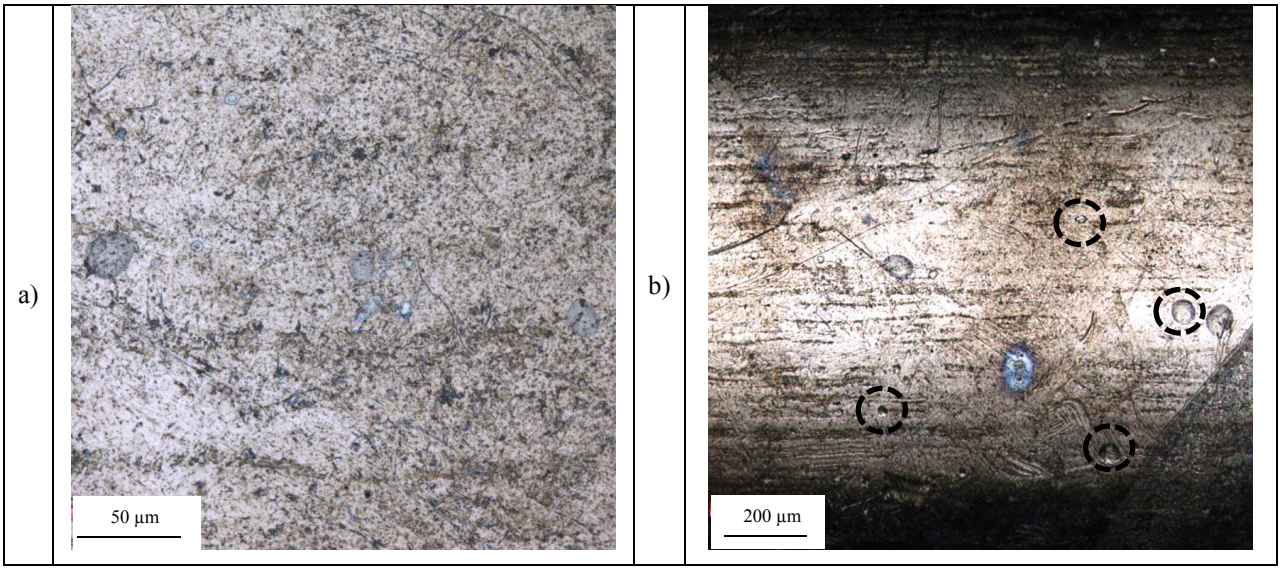

Figure 3.17 Optical characterizations of surface defects for straight shanks specimens after shot peening plus chemical polishing in two magnifications (a)500x and (b)100x.

Figure 3.16 (a) and (b) show lots of peening defects induced by shot peening in two magnifications. The peening defects have removed significantly after chemical polishing (condition 7) (Figure 3.17 (a)). Optical characterization of the surface after shot peening plus chemical polishing at lower magnification has shown in Figure 3.17 (b). It can be seen that after chemical polishing most of the peening impacts are removed, but still few peening defects have left as shown by dash circles in Figure 3.17 (b).

3.2.1.4 Layers in Compressive Residual Stress

Affected layers were characterized by residual stress measurements and optical inspections of the microstructure. Residual stress measurements show that specimens after mechanical polishing (conditions 0, 1, and 2) have no depth of compressive residual stress (Figure 3.18 (a)). Residual stress for the specimens that were machined and were chemically polished (conditions 3, 4, and 5) reached -600 MPa and affected only the first 25 microns of the material (shown by the dash line in Figure 3.18 (b)). Rough machining condition was induced residual stress at this depth, which was not removed completely by chemical

polishing. Specimens after shot peening (condition 6) have almost 180 microns depth of compressive residual stress (shown by the dash line in Figure 3.18 (c)). These measurements showed that specimens have 160 microns depth of compressive residual stress (indicated by the dash line in (Figure 3.18 (d)) after chemical polishing (condition 7). Compressive residual stress showing almost similar depth before and after chemical polishing (conditions 6 and 7). However, surface roughness after shot peening improved significantly by chemical polishing.

Microstructural characterizations of the layers below the surface are presented in Figure 3.19 (a)-(d). Deformed microstructures by the machining or shot peening processes etched faster (dark regions) than other regions in specimen's cross-section due to the presence of dislocations and they become darker than the other regions. These affected regions have been sized by white dash lines in Figure 3.19 (numbers between two lines show the length of affected microstructures in each condition).

a)

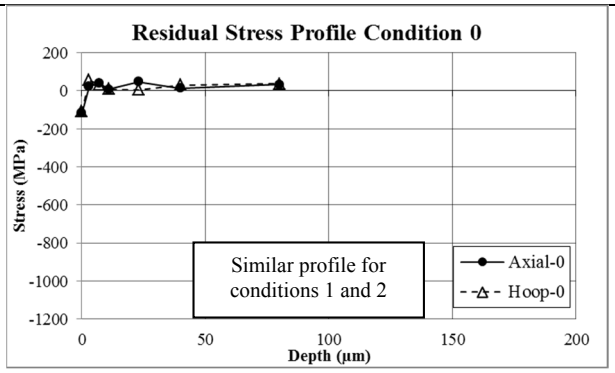

b)

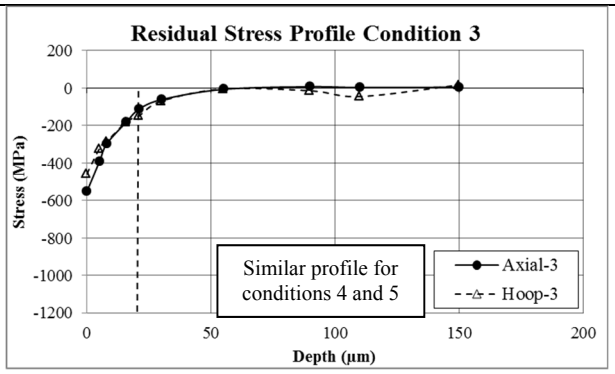

c)

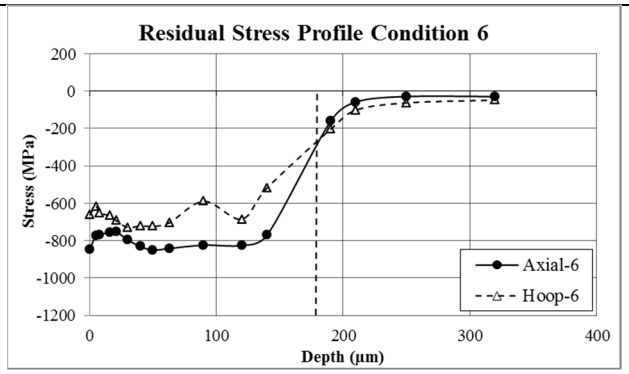

d)

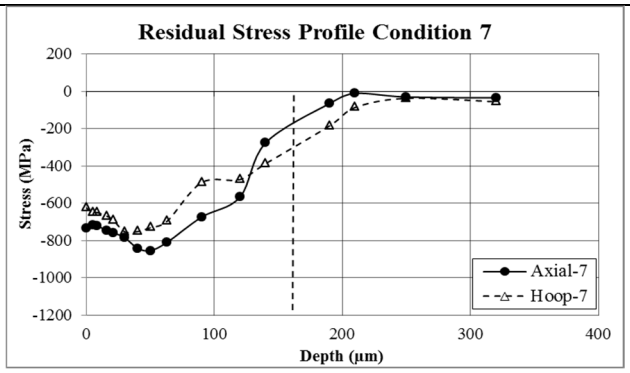

Figure 3.18 Residual stress profiles for the specimens (a) mechanical polishing, (b) chemical polishing, (c) shot peening, and (d) shot peening plus chemical polishing (see Table 3.1).

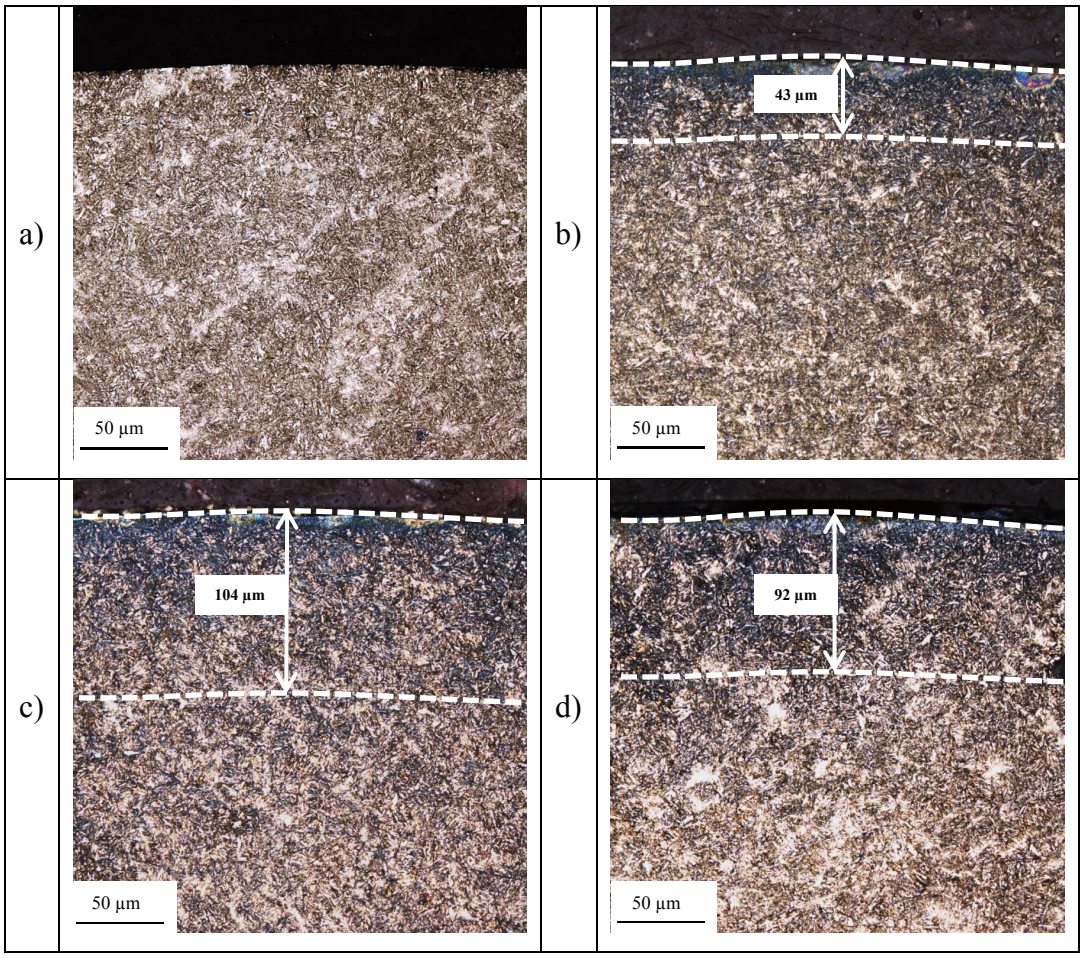

Figure 3.19 Optical characterizations of the deformed microstructures by machining process (a), (b) and shot peening process (c),(d).

3.2.2 Fatigue Test Results

Straight shank specimens were fatigue tested by rotating bending method at a constant stress level of 1000 MPa. Fatigue lives of the specimens in each condition are presented in Figure 3.20 in logarithmic scale. Specimens in each condition have separated by dash box. The first box at the bottom shows the fatigue lives for the specimens that were mechanically polished. The box in the middle shows the fatigue lives for the specimens that were chemically polished and fatigue lives in shot peened conditions have shown by the dash box on top.

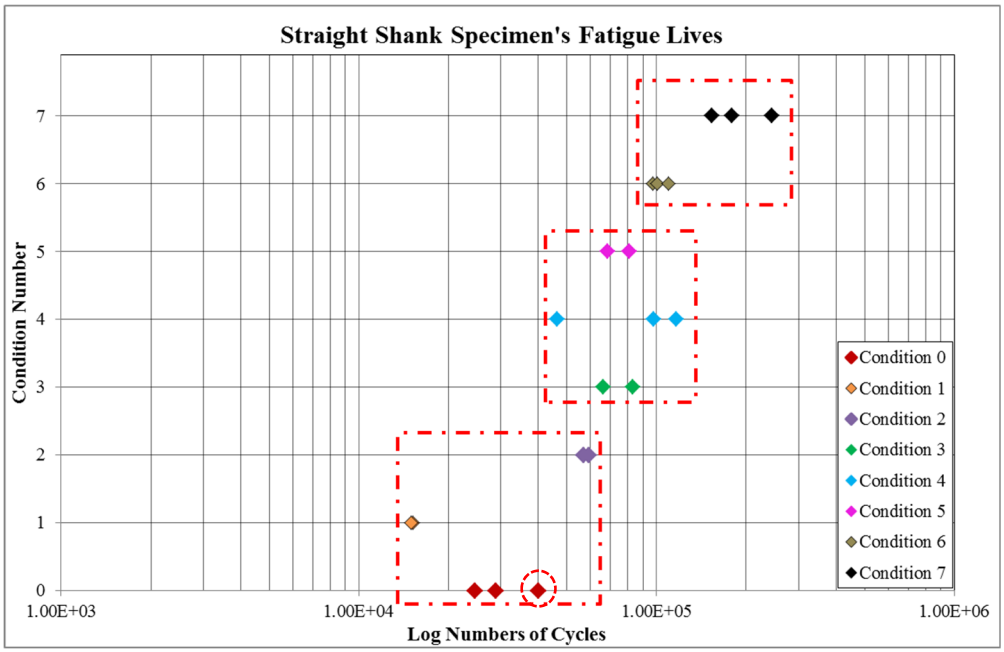

Figure 3.20 Fatigue lives of the straight shank specimens in different surface integrity conditions (see Table 3.1) at 1000 MPa stress level.

First dash box at the bottom (conditions 0, 1, and 2) shows that fatigue lives for the specimens in mechanical polishing condition do not have too much dispersion. In this box, specimens in condition 1 have lower fatigue lives compare to conditions 0 and 2. It means that high-strength steels provided by 'supplier A' have the lower fatigue life after stress relieving with batch method (condition 1) than inline method (condition 0). The other conclusion from mechanical polishing specimens after stress relieving with inline method is that 'supplier B' products (condition 2) have highest fatigue lives than 'supplier A' products. Dash circle in Figure 3.20 represents the specimen that was not broken completely and was plastically deformed.

The box in the middle shows the fatigue lives for the specimens in chemical polishing condition (conditions 3, 4 and 5). These specimens have the same average of fatigue lives. One of the specimens in condition 4 has failed at relatively low numbers of cycles suggesting a large dispersion of the results.

The dash box on top shows the fatigue behavior of shot peened specimens (conditions 6 and 7). Specimens in condition 6 were only shot peened with same peening intensity, and their fatigue lives are almost as good as the specimens in conditions 3, 4, and 5 (machining plus chemical polishing). Specimens in condition 7 (shot peening plus chemical polishing) have almost twice higher fatigue life compare to specimens in condition 6 but the fatigue lives have relatively large dispersion.

3.2.3 Characterizations after Fatigue Test

3.2.3.1 Fractography of Fracture Surface in Macroscale

Fractography of the fracture surface for the specimens in conditions 0, 1, and 2 (mechanical polishing) are shown in Figure 3.21. White arrows are showing the crack initiation sites for each specimen. Specimens in condition 1 and one of the specimens in condition 2 have multiple crack initiation sites, which shows that the stress level during fatigue test was relatively high for this material (Torres and Voorwald, 2002). For all the other conditions, one crack initiation was found as shown in Figure 3.22 and Figure 3.23.

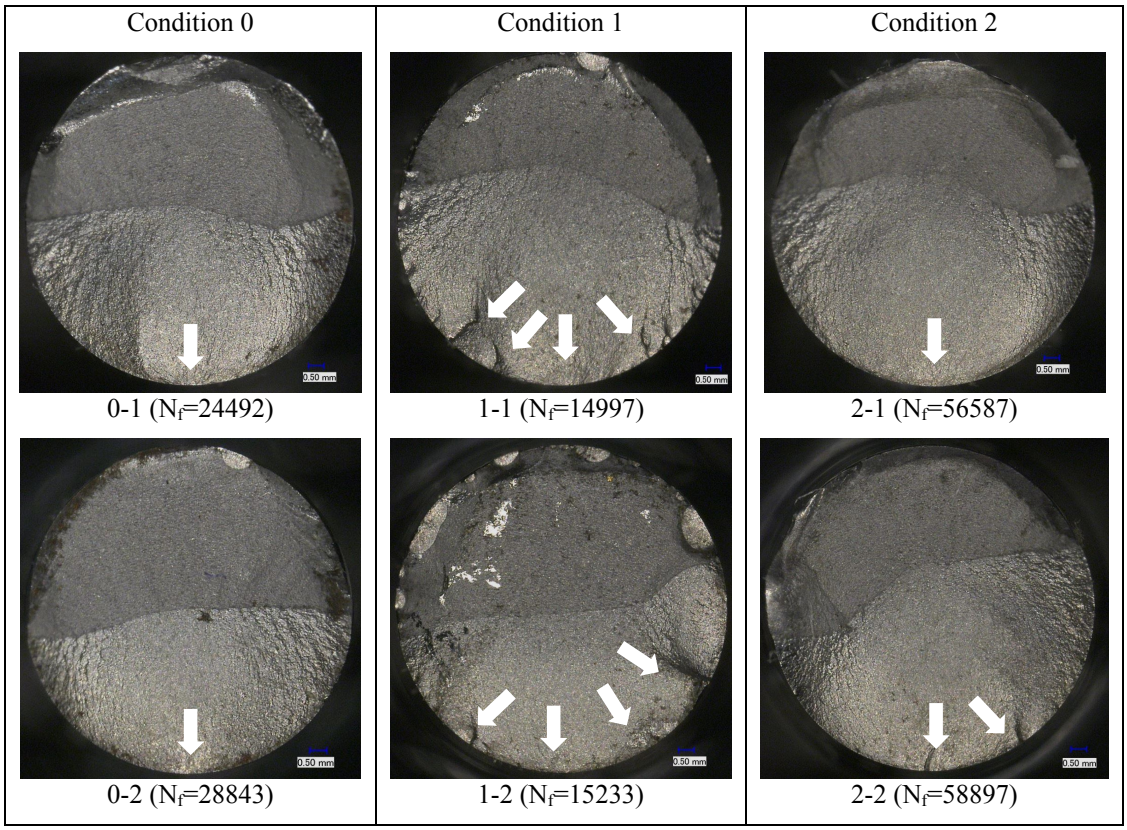

Figure 3.21 Fracture surface at macroscale for the mechanically polished specimens (conditions 0, 1, and 2).

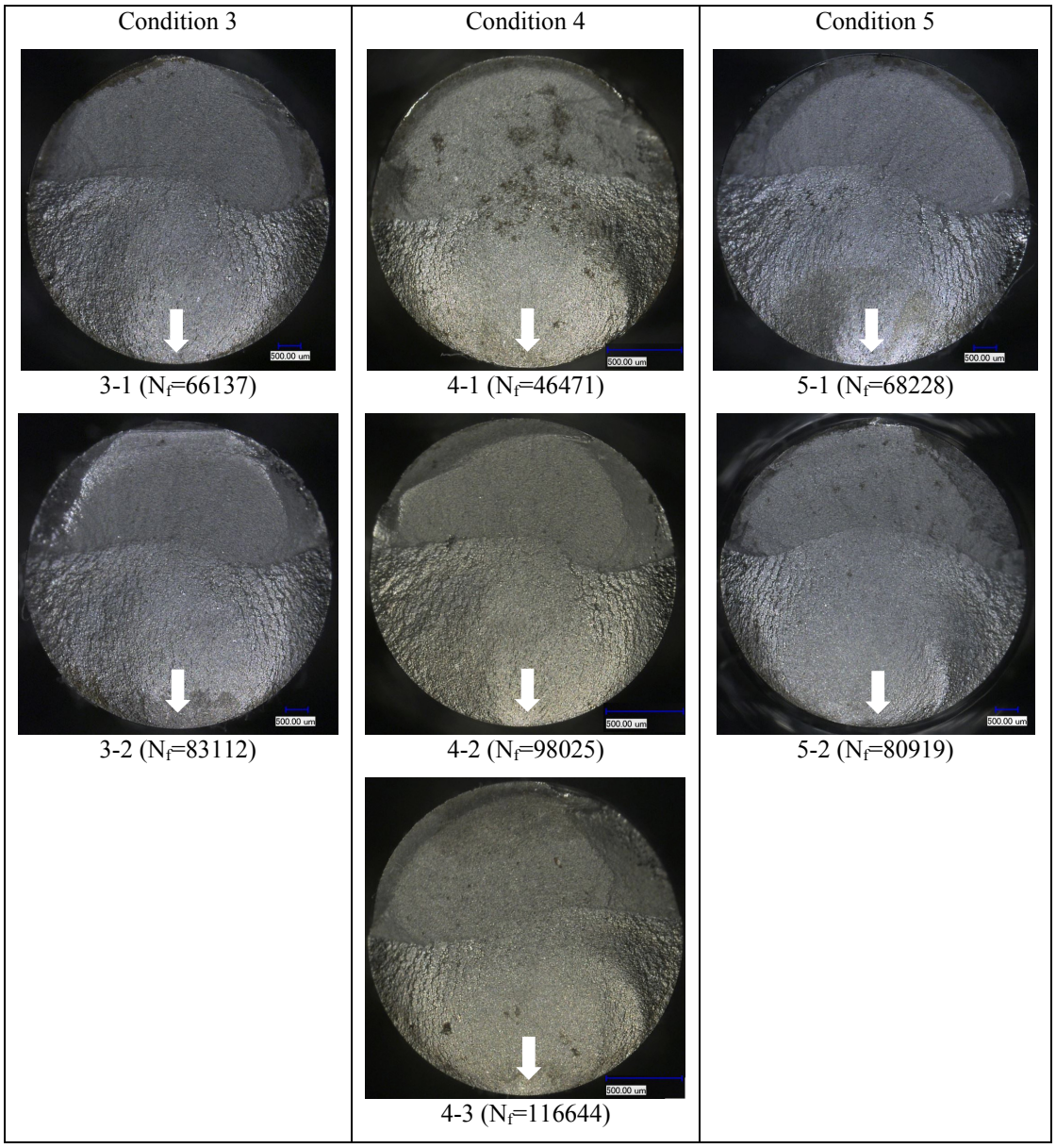

Figure 3.22 Fracture surface at macroscale for the chemically polished specimens (conditions 3, 4, and 5).

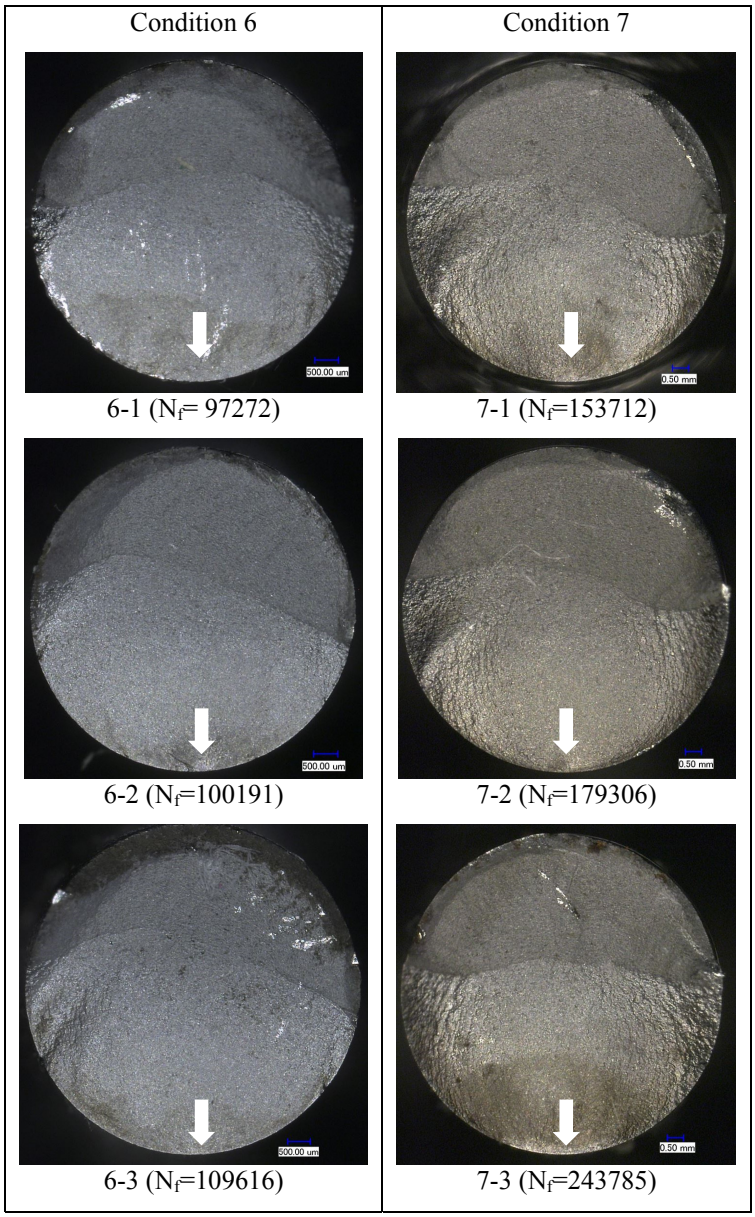

Figure 3.23 Fracture surface at macroscale for the shot peened specimens (condition 6) and shot peened plus chemically polished (condition 7).

3.2.3.2 Fractography of Fracture Surface in Microscale

Nucleation sites were characterized in more detail by fractography at a microscale. These characterizations show that failure of the specimens in conditions 0 and 1 are due to the inclusion particles (Figure 3.24 and Figure 3.25). Specimens in condition 0 were stress relieved with inline method, and in condition 2, specimens were stress relieved by batch method. Material for the specimens in both conditions was provided by 'Supplier A'. The fractography reveals that products of 'supplier A' have big inclusion particles and these inclusion particles cause failure in the materials. These inclusion particles are found at the surface (specimens 0-2, and 1-1), close to the surface (specimens 0-1) or inside the material with an almost 50 microns distance from the surface (Specimen 1-2). Size of these inclusion particles varies between 12 to 25 microns. Internal inclusion particle has 40 microns dimension (specimen 1-2), which is twice bigger than external inclusion particle. EDX analysis of these inclusion particles shows their chemical composition is Aluminum-Calcium (Al-Ca) (Figure 3.26).

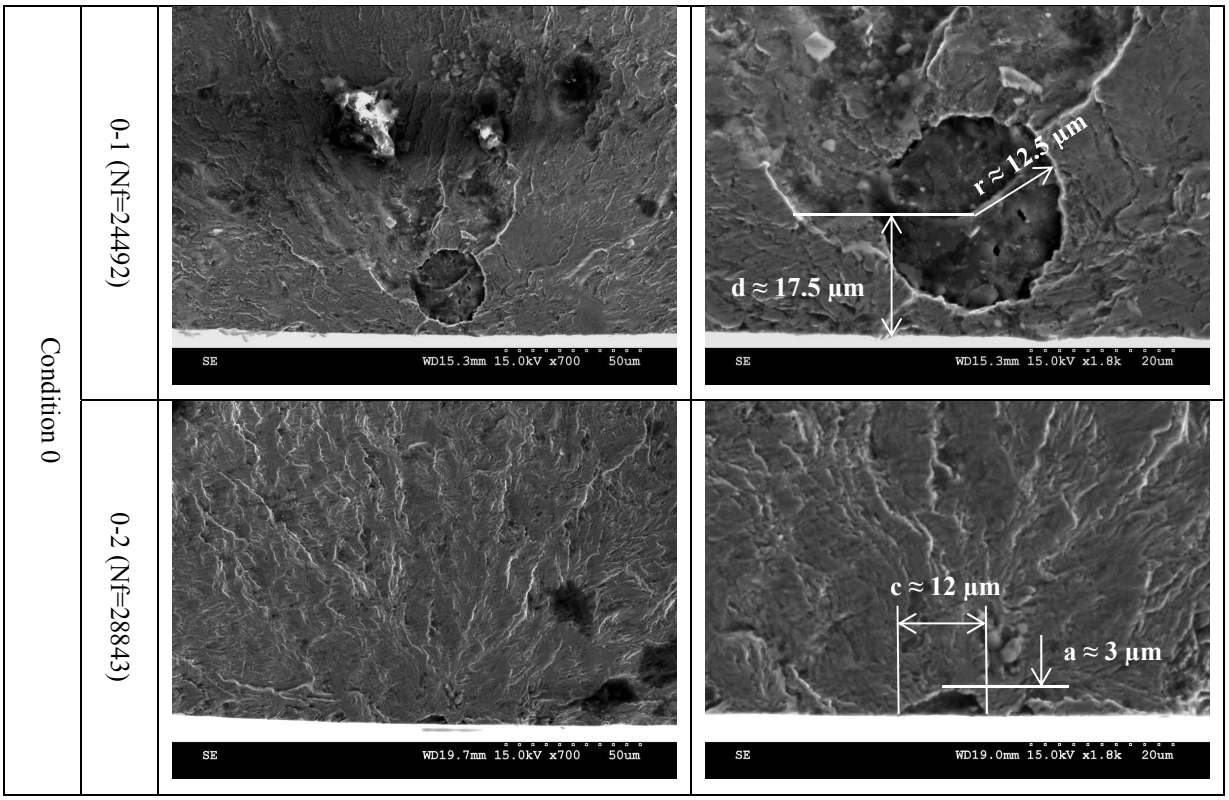

Figure 3.24 Fracture surface at microscale at the nucleation site for tow specimens in condition 0 at two scales.

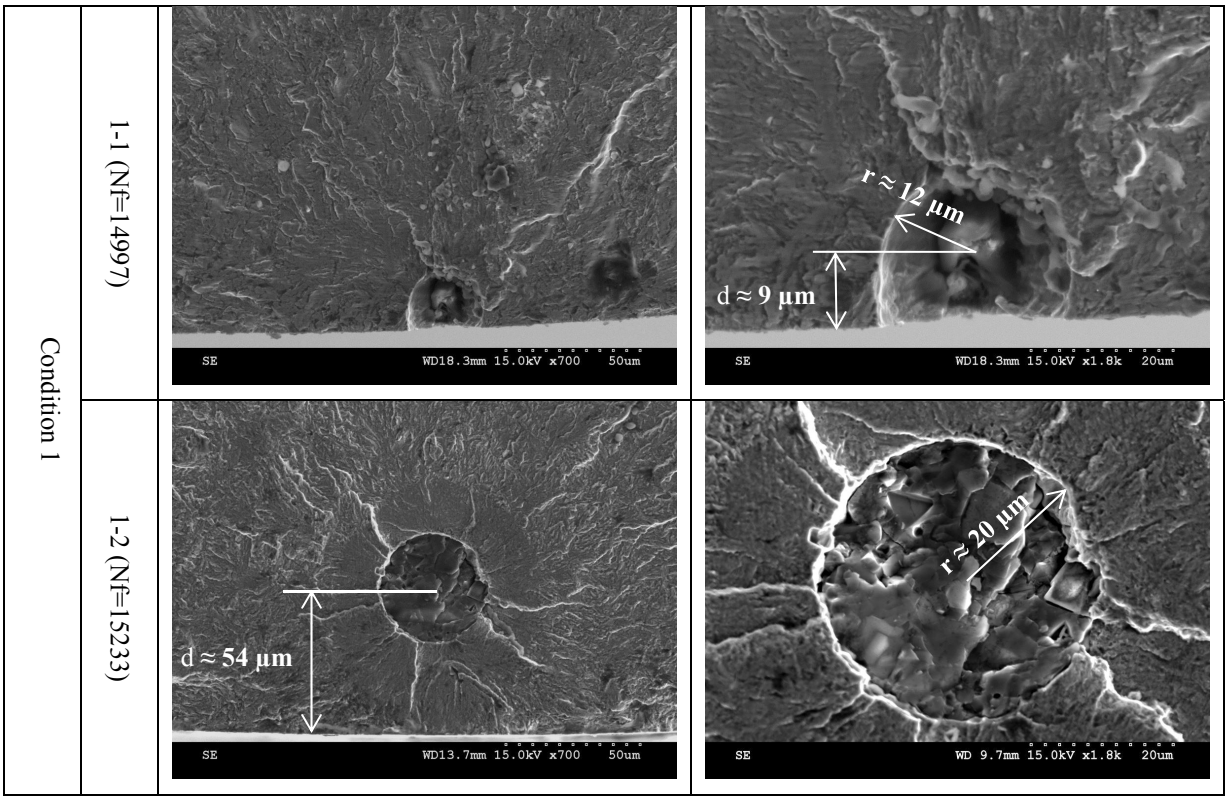

Figure 3.25 Fracture surface at two microscales around the nucleation site for the specimens in condition 1.

Internal inclusion particle and particles at the surface are relatively bigger in condition 1 compare to those in condition 0. Big inclusion particles in condition 1 would explain the failure at lower numbers of cycles for the specimens in this condition 1. However, in these two conditions the same supplier has been provided the high-strength steels and as the various stress relieving methods do not affect the particle size, the average life difference is may be due to a statistical effect on particle size, or at some other degree the effect of matrix hardness.

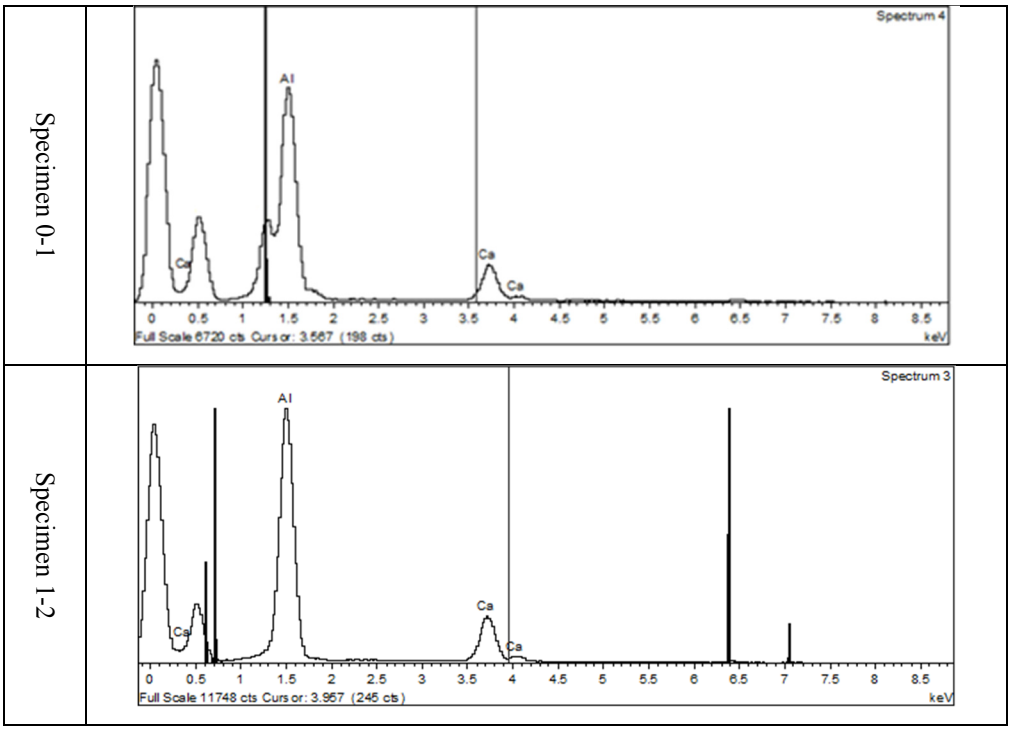

Figure 3.26 EDX analysis shows Al-Ca element for the inclusion particles.

Failures for the specimens in condition 2 are also due to inclusion particles. They are found at the surface (Figure 3.27) however, the particles are not found at the nucleation site, but their shape is similar to the shape of the inclusion particles. Their sizes are much smaller compared to the specimens in condition 0 and 1. They are most probably Al-Ca particles too. Specimens in this condition were provided by 'Supplier B' and stress relieved by inline method.

Stress raiser (k_t) would explain more the reason of failure at different numbers of cycles for the specimens 0-2, 1-1, 2-1, and 2-2. In this study, calculation of the stress raiser has not been performed for these specimens, but stress raiser geometries have been documented below (APPENDIX II).

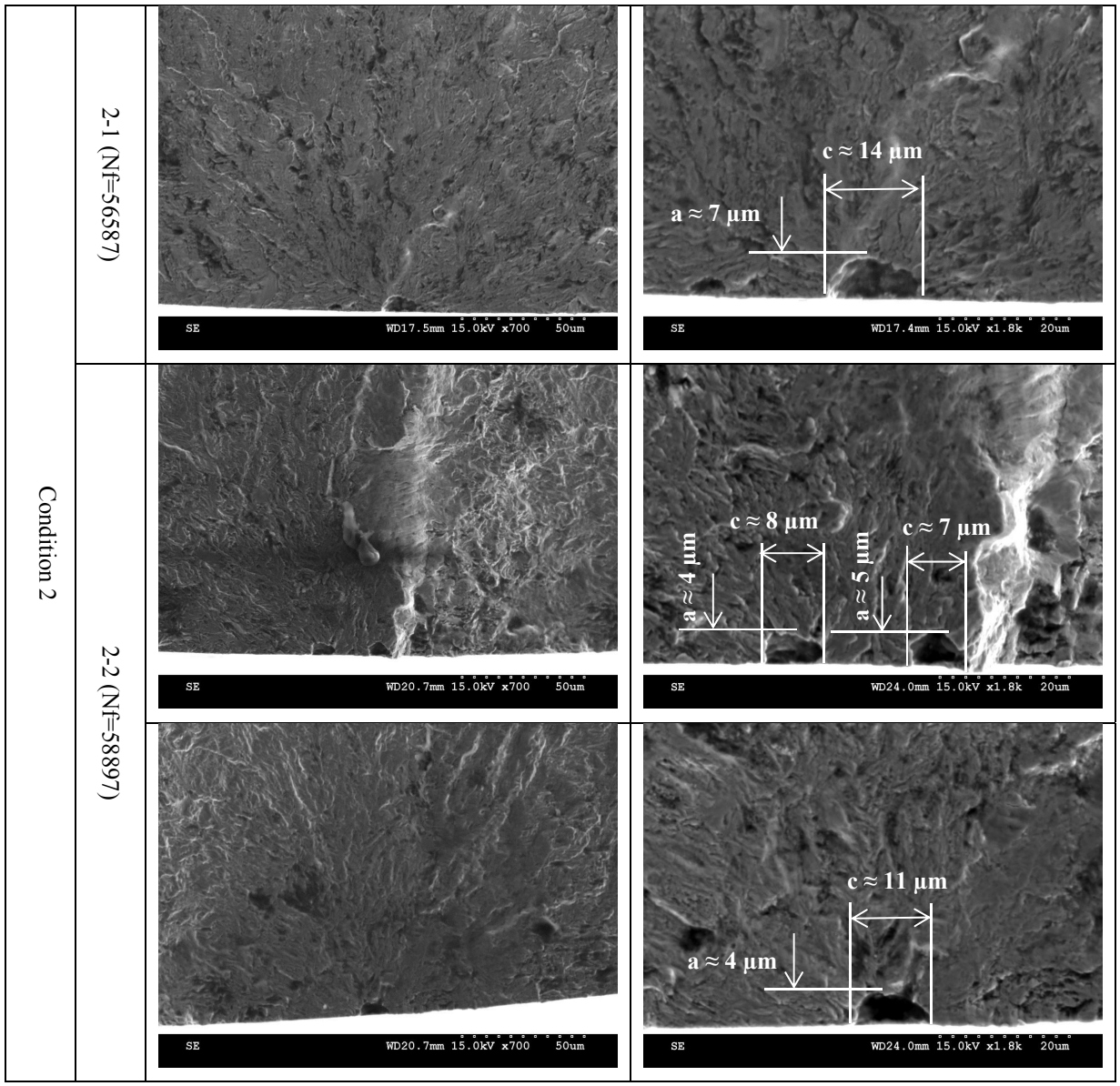

Figure 3.27 Fracture surface at microscale close to the nucleation site for three specimens in condition 2 with two scale.

Specimens for which crack nucleation takes place at the surface have optically observed from the side (Figure 3.28). White boxes in Figure 3.28 are showing the location of the nucleation site seen on the side of the specimen. These optical observations showed that no specific defect is found at the outer surface. The inclusion particles in the specimens 0-1 and 1-2 are not at the surface and they have not seen optically on the side.

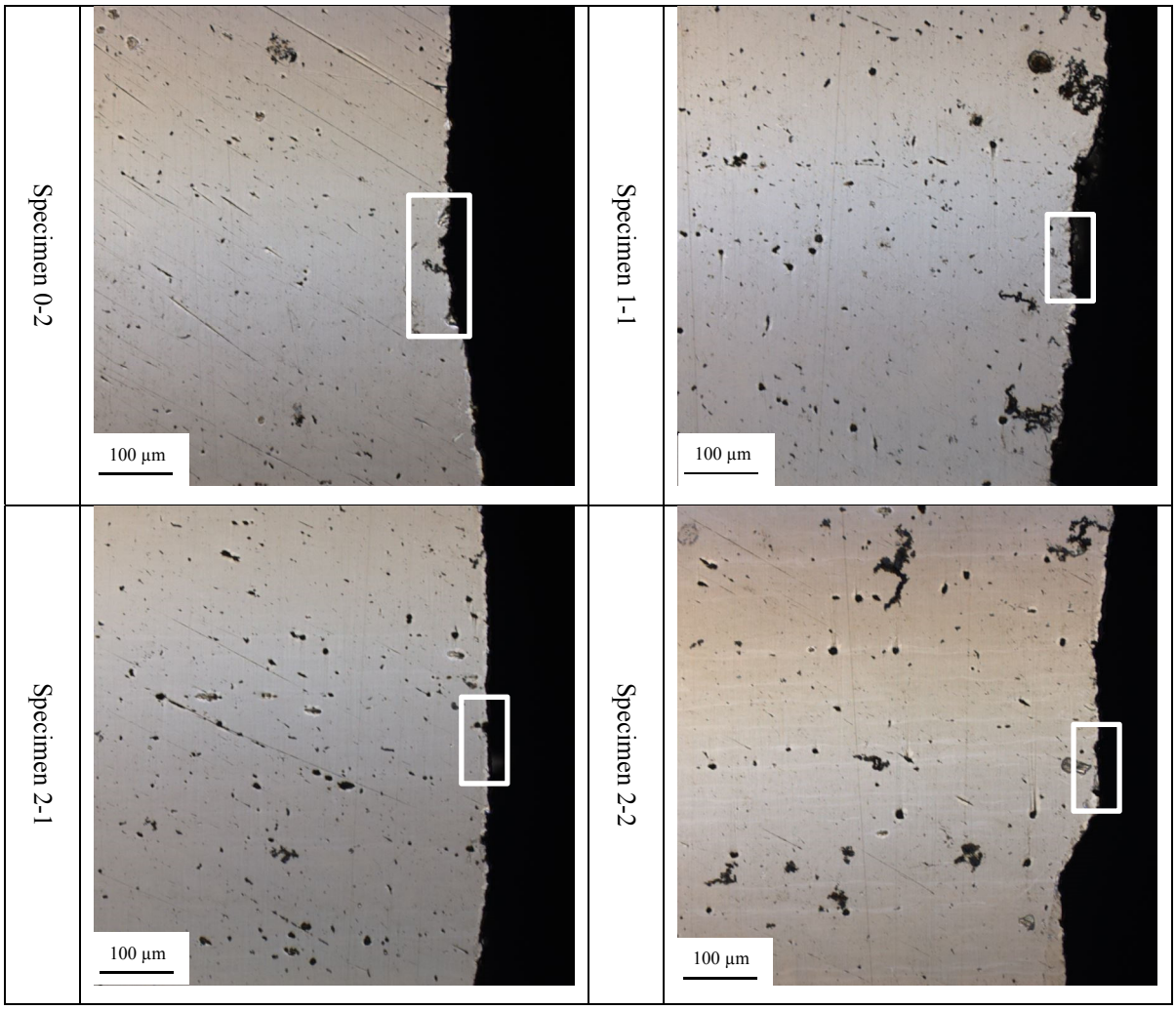

Figure 3.28 Optical observation from the side of fatigue samples where crack nucleation located for the conditions 0, 1, and 2.

Numbers of secondary cracks were measured for the specimens in mechanical polishing conditions (0, 1, and 2) and they have presented in Table 3.2. Numbers of secondary cracks for the specimens in condition 1 are relatively more than conditions 0 and 3. Zheng and al. (2012) have reported that formation of secondary cracks resulted in absorbing more energy, relaxing stress concentrations, and reduced the crack growth rate in bainitic steels. However, specimens in condition 1, failed at the lowest numbers of cycles.

Table 3.2 Numbers of secondary cracks in one cm^2 for the specimens that were mechanically polished (see Table 3.1).

Specimen Number	Supplier	Stress relieving	Numbers of secondary cracks per cm^2
0-1	A	Inline	16
0-2	A	Inline	20
1-1	A	Batch	28
1-2	A	Batch	35
2-1	B	Inline	8
2-2	B	Inline	11

Fracture surfaces of the specimens in condition 3 are shown in Figure 3.29. This figure shows that failure for the specimen 3-1 is due to the inclusion particle. The other specimens in this condition (specimen 3-2) failed due to a severe surface defect. The inclusion particle (Al-Ca (Figure 3.30)) has 13 microns size, which is relatively smaller than the particles found in the same material in conditions 0 and 1. Optical characterization of the outer surface for the specimen 3-2 shows failure at the surface is due to the machining defects, which were not removed by chemical polishing (Figure 3.33).

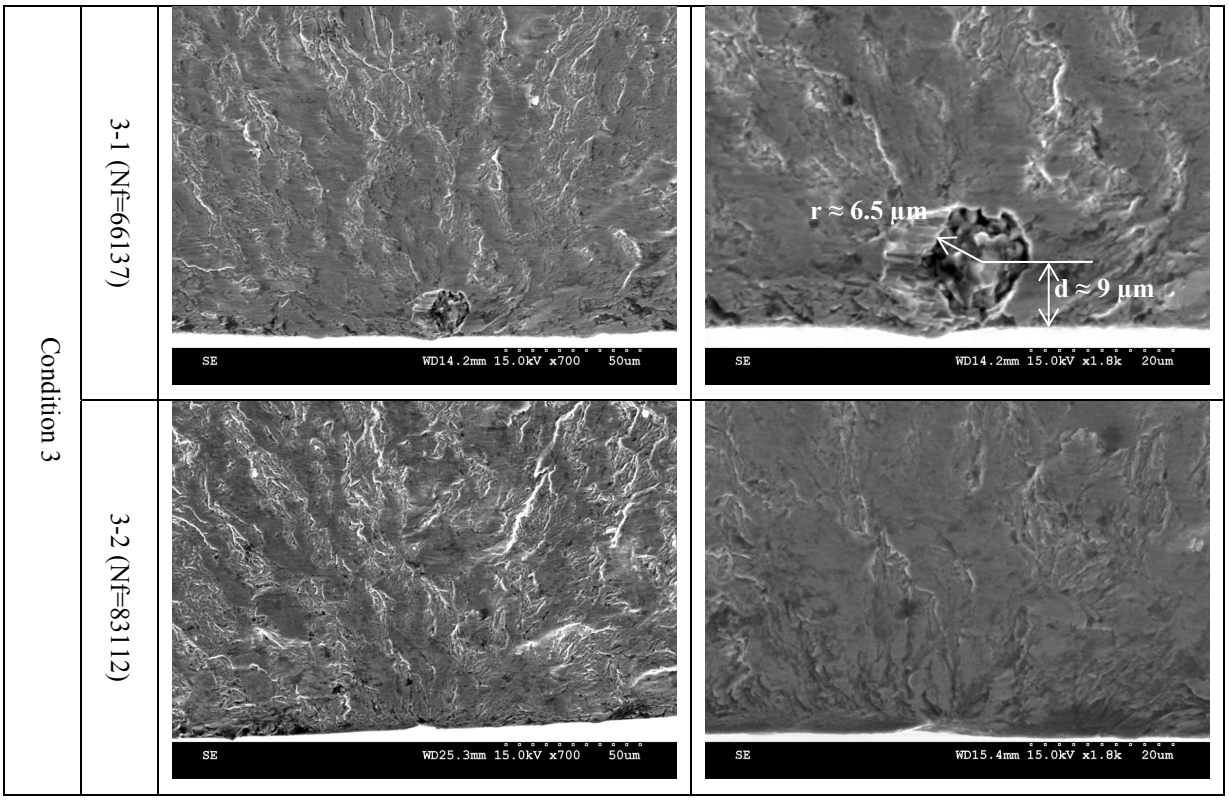

Figure 3.29 Fracture surface at microscale close to the nucleation site for three specimens in condition 3 with two scales.

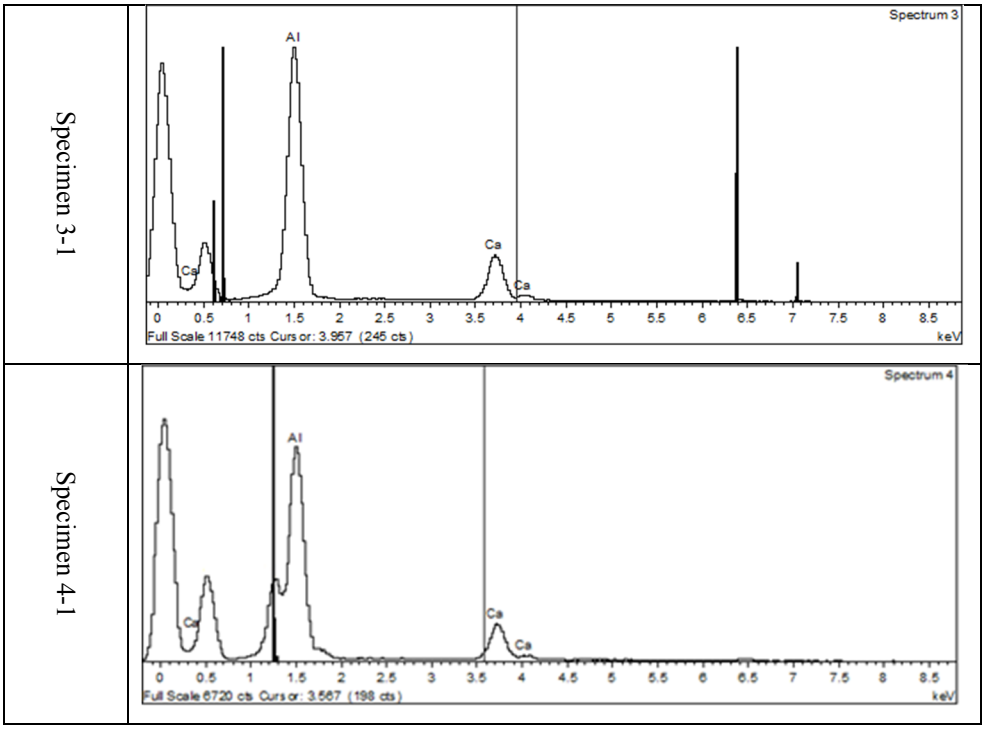

Figure 3.30 EDX analysis shows Al-Ca element for the inclusion particles.

The specimens in condition 4 failed due to the presence of inclusion particle and surface defect (Figure 3.31). Specimen 4-1 has big Al-Ca (Figure 3.30) inclusion particle and failed at a very low number of cycles compare to the other specimens in this condition. Specimens 4-2 and 4-3 show that if no big particles are found at the surface of the specimen, failure at a high number of cycles initiated from the surface or very small inclusion particle. In particular, the surface defect for the specimen 4-2 is the machining defect that was not removed by chemical polishing process (Figure 3.33).

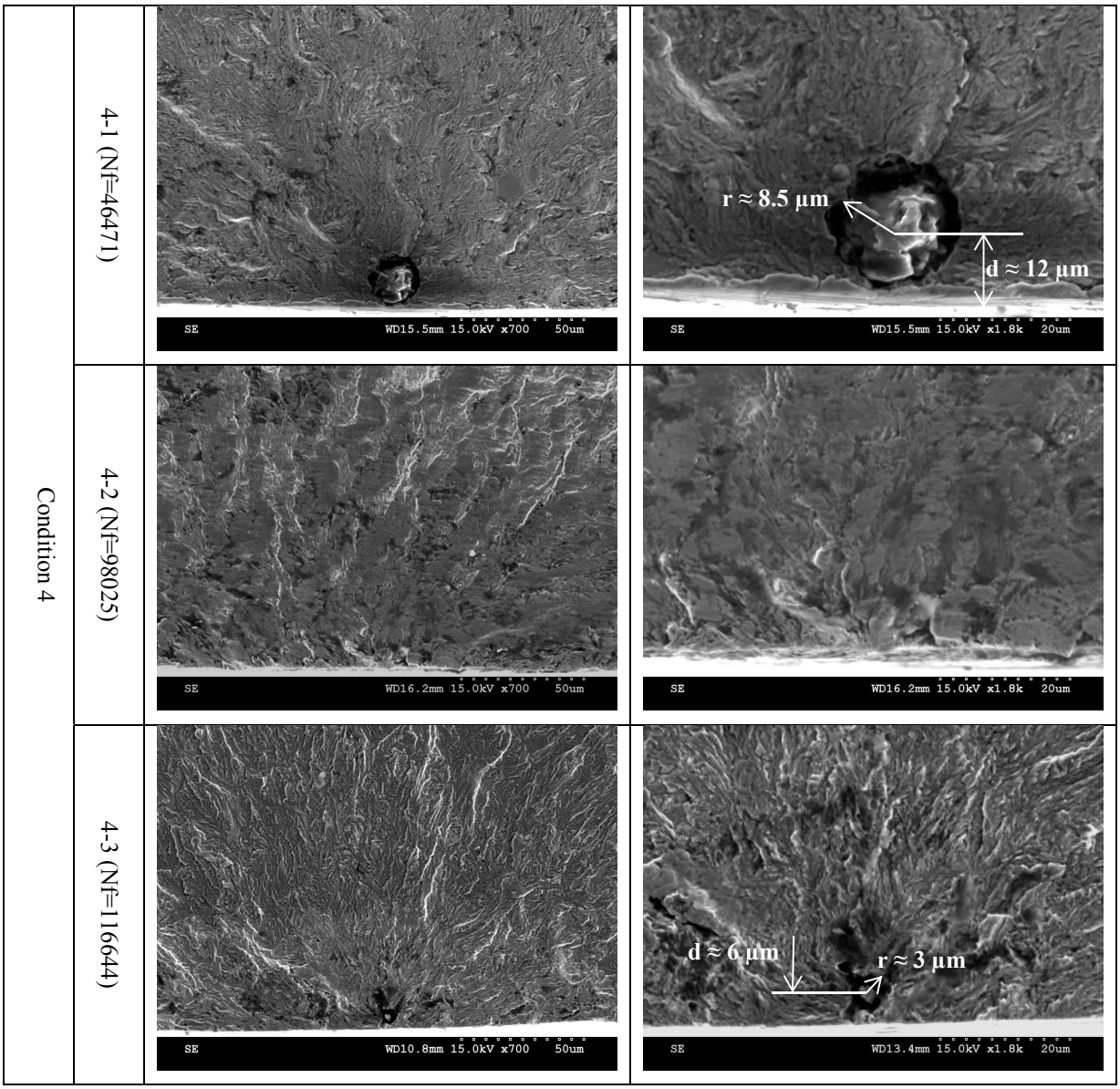

Figure 3.31 Fracture surface at a microscale around the nucleation site for three specimens in condition 4 with two scales.

Stress raiser (k_t) needs to be estimated for the specimens 3-1 and 3-2 in order to understand the reason of similar fatigue life for the specimens in this condition, but their geometries are reported below (APPENDIX II). Furthermore, fatigue life changes in condition 4 could be explained by the calculation of the stress raiser.

Failures for the both specimens in condition 5 are due to the surface defects and not inclusion as shown in Figure 3.32. Specimen 5-2 shows two crack initiation sites that are presented by white arrows in Figure 3.32. The optical observation of the nucleation site location on the side of the samples has presented in Figure 3.33. This figure shows that surface defects are the machining marks, which were not removed by chemical polishing.

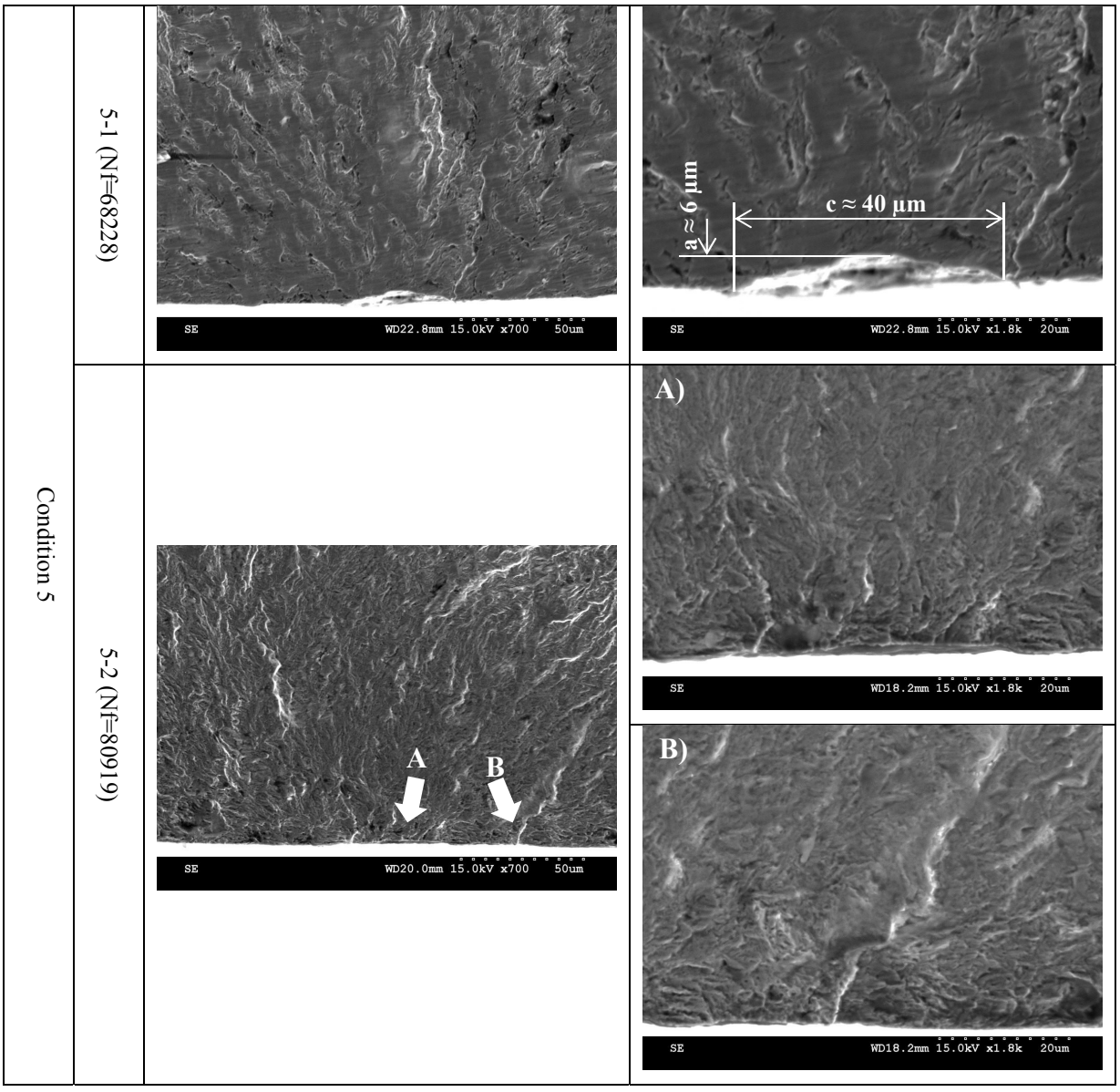

Figure 3.32 Fracture surface at a microscale close to the nucleation site for two specimens in condition 5 with two scales.

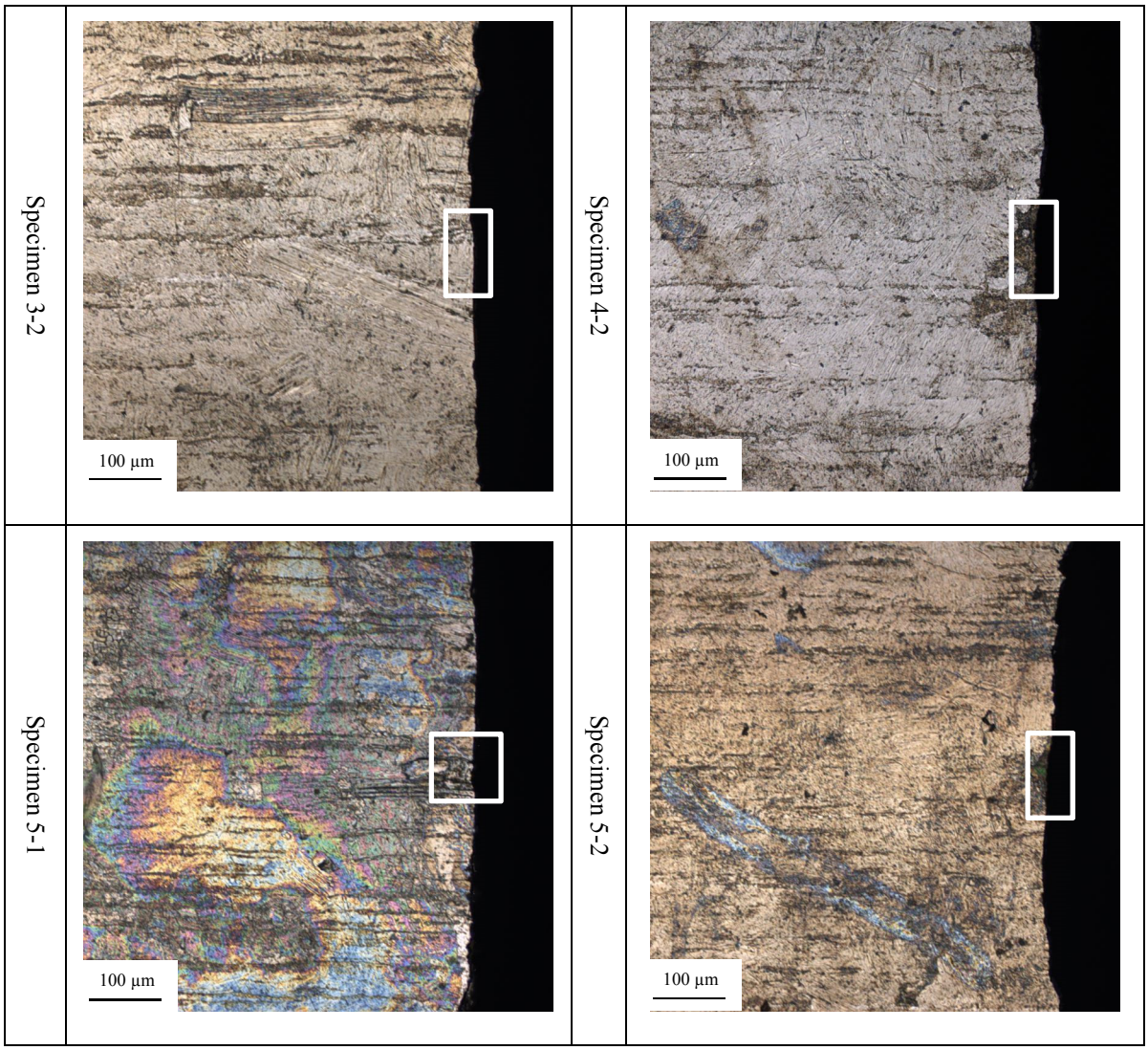

Figure 3.33 Optical observation from the side of fatigue samples where crack nucleation located for the conditions 3, 4, and 5.

Optical observations from the side of the specimens 3-1, 4-1, and 4-3 were not reported as they failed due to the internal inclusion particle. Due to the defects at the surface after chemical polishing, the characterizations of the secondary cracks were not possible with an optical microscope for these specimens.

The surface defects from applied shot peening are the origin of the failure in condition 6 (Figure 3.35). Optical characterizations at the side of the specimens show that shot peening process induces too many defects at the surface (Figure 3.34). 'Supplier A' is the material provider of the specimens in condition 6. 'Supplier A' products were failed because of Al-Ca inclusion particle as in conditions 0 and 4. However, analysis of the fracture surfaces of the specimens that were only shot peened (condition 6) shows that inclusion particles are not a failure reason and peening defects are controlling the fatigue life.

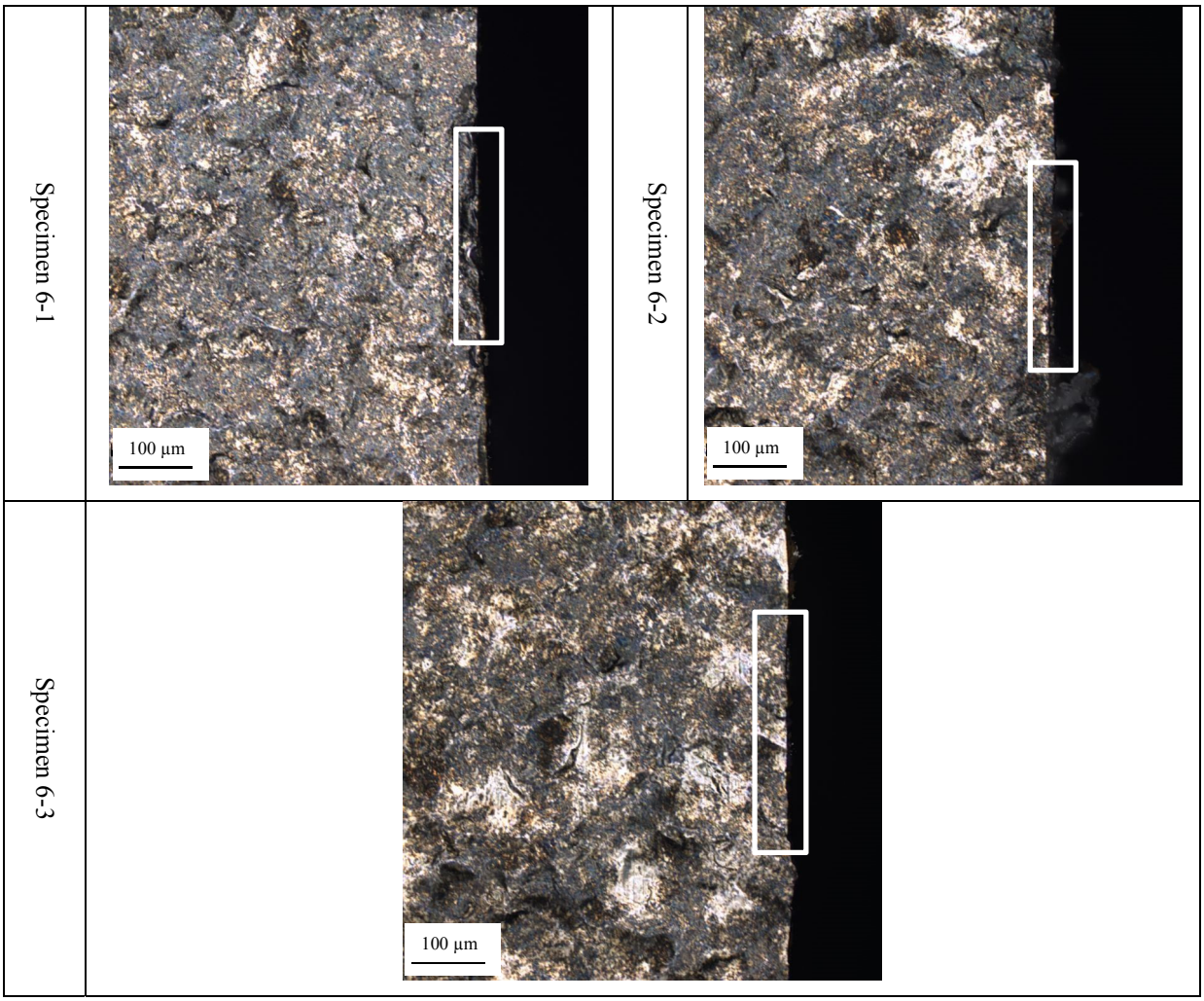

Figure 3.34 Optical observation of the nucleation location from the side of fatigue samples in the condition 6.

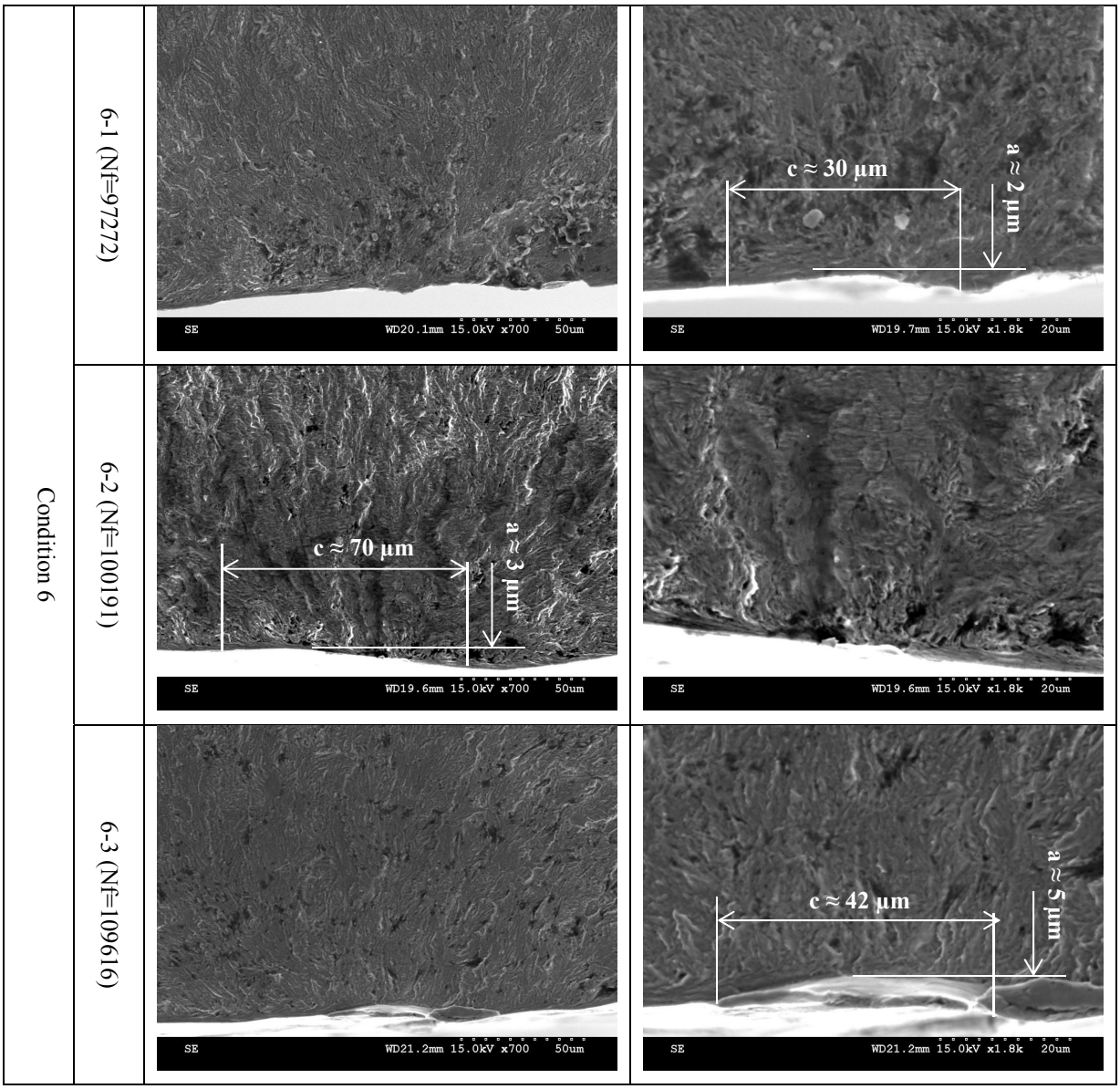

Figure 3.35 Fracture surface at a microscale close to the nucleation site for three specimens in condition 6 with two scales.

Chemical polishing does not prevent failure to take place at the surface (Figure 3.37). Failure in specimen 7-3 is due to the peening defect. However, cracks in specimen 7-1 and 7-2 initiated from a flat surface and no defect or stress concentration can be found. Most probably, surface defects in these specimens have been induced by shot peening process, and these defects were not removed completely by chemical polishing. Figure 3.36 shows optical observation from the side view of crack nucleation location.

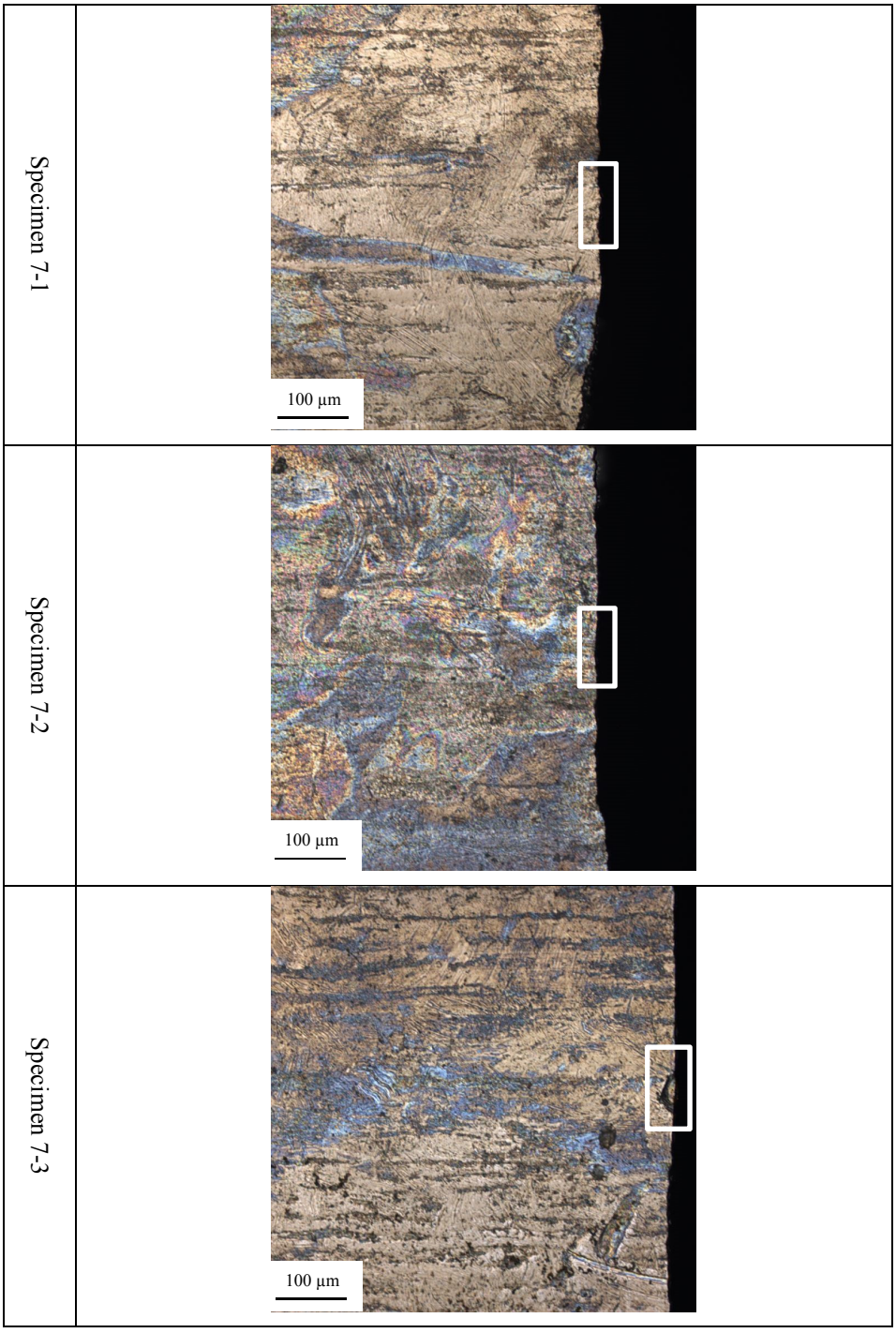

Figure 3.36 Optical observation of the nucleation location from the side of fatigue samples in condition 7.

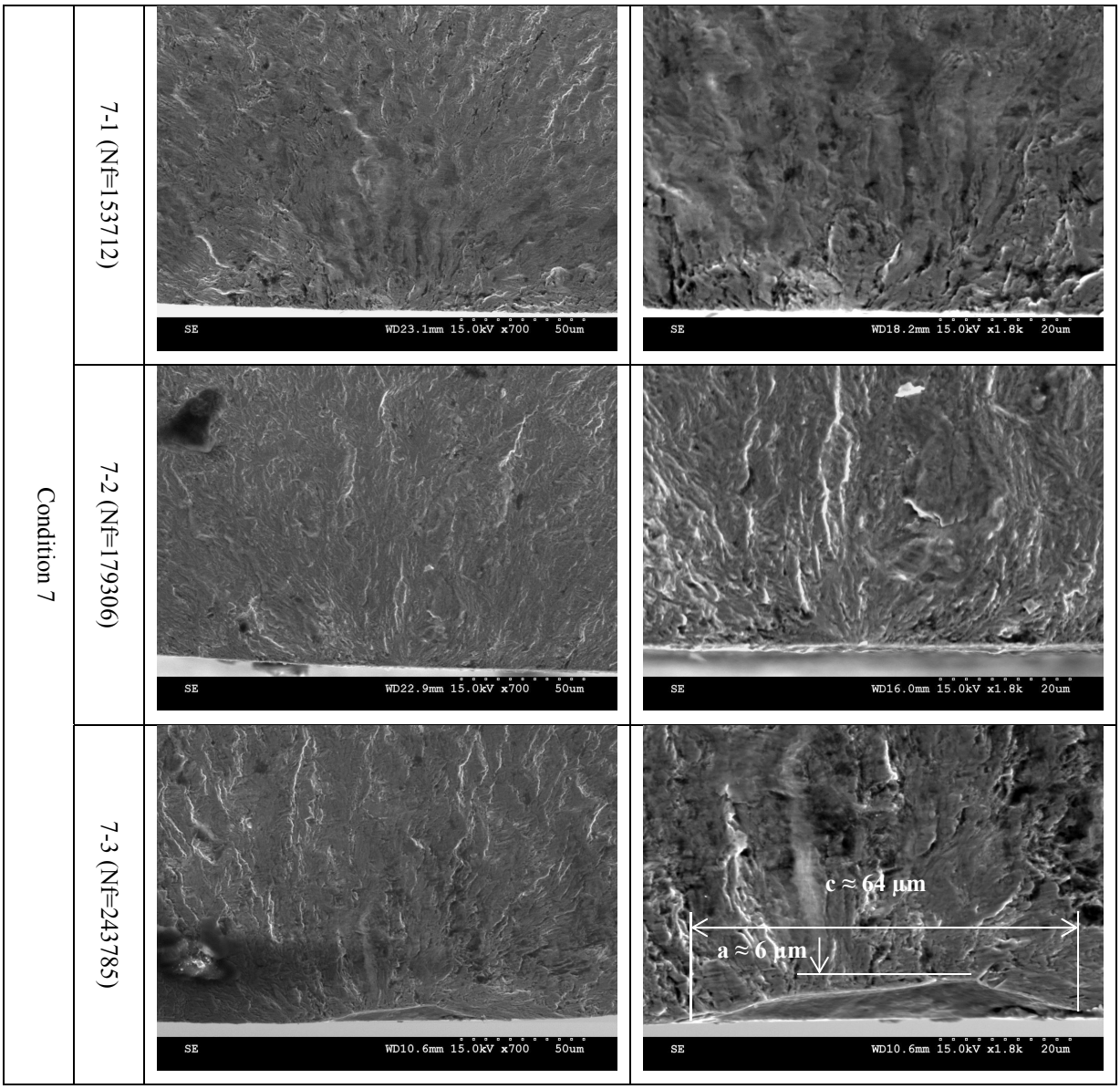

Figure 3.37 Fracture surface at a microscale close to the nucleation site for two specimens in condition 7 with two scales.

The summary of the numbers of crack initiation sites, failure reason, the size of the inclusion particles, and the size of surface defects have been detailed in Appendix II.

3.2.3.3 Stress Relaxation

Residual stress of the chemically polished specimens (conditions 3, 4, and 5) before fatigue test and after fatigue test has been measured and their results are presented in Figure 3.38 (a) and (b) in axial and hoop directions respectively. Stress relaxation has increased almost 20 % (from 40% to 60%) in condition 4 as specimens failed at higher numbers of cycles. The other two conditions in Figure 3.38 (conditions 3 and 5) failed at almost same numbers of cycles but they have different stress relaxation. Stress relaxation of the specimens in condition 5 is 10% more than condition 3 suggesting different behavior of the steels provided by two suppliers during fatigue test. 'Supplier A' was a material provider of the specimens in condition 3 has lower microhardness value in its products than the supplier 'B', which provided the steels for condition 5 (Figure 3.11) suggesting that stress relaxation is less in soft steels.

Figure 3.39 (a) and (b) show the stress relaxation of the specimen in conditions 6 and 7. Stress relaxation has increased significantly (almost 30%) after shot peening and chemical polishing (condition 7) compare to only shot peened specimens (condition 6). Stress relaxation for condition 6 was less than 40 % while in condition 7 it was 60% thus it could conclude that chemical polishing removes the hard layers with lots of dislocations.

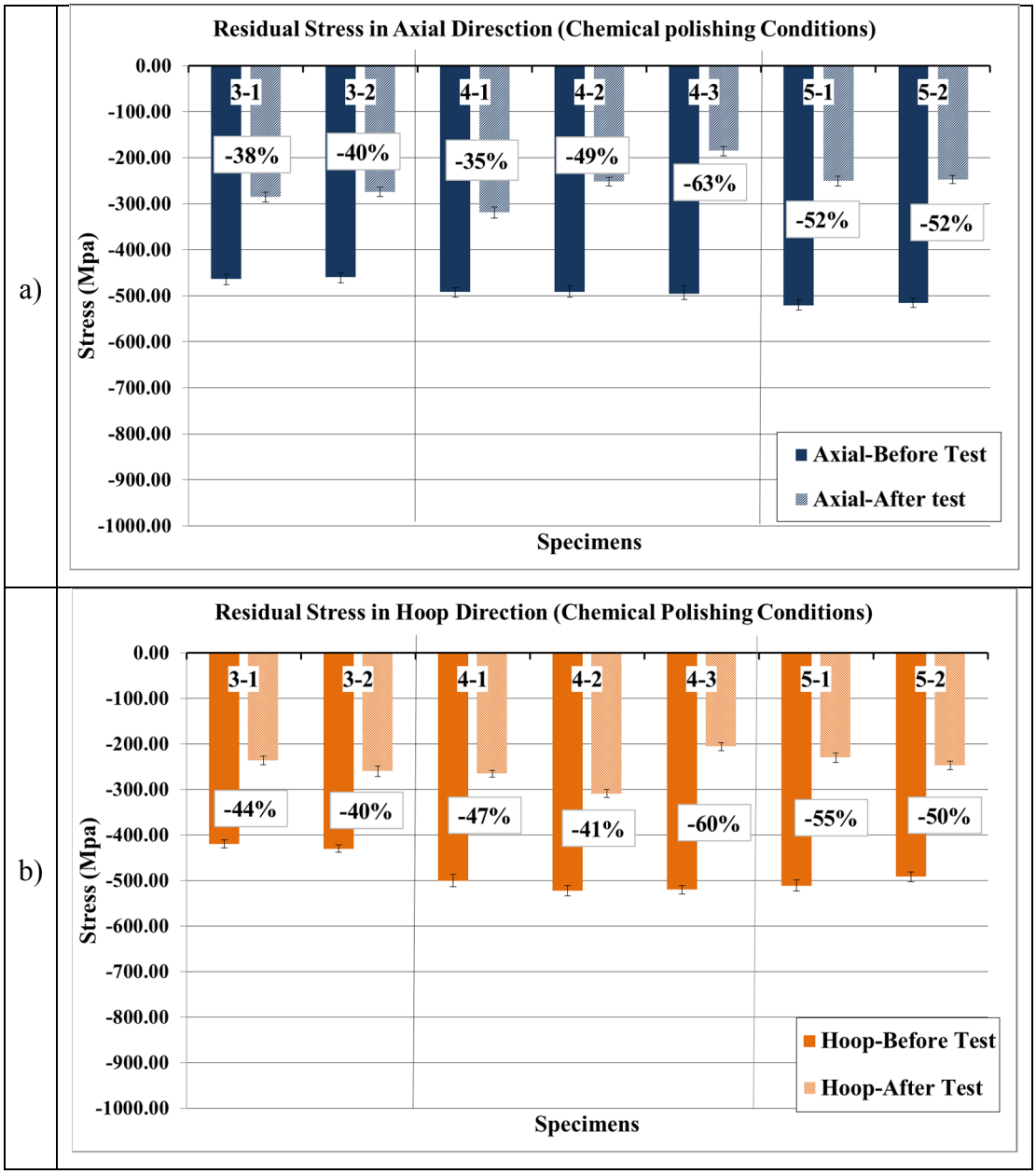

Figure 3.38 Surface residual stress measurements before and after fatigue test in axial (a) and hoop (b) directions showing the stress relaxation of the specimens in conditions 3, 4, and 5 (see Table 3.1).

a)

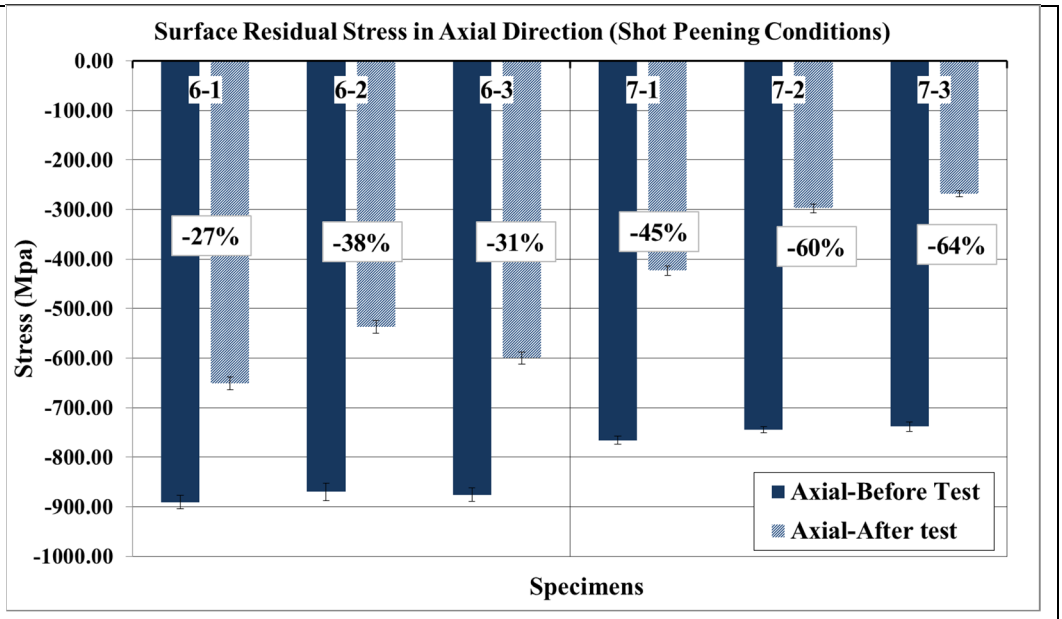

b)

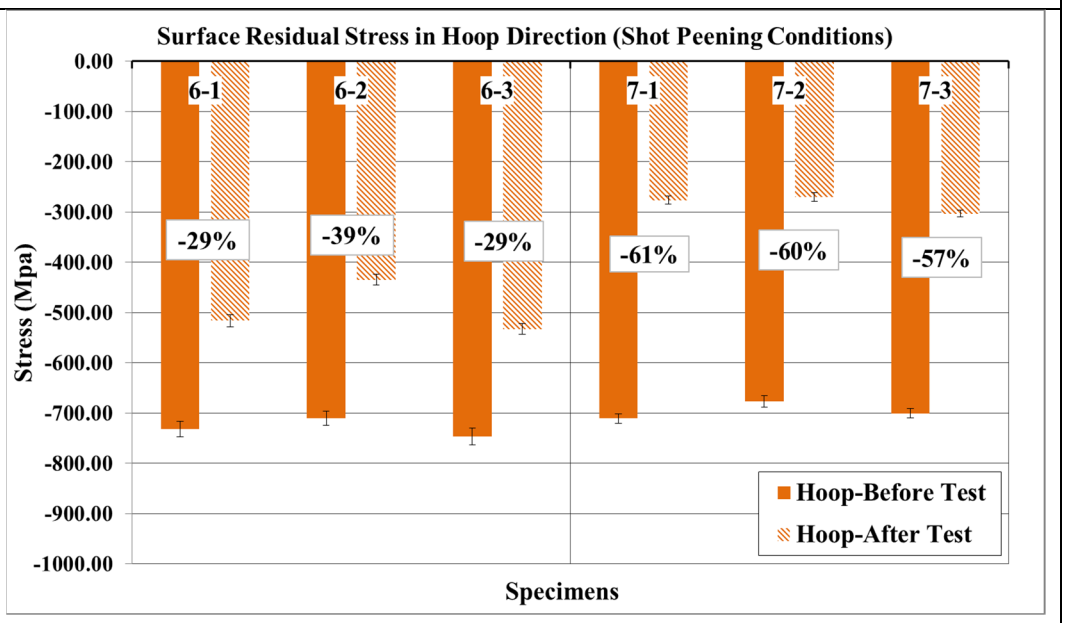

Figure 3.39 Surface residual stress measurements before and after fatigue test in axial (a) and hoop (b) directions showing the stress relaxation of the specimens in conditions 6 and 7 (see Table 3.1).

3.2.3.4 FWHM

Indirect measurements of the dislocation density can be done by using the FWHM results obtained from the XRD peaks. Figure 3.40 (a) and (b) show the FWHM results for the mechanical polishing conditions (0, 1, and 2). Dislocation density decreased more than 10% for the specimens in condition 1 suggesting more material softening for the specimens provided by supplier 'A' and stress relieved with batch method.

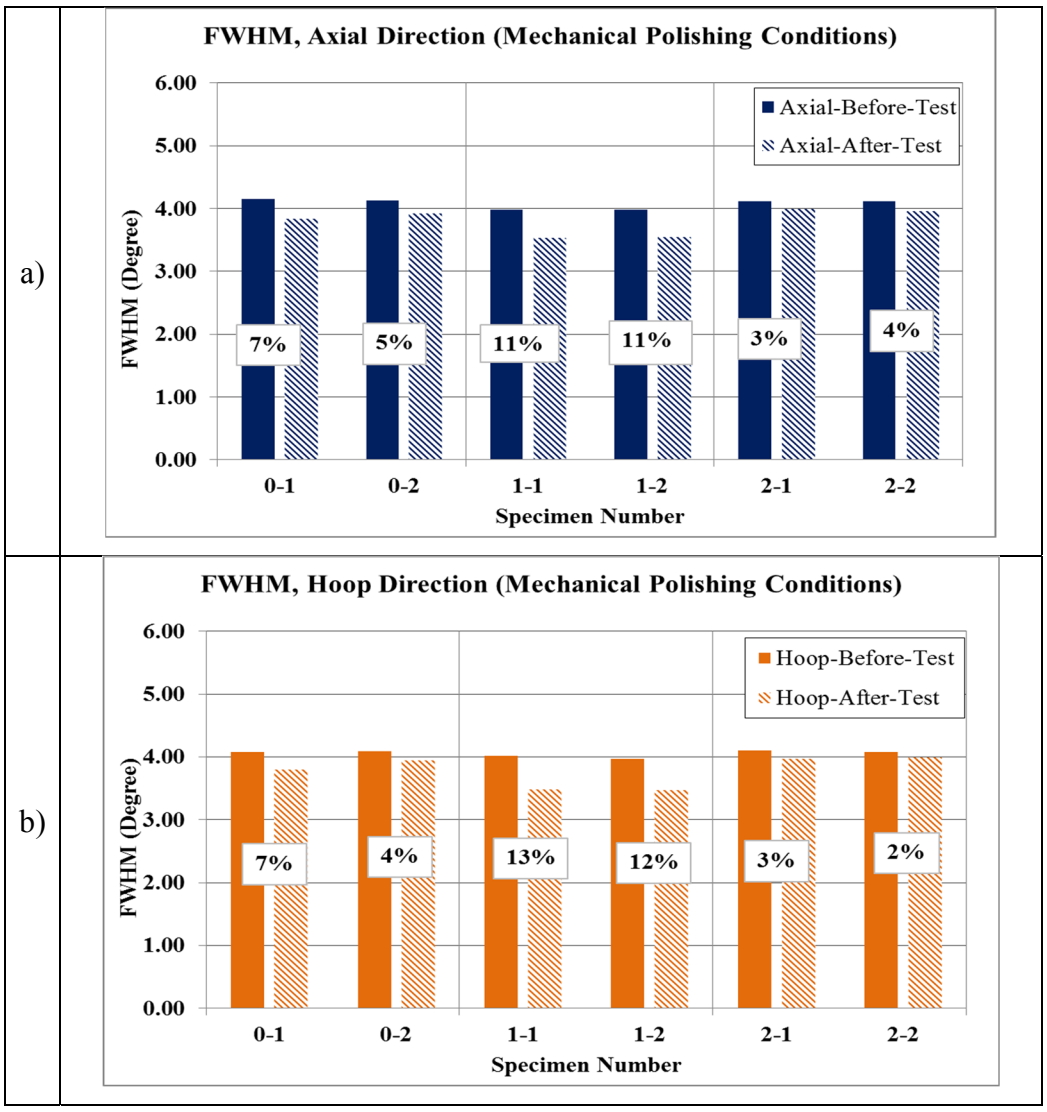

Figure 3.40 FWHM measurements showing the dislocation density before and after fatigue test for the specimens that were mechanically polished.

Specimens that were chemically polished (conditions 3, 4, 5) display a reduction in dislocation density (Figure 3.41 (a) and (b)), which may also reduce the sensitivity of the surface to the presence of inclusion particles.

a)

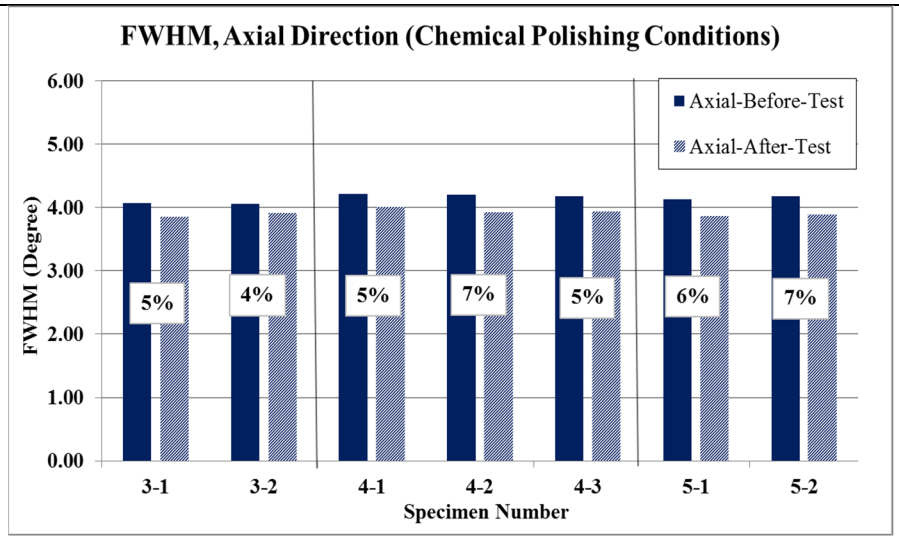

b)

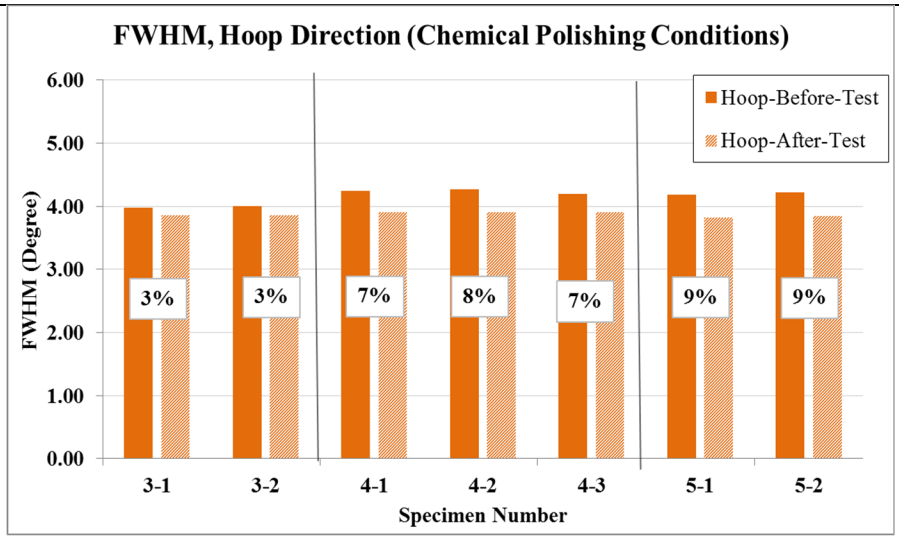

Figure 3.41 FWHM measurements showing the dislocation density before and after fatigue test for the specimens that were chemically polished.

In condition 7, specimens were shot peened and chemically polished, and FWHM decreased significantly compared to the only shot peened specimens (condition 6) (Figure 3.42). It shows chemical polishing removes the layers that have a very high density of dislocations.

a)

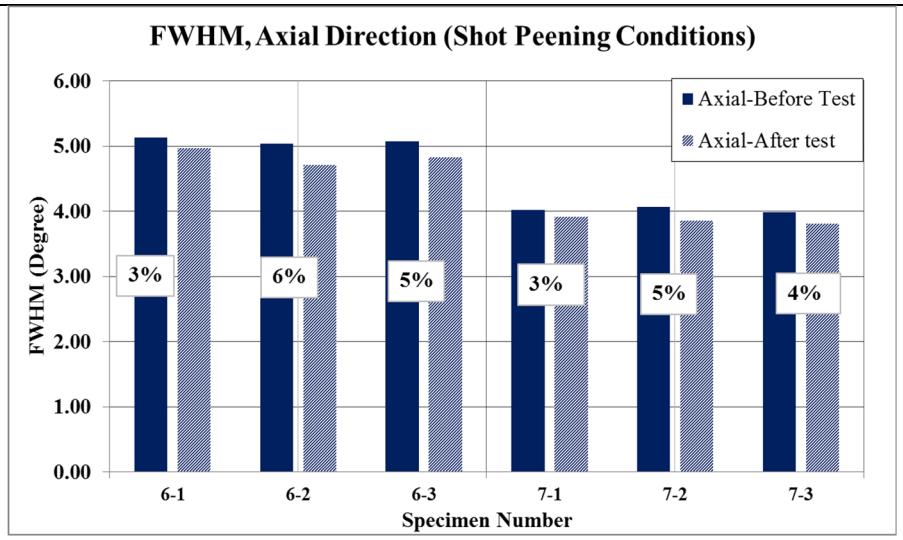

b)

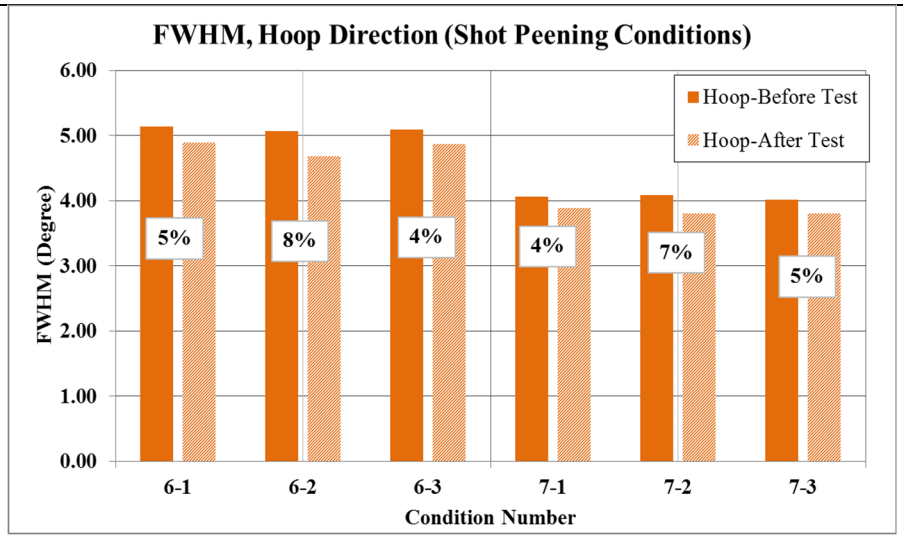

Figure 3.42 FWHM measurements showing the dislocation density before and after fatigue test for the specimens in condition 6 and 7.

3.2.3.5 Microhardness Measurement

During rotative fatigue tests, only the surface regions of the specimens were highly stressed, therefore, only the few hundreds of microns below the surface in these specimens were affected during fatigue test. Microhardness measurements at this region are shown in Figure 3.43 (a) for the conditions 0 and 1 and (b) for the conditions 0 and 2. Specimens in these conditions are mechanically polished and they do not have a surface defect and residual stress. Microhardness profiles have been compared before and after fatigue test for supplier 'A' products after both methods of stress relieving (Figure 3.43 (a)) showing relatively lower microhardness profile up to 75 microns below the surface for the specimen stress relieved with batch method (condition 1). In deeper layers, both conditions are showing the same profile, which is below the initial microhardness profile suggesting material softening during fatigue test up to 125 microns below the surface for both stress relieving methods.

Microhardness profiles for both suppliers after stress relieving with inline methods has presented in Figure 3.43 (b) showing almost similar microhardness profiles, which below the initial microhardness profile up to 125 microns in depth suggesting similar the same depth and material softening after inline method of stress relieving for both suppliers.

a)

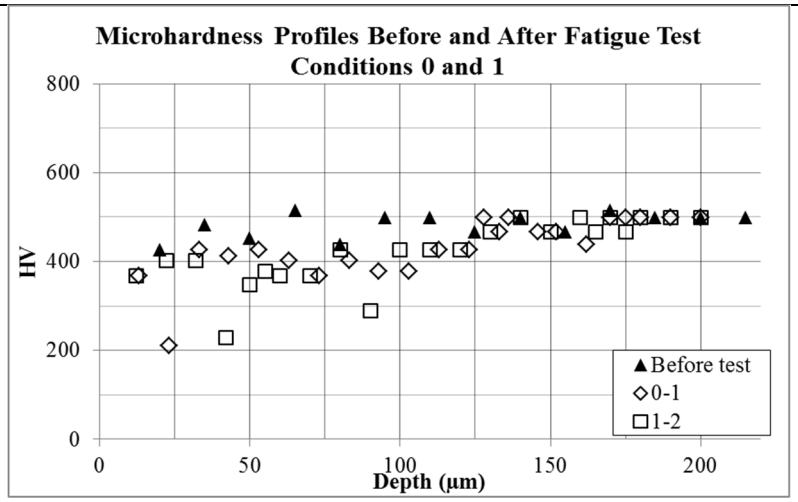

b)

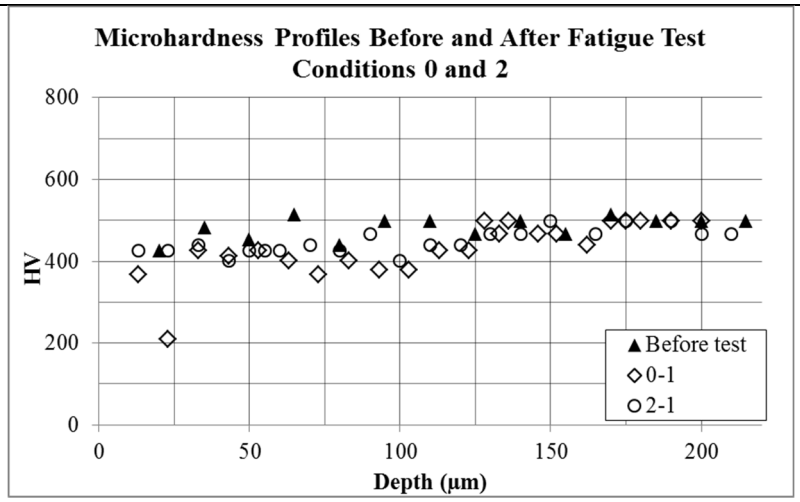

Figure 3.43 Comparing the microhardness at the surface before fatigue test (▲) and after fatigue test for the (a) conditions 0 and 1, (b) conditions 0 and 2.

Microhardness measurements for the specimens that were chemically polished after machining (conditions 3, 4, and 5) have shown in Figure 3.44 (a) and (b). Initial microhardness profile (before fatigue test) have a relatively similar trend with the profiles after fatigue test suggesting constant material properties during fatigue test in these conditions. However, the first 50 microns below the surface shows the higher microhardness values after fatigue test (particularly condition3) compare to the values before fatigue test suggesting the effect of compressive residual stress.

a)

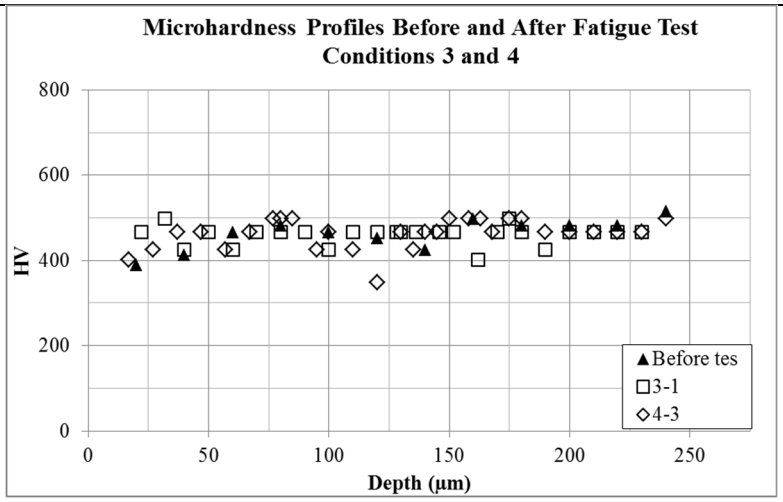

b)

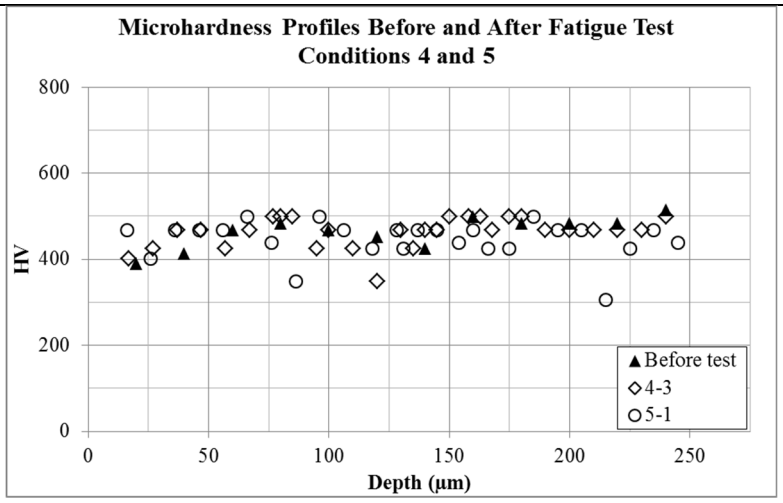

Figure 3.44 Comparing the microhardness at the surface before fatigue test (▲) and after fatigue test for the (a) conditions 3 and 4, (b) conditions 4 and 5.

Specimens after shot peening (conditions 6 and 7) shows lower microhardness values after fatigue test as shown in Figure 3.45 (a) and (b). Only shot peened specimen (condition 6) has almost same hardness values at first 60 microns below the surface compare to the initial values before fatigue test. However, in deeper layers, hardness values in this condition have relatively lower values (Figure 3.45 (a)) suggesting the effect of material softening during fatigue test in this condition. The material softening after shot peening was obverted for the coil springs specimens that were double shot peened (see Figure 3.8).

Chemical polishing removed the hard layers after shot peening as Figure 3.45 (b) shows the lower microhardness values after 50 microns below the surface. Lower microhardness values have continued up to 200 microns below the surface presenting the effect of material softening due to the fatigue test. In deeper layers, the material has similar microhardness value with the ones before fatigue test.

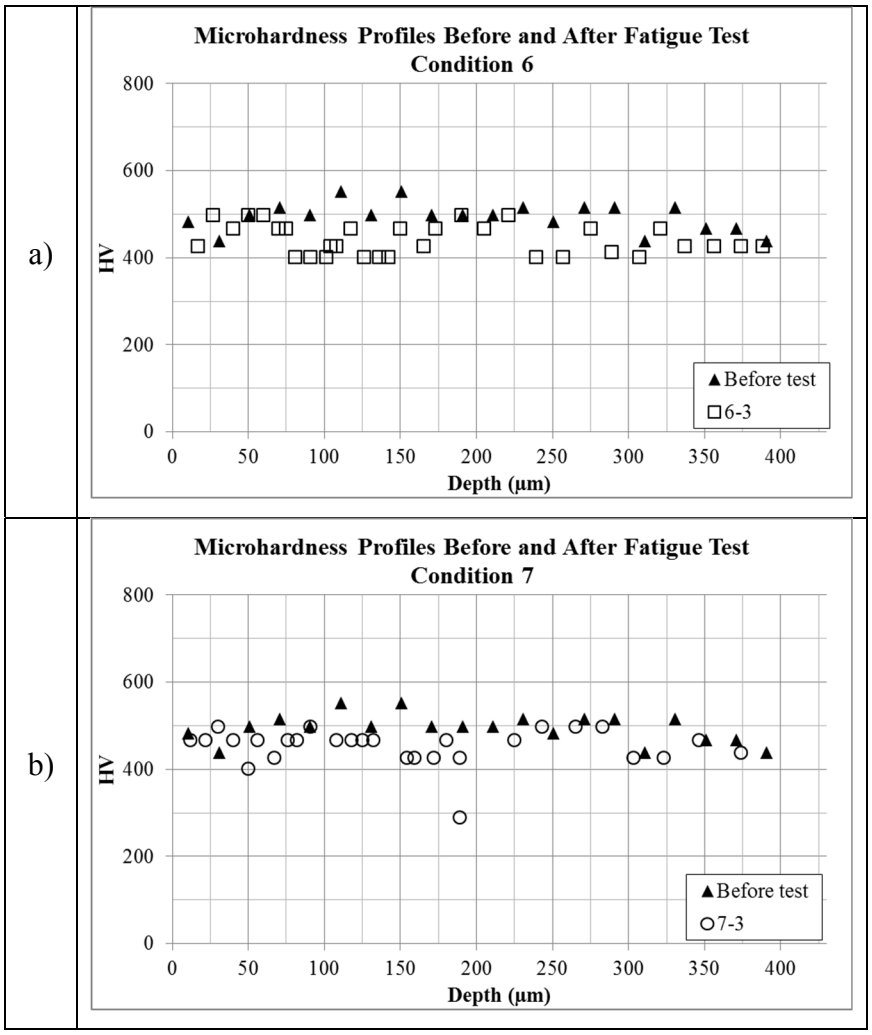

Figure 3.45 Microhardness measurements at the surface for the specimens in conditions 6 and 7 showing same microhardness profile at the surface and in depth.

CONCLUSIONS

This master thesis investigated the reason for fatigue life discrepancy of the coil springs that are used in automotive engine systems. Fatigue life in these springs varies in the range of 10^4 to 10^5 while they had same material properties and production conditions. This study showed coils with low life cycles (10^4) and high life cycles (10^5) had different initial material properties. The coils broken at low numbers of cycles had different microhardness at the surface and in depth compare to high cycle coils. This difference of microhardness was explained by the microstructural point of view. Both steels have the same composition and both have bainitic-martensitic structures. The coil springs with low life cycles have smaller bainitic structures than the coils with high life cycles. Microstructure of low life cycle coils is mostly martensitic, which decreases the performance of these coils. Crack nucleation site in coil springs was close to the surface (<30 μm) suggesting that applied double shot peening process was not optimized.

This work also studied the fatigue life of high-strength steels in different surface integrity conditions. It was found that Al-Ca inclusion particles in the material are the normal source of failure for the steels if no surface defects are found at the surface. The size of the inclusion particles is different in two material providers. The size of the particles and their positions relative to the surface controlled the number of cycles to rupture. The chemical polishing does not remove the surface defects completely and leaving some valley at the surface in the case of machining or shot peening. Surface shot peening induced good depth of compressive residual stress (180 microns), while surface after shot peening has lots of peeing defects generating stress concentrations. These stress concentrations are the main reason for the nucleation of cracks that lead to the rupture of the specimen. In the present conditions, inclusion particles are not the main reason of failure after shot peening. Fatigue life after shot peening is controlled by peening defects. These peening defects seem to include roughness impact and micro-cracks. Fatigue life improves only twice after the shot peening and chemical polishing method used in the present work.

This study concluded that double shot peening using the big shot as a first peening and small shot size in second peening or single shot peening with less peening intensity could improve the fatigue life more.

RECOMMENDATIONS

This section will give some recommendations that will be useful to improve the quality, fatigue life, and complete the present work.

- In addition to the mechanical properties of the high-strength steels, their microstructures also should be verified.

- Surface roughness should be improved after shot peening process. For this regard, double shot peening, with different shot size is suggested. First peening with big shot size (≥0.8 mm) and second peening with small shot size (≤0.6 mm) are classically used (Vielma, Llaneza and Belzunce, 2014). Both steps have to be optimized, as introduced defects in the material cannot be removed later in the production line.

- Chemical polishing seems to improve the fatigue property but cannot remove severe surface defects that are introduced earlier in the production process.

- It is suggested to run more rotating bending test (R=-1) for the specimens. Different microstructures and various peening sequence should be tested. These microstructures can be included tempered martensite, various amounts of bainite-martensite, and fully bainitic structures. The stress level can be similar to the present study to have a comparable result, but other stress ranges can be tested to design *S*-*N* curve.

APPENDIX I

PROPAGATION ELLIPSE MEASUREMENTS

Fracture toughness (K_C) described the resistance to a fracture in the material (Hertzberg, Vinci and Hertzberg, 2012) and calculated from the Equation A I-1. In this equation, 'σ' is applied stress and 'a_c' is critical flaw size of the material. Assuming that fatigue test performs at constant stress level, 'K_C' has proportional to square root of 'a_c' on the fracture surface (Equation A I-2) (Dao and Sellami, 2012).

$$K_c = Y\sigma \sqrt{\pi a_c} \qquad \text{(A I-1)}$$

$$K_c \; \alpha \; \sqrt{a_c} \qquad \text{(A I-2)}$$

The big and small diameters of the propagation ellipse on the coil specimens represent the depth and width of the flaw on the fracture surface. Propagation ellipse diameters were measured by using the profile measurements method with Lext microscope. In this method, two perpendicular lines were drawn representing the big diameter (a) and small diameter (b) in the propagation ellipses as shown in Figure A I-1. The length of the measurements for both perpendicular lines needs to be adjusted based on the propagation ellipse size. The value of the measurement is shown as a length (arrow in Figure A I-3).

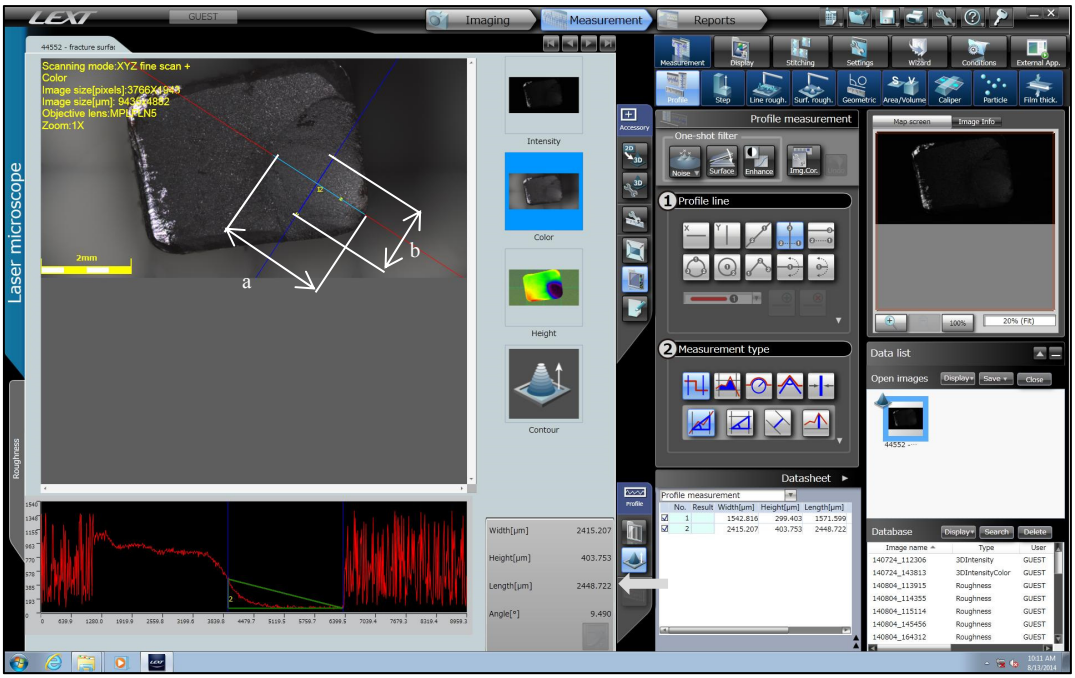

Figure-A I–1 Propagation ellipse measurements for specimen failed at 44552 cycles.

The total area of the propagation ellipse (A in Table-A I-1) was calculated by having big and small diameters and using Equation A I-3. Table-A I-1 shows the values of the diameters and the total area of the propagation ellipse for each coil specimen.

$$A = \pi ab \qquad \text{(A I-3)}$$

Table A I-1 Results of the propagation ellipse measurements showing big diameter 'a', small diameter 'b', and total area 'A' for all the broken coil specimens.

Nf	a (μm)	b (μm)	A (μm^2)
44552	242	154	117021
49758	210	143	94294
60758	295	183	169513
195391	283	230	204383
200319	310	174	169372
320225	250	173	135805

APPENDIX II

SUMMARY OF THE STRESS RAISER DIMENSIONS

Table A II-1 presents the summary of the characterizations on the fracture surfaces for the specimens with eight different surface integrity conditions.

Table A II-1 Presenting the summary of the fractography.

Condition	Specimen No.	No. initiation sites	Failure reason	Inclusion size (μm)	Surface defect size (μm)	Distance from surface (μm)	Nf
0	0-1	1	Internal Inclusion	r ≈ 12.5, d ≈ 17.5	-	-	24492
	0-2	1	Missed inclusion at surface	-	a ≈ 3 c ≈ 12	-	28843
1	1-1	1	Missed inclusion at surface	r ≈ 12, d ≈ 9	-		14997
	1-2	1	Internal Inclusion	r ≈ 20, d ≈ 54	-		15233
2	2-1	1	Missed inclusion at surface	-	a ≈ 7 c ≈ 14	-	56587
	2-2	3	Missed inclusion at surface	-	a1 ≈ 4, a2 ≈ 5, a3 ≈ 4 c1 ≈ 8, c2 ≈ 7, c3 ≈ 11	-	58897
3	3-1	1	Inclusion close to surface	r ≈ 6.5, d ≈ 9	-		66137
	3-2	1	Machining defect	-	-	-	83112
4	4-1	1	Inclusion close to surface	r ≈ 8.5, d ≈ 12	-	-	46471
	4-2	1	Machining defect	-	-	-	98025
	4-3	1	Inclusion close to surface	r ≈ 3, d ≈ 6	-		116644
5	5-1	1	Machining defect	-	a ≈ 6 c ≈ 40	-	68228
	5-2	2	Machining defect	-	-	-	80919
6	6-1	1	Peening defect	-	a ≈ 2 c ≈ 30	-	97272
	6-2	1	Peening defect	-	a ≈ 3 c ≈ 70	-	100191
	6-3	1	Peening defect	-	a ≈ 5 c ≈ 42	-	109616
7	7-1	1	Remained peening defect	-	-	-	153712
	7-2	1	Remained peening defect	-	-	-	179306
	7-3	1	Remained peening defect	-	a ≈ 6 c ≈ 64	-	243785

BIBLIOGRAPHY

ASTM. 2007. *Preparation of Metallographic Specimens*. 12.p.

ASTM. 2012. *Knoop and Vickers Hardness of Materials*. United States: 43.p.

ASTM. 2014. *Steel Wire, Carbon and Alloy Specialty Spring Quality*. 5.p.

ASTM. 2015. *Conducting Force Controlled Constant Amplitude Axial Fatigue Tests of Metallic Materials*. 6.p.

Balseal. 2016. *Electropolishing of metal surfaces and its effect on Bal Seal spring-energized seal performance*. Summary. USA: Bal Seal Engineering Inc., p.1-4.

Bramfitt, B. L. 2002. « Structure/Property Relationships in Irons and Steels ». In *Metals Handbook Desk Edition*, sous la dir. de Davis, J.R., Second: American Society for Metals. p. 153-173.

Campbell, F.C. 2008. « The Iron-Carbon System ». In *Elements of Metallurgy and Engineering Alloys*. ASM International. p. 167-168.

Canonico, D.A. 1991. « Stress-relief Heat treating of Steel ». In *Heat treating*. Vol. 4. ASM International. p. 33-34.

Chang, W.R., M. Hirvonen and R. Grönqvist. 2004. « The effects of cut-off length on surface roughness parameters and their correlation with transition friction ». *Safety Science,* vol. 42, n^{o} 8, p. 755-769.

Dao, N. H., and H. Sellami. 2012. « Stress intensity factors and fatigue growth of a surface crack in a drill pipe during rotary drilling operation ». *Engineering Fracture Mechanics,* vol. 96, p. 626-640.

Daubenspeck, B. R. 2010. « Extrapolation Techniques For Very Low Cycle Fatigue Behavior Of a Ni-Base Superalloy ». Florida, University of Central Florida.p.97.

Dove, A.B. 1990. « Steel Wire ». In *Properties and selection: irons, steels, and high performance alloys*. Vol. 1. American Society of Metals (ASM). p. 277-288.

Dubey, J. S., H. Chilukuru, J. K. Chakravartty, M. Schwienheer, A. Scholz and W. Blum. 2005. « Effects of cyclic deformation on subgrain evolution and creep in 9–12% Cr-steels ». *Materials Science and Engineering: A,* vol. 406, nº 1–2, p. 152-159.

Guagliano, M., and L. Vergani. 2004. « An approach for prediction of fatigue strength of shot peened components ». *Engineering Fracture Mechanics,* vol. 71, nº 4–6, p. 501-512.

Gur, H. C., and S. Savas. 2012. « Measuring the Surface Residual Stresses in Shot Peened Steel Components by Magnetic Barkhausen Noise Method ». In *18th World Conference on Nondestructive Testing*. (Durban, South Africa), p. 1-7.

Hertzberg, R.W., R.P. Vinci and J.L. Hertzberg. 2012. « Deformation and Fracture Mechanics of Engineering Materials ». In.: Wiley. p. 330.

Htun, M., S. Kyaw and K. Lwin. 2008. « Effect of Heat Treatment on Microstructures and Mechanical Properties of Spring Steel ». *Metals, Materials and Minerals,* vol. 18, nº 2, p. 7.

Ishigami, H., K. Matsui, Y. Jin and K. Ando. 2000. « Technical note A study on stress, reflection and double shot peening to inrease compressive residual stress ». *Fatigue & Fracture of Engineering Materials & Structures,* vol. 23, nº 11, p. 959-963.

ISO. 2010. *Metallic materials – Rotating bar bending fatigue testing*. ISO 1143:2010. Switzerland: 32.p.

Izumida, H., S. Matsumoto and T. Murai. 2016. *History and Future of High-Fatigue-Strength Steel Wire for Automotive Engine Valve Spring*. Coll. « SEI TECHNICAL REVIEW », p.1-6.

Kostilnik, T. 1994. « Shot Peening ». In *Surface Engineering*. Vol. 5. American Society of Metals (ASM). p. 126-135.

Kovacs, B. 1991. « Heat Treating of Gray Irons ». In *Heat treating*. Vol. 4. ASM International. p. 670-681.

Lee, C. S., D. M. Li, K. A. Lee, S. J. Yoo and W. J. Nam. 1998. « Microstructural influence on fatigue properties of a high-strength spring steel ». *Materials Science and Engineering: A,* vol. 241, nº 1–2, p. 30-37.

Nam, W., C. Lee and Y. Deok. 2000. « Effects of alloy additions and tempering temperature on the sag resistance of Si–Cr spring steels ». *Materials Science and Engineering: A,* vol. 289, nº 1–2, p. 8-17.

Porteiro, J. L. 2010. « Spring design optimization with fatigue ». United State of America, University of South Florida. < http://scholarcommons.usf.edu/etd/1742 >.p.77.

Prawoto, Y., M. Ikeda, S.K. Manville and A. Nishikawa. 2008. « Failure Analysis of Automotive Suspension Coil Springs ». *Iron & steel technology,* vol. 5, p. 35-48.

Puls-Tech. 2016. « portable X-ray residual stress measuring device μ-X360 ». < http://www.meidenshoji.co.jp/business/measurement/prod_03/index.html >. Viewed 05-19.

Quesnel, D. J., M. Meshii and J. B. Cohen. 1978. « Residual stresses in high strength low alloy steel during low cycle fatigue ». *Materials Science and Engineering,* vol. 36, nº 2, p. 207-215.

SAE. 2015. *Steel, Spring Wire 1.4Si - 0.65Cr*. USA: SAE International 4.p.

Sarna, S. K. 2013. « Spring Steels ». In *Ispat Digest*. < http://ispatguru.com/spring-steels/ >. Viewed 10/20.

Sauzay, M., H. Brillet, I. Monnet, M. Mottot, F. Barcelo, B. Fournier and A. Pineau. 2005. « Cyclically induced softening due to low-angle boundary annihilation in a martensitic steel ». *Materials Science and Engineering: A,* vol. 400–401, p. 241-244.

Sauzay, M., B. Fournier, M. Mottot, A. Pineau and I. Monnet. 2008. « Cyclic softening of martensitic steels at high temperature—Experiments and physically based modelling ». *Materials Science and Engineering: A,* vol. 483–484, p. 410-414.

Serbino, E. M., and A. P. Tschiptschin. 2014. « Fatigue behavior of bainitic and martensitic super clean Cr–Si high strength steels ». *International Journal of Fatigue,* vol. 61, p. 87-92.

SMI. 2002. *Handbook of Spring Design*. Spring Manufacturers Institute, Incorporated, p 119.

Song, P. S., and C. C. Wen. 1999. « Crack closure and crack growth behaviour in shot peened fatigued specimen ». *Engineering Fracture Mechanics,* vol. 63, nº 3, p. 295-304.

Suda, S., and N. Ibaraki. 2005. « The Past and Future of High-strength Steel for Valve Springs ». *Kobelco Technology Review*, nº 2005, p. 5.

Tekeli, S. 2002. « Enhancement of fatigue strength of SAE 9245 steel by shot peening ». *Materials Letters,* vol. 57, nº 3, p. 604-608.

Terentyev, D. A., G. Bonny and L. Malerba. 2008. « Strengthening due to coherent Cr precipitates in Fe-Cr alloys: Atomistic simulations and theoretical models ». *Acta Materialia,* vol. 56, nº 13, p. 3229-3235.

Torres, M. A. S., and H. J. C. Voorwald. 2002. « An evaluation of shot peening, residual stress and stress relaxation on the fatigue life of AISI 4340 steel ». *International Journal of Fatigue,* vol. 24, nº 8, p. 877-886.

Totten, G.E. 2006. « Effect of Alloying Elements on Heat Treatment Processing of Iron-Carbon Alloys ». In *Steel Heat Treatment: Metallurgy and Technologies*. Taylor & Francis. p. 166-171.

Uematsu, Y., T. Kakiuchi, K. Tokaji, K. Nishigaki and M. Ogasawara. 2013. « Effects of shot peening on fatigue behavior in high speed steel and cast iron with spheroidal vanadium carbides dispersed within martensitic-matrix microstructure ». *Materials Science and Engineering a-Structural Materials Properties Microstructure and Processing,* vol. 561, p. 386-393.

Vielma, A. T., V. Llaneza and F. J. Belzunce. 2014. « Effect of coverage and double peening treatments on the fatigue life of a quenched and tempered structural steel ». *Surface and Coatings Technology,* vol. 249, p. 75-83.

Wahl, A.M. (34-38). 1944. *Mechanical springs*, First edition. USA: Penton, p 463.

Wang, J. S., C. C. Hsieh, H. H. Lai, C. W. Kuo, P. T. Y. Wu and W. T. Wu. 2015. « The relationships between residual stress relaxation and texture development in AZ31 Mg alloys via the vibratory stress relief technique ». *Materials Characterization,* vol. 99, p. 248-253.

Yamada, Y., and T. Kuwabara. 2007. « A Guide to Spring Material Selection ». In *Materials for Springs*. Springer Berlin Heidelberg. p. 377.